



**ScuDo**  
Scuola di Dottorato ~ Doctoral School  
WHAT YOU ARE, TAKES YOU FAR

Doctoral Dissertation  
Doctoral Program in Mechanical Engineering (30<sup>th</sup> Cycle)

# **Concept of an exoskeleton for industrial applications**

**With modulated impedance based on  
Electromyographic signal recorded from the  
operator**

By

**Daniele Borzelli**

\*\*\*\*\*

**Supervisor:**

Prof.ssa Laura Gastaldi

**Doctoral Examination Committee:**

Prof. Benedetto Allotta, Referee, University of Florence

Prof. Yanan Li, Referee, University of Sussex

Politecnico di Torino  
2018



## **Declaration**

I hereby declare that, the contents and organization of this dissertation constitute my own original work and does not compromise in any way the rights of third parties, including those relating to the security of personal data.

Daniele Borzelli

2018

\* This dissertation is presented in partial fulfillment of the requirements for **Ph.D. degree** in the Graduate School of Politecnico di Torino (ScuDo).







## **Abstract**

The introduction of an active exoskeleton that enhances the operator power in the manufacturing field was demonstrated in literature to lead to beneficial effects in terms of reducing fatiguing and the occurrence of musculo-skeletal diseases. However, a large number of manufacturing operations would not benefit from power increases because it rather requires the modulation of the operator stiffness. However, in literature, considerably less attention was given to those robotic devices that regulate their stiffness based on the operator stiffness, even if their introduction in the line would aid the operator during different manipulations respect with the exoskeletons with variable power.

In this thesis the description of the command logic of an exoskeleton for manufacturing applications, whose stiffness is modulated based on the operator stiffness, is described. Since the operator stiffness cannot be mechanically measured without deflecting the limb, an estimation based on the superficial Electromyographic signal is required.

A model composed of 1 joint and 2 antagonist muscles was developed to approximate the elbow and the wrist joints. Each muscle was approximated as the Hill model and the analysis of the joint stiffness, at different joint angle and muscle activations, was performed. The same Hill muscle model was then implemented in a 2 joint and 6 muscles (2J6M) model which approximated the elbow-shoulder system. Since the estimation of the exerted stiffness with a 2J6M model would be quite onerous in terms of processing time, the estimation of the operator end-point stiffness in real-time would therefore be questionable. Then, a linear relation between the end-point stiffness and the component of muscle activation that does not generate any end-point force, is proposed.

Once the stiffness the operator exerts was estimated, three command logics that identifies the stiffness the exoskeleton is required to exert are proposed. These

proposed command logics are: Proportional, Integral 1 s, and Integral 2 s. The stiffening exerted by a device in which a Proportional logic is implemented is proportional, sample by sample, to the estimated stiffness exerted by the operator. The stiffening exerted by the exoskeleton in which an Integral logic is implemented is proportional to the stiffness exerted by the operator, averaged along the previous 1 second (Integral 1 s) or 2 seconds (Integral 2 s). The most effective command logic, among the proposed ones, was identified with empirical tests conducted on subjects using a wrist haptic device (the Hi5, developed by the Bioengineering group of the Imperial College of London). The experimental protocol consisted in a wrist flexion/extension tracking task with an external perturbation, alternated with isometric force exertion for the estimation of the occurrence of the fatigue. The fatigue perceived by the subject, the tracking error, defined as the RMS of the difference between wrist and target angles, and the energy consumption, defined as the sum of the squared signals recorded from two antagonist muscles, indicated the Integral 1 s logic to be the most effective for controlling the exoskeleton.

A logistic relation between the stiffness exerted by the subject and the stiffness exerted by the robotic devices was selected, because it assured a smooth transition between the maximum and the minimum stiffness the device is required to exert. However, the logistic relation parameters are subject-specific, therefore an experimental estimation is required. An example was provided.

Finally, the literature about variable stiffness actuators was analyzed to identify the most suitable device for exoskeleton stiffness modulation. This actuator is intended to be integrated on an existing exoskeleton that already enhances the operator power based on the operator Electromyographic signal. The identified variable stiffness actuator is the DLR FSJ, which controls its stiffness modulating the preload of a single spring.

# Contents

1. Introduction to exoskeletons .....	1
1.1 Exoskeleton definition and generations.....	2
1.2 Fields of use of exoskeletons.....	6
1.3 Potential effects of industrial exoskeletons on workers .....	12
1.4 Standards and current legislation on collaborative robotics.....	15
1.5 Exoskeletons with variable impedance.....	18
1.5.1 Arm impedance.....	19
1.5.2 The real-time impedance control in robotic manipulators.....	19
1.5.3 Exoskeletons and impedance .....	20
2. Exoskeleton concept .....	22
2.1 Machining classification.....	22
2.2 Human-Exoskeleton interface functional blocks.....	26
2.2.1 The ‘Human arm system’ block.....	27
2.2.2 The ‘Exoskeleton system’ block.....	28
3. The upper limb models .....	30
3.1 Musculo-tendon system model.....	30
3.1.1 The active element .....	32
3.1.2 The parallel spring .....	33
3.1.3 The serial spring.....	34
3.1.4 The musculo-tendon system .....	35
3.2 1J2M: 1 joint and 2 antagonist muscles model .....	36

---

3.2.1 Joint model.....	38
3.2.2 Equations for force balancing .....	41
3.2.3 The elbow model .....	44
3.2.4 The wrist model .....	49
3.2.4.4 Wrist rotational stiffness .....	52
3.3 2J6M: 2 joints and 6 muscles model .....	54
3.3.1 Implications of muscle redundancy .....	54
3.3.2 The model of 2 joints and 6 muscles .....	59
3.3.3 Model simulations.....	62
3.3.4 Equations for end-point force calculation.....	64
3.3.5 Equations for end-point stiffness calculation.....	64
3.3.6 The projection of the muscle activation onto the null space.....	67
3.3.7 The stiffness ellipse fitting.....	68
4. The exoskeleton command logic .....	71
4.1 The Hi5 .....	72
4.1.1 Mechanical specifications.....	73
4.1.2 Software and control.....	74
4.1.3 Ergonomic aspects .....	75
4.1.4 Redundant safety.....	75
4.1.5 Real-time performance .....	76
4.2 Experimental protocol .....	76
4.2.1 Participants.....	76
4.2.2 Setup .....	76
4.2.3 Surface electromyography .....	77
4.2.4 Protocol.....	78
4.2.4.1 Zero setting, wrist range of motion definition, and normalization .....	79

---

4.2.4.2 Initial maximum voluntary torque ( $MVT_i$ ).....	80
4.2.4.3 The Borg rating of perceived exertion scale.....	81
4.2.4.4 Visual feedback.....	82
4.2.4.5 Isometric force task.....	83
4.2.4.6 Tracking task.....	84
4.2.4.7 Command logics .....	85
4.2.4.8 Repetitions .....	87
4.2.4.9 Final maximum voluntary torque ( $MVT_f$ ) and last Borg perceived exertion.....	88
4.2.4.10 Statistics .....	88
4.3 Analysis .....	88
4.3.1 Initial Maximum voluntary torques .....	88
4.3.2 Perceived fatigue.....	89
4.3.3 The frequency median.....	90
4.3.4 Task error during tracking task.....	92
4.3.5 Energy consumption during the tracking task .....	95
4.3.6 Conclusions.....	97
4.4 The command parameters.....	98
4.4.1 Co-activation below which no stiffening is exerted .....	99
4.4.2 Co-activation above which the maximum stiffening is exerted ...	100
4.4.3 Co-activations which linearly scale with the exerted stiffening ...	101
4.4.4 Example of the relation between co-activation and exoskeleton stiffness.....	104
5. Selection of the variable stiffness actuators.....	106
5.1 Actuators for the exoskeleton stiffness modulation .....	107
5.1.1 Variable impedance actuators definition .....	107
5.1.2 Active impedance by control .....	109
5.1.3 Inherent compliance.....	109

5.1.3 Fixed compliance .....	109
5.1.4 Adaptable compliance properties.....	110
5.1.4.1 Spring preload.....	111
a) Antagonistic springs with antagonistic motors.....	112
b) Antagonistic springs with independent motors .....	112
c) Preload adjustment of single spring.....	113
5.1.4.2 Changing transmission between load and spring.....	115
a) Lever length .....	115
b) Nonlinear mechanical interlink .....	116
c) Continuous variable transmission.....	116
5.1.4.3 Physical properties of spring.....	116
a) Changing of the cross-section area .....	117
b) Active spring length.....	117
5.2 Identification of the actuator .....	117
5.2.1 Use-cases .....	118
5.2.2 Design concepts .....	119
5.2.3 Selection of the VSA .....	120
5.3 Safety systems .....	123
6. Conclusions.....	124
7. References.....	129
8. Appendix A: The administrated Borg scale.....	146
9. Appendix B: The DLR FSJ data sheet.....	148



# List of Figures

Figure 1.1: Example of first generation exoskeleton. The Hardiman .....	3
Figure 1.2: Examples of exoskeletons of the second generation. A: The BLEEX. B: ALEX. C: ARMin .....	4
Figure 1.3: Examples of exoskeletons of the third generation. A: Exoskeleton described in (Rosen et al., 2001); B: Exoskeleton described in (Cavallaro et al., 2006); C: Exoskeleton described in (Fleischer & Hommel, 2008); D: Exoskeleton described in (S. Lee & Sankai, 2002); E: Exoskeleton described in (Lucas et al., 2004); F: Exoskeleton described in (Mulas et al., 2005). .....	5
Figure 1.4: Examples of exoskeletons of the fourth generation. A: Exoskeleton described in (Bhagat et al., 2016); B: Exoskeleton described in (Contreras-Vidal & Grossman, 2013); C: Exoskeleton described in (Kilicarslan et al., 2013); D: Exoskeleton described in (S. Wang et al., 2015); E: Exoskeleton described in (Soekadar et al., 2015). .....	6
Figure 1.5: Examples of exoskeletons for military purpose. A: Hardiman. B: HULC. C: BLEEX. D: Hercule. E: Talos. ....	7
Figure 1.6: Examples of commercial exoskeletons for rehabilitation purpose. A: Hal. B: Honda Motor Company exoskeletons. C: ReWalk. D: Rco Bionics rehabilitation exoskeleton. E: ArmIn. F: ABLE. G: KMI Hand Mentor. ....	9
Figure 1.7: Examples of exoskeletons and robotic devices for the industrial field. A: X-Ar. B: Exhauss stronger exoskeleton. C: Exoskeleton developed by Levitate technologies. D: PLAD. E: Laevo. F: Power Loader. G: Muscle Suit. H: Chairless chair. I: Zero-G. L: Fortis. ....	11
Figure 1.8: Examples of exoskeletons for agricultural purposes. A. The exoskeleton developed at the Tokyo University of Agriculture and Technology. B. The Happy back. ....	12
Figure 2.1: Example of the actions exerted during the use of a screwdriver. The operator needs to exert a force (green arrow) and a torque (blue arrow). If the screw axis (black dotted line) is not aligned with the exerted force, the operator needs to increase the stiffness along the directions orthogonal to the force (red arrows and plane) such to avoid the screwdriver to lose contact with the screw. ....	23
Figure 2.2: Iconic machining of different tasks. ....	25

Figure 2.3: Concept of human-exoskeleton interaction. ....	27
Figure 3.1: Skeletal muscle structure. The belly is the middle thicker part of the muscle while the tendons connect the muscle with the bones. The origin is the attachment to the stationary end of the muscle and the insertion is the attachment to the mobile end of the muscle .....	31
Figure 3.2: The Hill musculo-tendon model. A. The musculo-tendon system is modeled with an active element (A) and a parallel spring ( $k_p$ ), which modulate the action of the muscle belly, and a serial spring ( $k_s$ ) which modulates the tendons action. B. The force exerted by the serial spring, depending on the relative length of the tendons ( $l_s/l_{s0}$ ). C. The force exerted by the muscle belly (black) as the sum of the action exerted by the parallel spring (green) and the active element (red) depending on the relative length of the belly ( $l_p/l_{popt}$ ) .....	31
Figure 3.3: The force exerted by the active element depending on the muscle activation and on the length of the belly segment. The force is normalized to the maximum force the muscle active element could exert, the belly length is normalized to its optimal length, and the muscle activation is normalized to the MVC. ....	33
Figure 3.4: The passive parallel spring force, normalized to the maximum force the muscle active element could exert, depends on the length of the belly segment, normalized to its optimal length. ....	34
Figure 3.5: The passive serial spring force, normalized to the maximum force the muscle could exert, depends on the length of the tendon, normalized to the tendon slack length. ....	35
Figure 3.6: Force exerted by the muscle segment (left) in relation to its length at different activations of the active element (color coded and normalized to the MVC). Force exerted by the musculo-tendon system (right) in relation to its length at different activations (color coded and normalized to the MVC). ....	36
Figure 3.7: The model made of 1 joint and 2 muscles could approximate both an elbow joint (left) and a wrist joint (right). ....	37
Figure 3.8: Model of human elbow or wrist joints.....	38
Figure 3.9: The muscle model implemented in the Simulink software. Left: the elbow model in which the only BRD and TriLat muscles are displayed. Right: the wrist model in which the only FCR and ECRL muscles are displayed. ....	40

- 
- Figure 3.10: Comparison between the muscle torque-joint angle curves of the BRD (muscle 1) calculated with the model presented in this chapter (continuous line) respect with the one calculated with the musculo-skeletal modeling software OpenSim (dotted line) for different muscle activations.....41
- Figure 3.11: The forces exerted by the two muscles.....42
- Figure 3.12: Intersections between the characteristics of the torque, related to the musculo-tendon length, exerted by the two muscles for different elbow flexion, at different level of activation of muscle 1 (BRD, colored) and 2 (TriLat, gray scale). .....44
- Figure 3.13: Relation between the torque related to the elbow flexion, exerted by the two antagonistic muscles, at different level of activation of muscle 1 (colored) and 2 (gray scale). Muscle activations are not equally spaced. ....45
- Figure 3.14: Activation of muscle 2 necessary to balance the torque exerted by muscle 1, for different elbow flexions. The different level of muscle 1 activations are reported with different colors. Muscle 1 activations are not equally spaced. In light yellow the surface in which stiffness could be modulated is identified. ....46
- Figure 3.15: Rotational stiffness of the muscles. The stiffness of muscle 1 is represented with a colored scale, each muscle 1 activation is represented with a different color. The stiffness of muscle 2 is represented with a gray scale, the muscle 2 activation, whose torque balanced the torque exerted by muscle 1, is represented with a different level of gray.....47
- Figure 3.16: Stiffness of the elbow at different elbow flexions and muscle 1 activations, are reported with different colors. ....49
- Figure 3.17: The 1J2M modeled as a wrist .....49
- Figure 3.18: Intersections between the characteristics of the torque, related to the musculo-tendon length, exerted by the two muscles for different wrist flexion, at different level of activation of muscle 1 (colored) and 2 (gray scale). .....50
- Figure 3.19: Relation between the torque related to the wrist flexion, exerted by the two antagonistic muscles, at different level of activation of muscle 1 (colored) and 2 (gray scale). Muscle activations are not equally spaced. ....51
- Figure 3.20. Activation of muscle 2 necessary to balance the torque exerted by muscle 1, for different wrist angles. The different level of muscle 1 activations are reported with different colors. Muscle 1 activations are not equally spaced.....52

Figure 3.21: Rotational stiffness of the muscles. The stiffness of muscle 1 is represented with a colored scale, each muscle 1 activation is represented with a different color. The stiffness of muscle 2 is represented with a gray scale, the muscle 2 activation, whose torque balanced the torque exerted by muscle 1, is represented with a different level of gray.....53

Figure 3.22. Stiffness of the wrist at different elbow flexions and muscle 1 activations, are reported with different colors. ....54

Figure 3.23: Example of the identification of the projection of the muscle activation onto the row and the null spaces. Left: model made of one joint and two identical antagonist muscles ('Muscle 1' and 'Muscle 2', blue lined). The positive direction of the force is represented as a green arrow ( $F_x$ ). Right: The muscle space on whose axes are reported the muscle activations (Muscle 1 on the x axis and Muscle 2 on the y label). The null (red) and row (green) spaces are identified. An example of muscle activations ([0.1 0.8], blue) together with its projection on the null (magenta) and the row (cyan) spaces are reported. ....55

Figure 3.24: Example of the identification of the projection of the muscle activation onto the row and the null spaces. Left: model made of one joint and three muscles two muscles ('Muscle 1' and 'Muscle 2', blue lined) antagonist to a third one ('Muscle 3'). The positive direction of the force is represented as a green arrow ( $F_x$ ). Right: The muscle space on whose axes are reported the muscle activations (Muscle 1 on the x axis, Muscle 2 on the y label, and Muscle 3 on the z label). The null (red plane) and row (green line) spaces are identified. An example of muscle activations ([0.1 0.4 0.8], blue) together with its projection on the null (magenta) and the row (cyan) spaces are reported.....57

Figure 3.25: Elbow shoulder system approximated with a 6M2J musculoskeletal model. The muscles (shoulder monoarticular in blue, elbow monoarticular in green and biarticular in red) are approximated with an Hill muscle model. ....59

Figure 3.26: The elbow-shoulder system and the modeled muscles.....60

Figure 3.27: Relation between the torque related to the elbow flexion, exerted by the two antagonistic muscles, at different level of activation of muscle 1 (colored) and 2 (gray scale). Muscle activations are not equally spaced. ....62

Figure 3.28: Workspace of the upper limb model. The physiological workspace (black line) and the workspace of the model (blue line) are plotted. The positions in which the endpoint stiffness is calculated are reported (red circles). ....63

Figure 3.29: Examples of end-point stiffness calculated for different arm configurations and muscle activations. In the first column the only BRD muscle is activated at different levels, while all the other muscles have a zero activation. In the second column both the PectMaj and the DeltP are activated of the same value, while all the other muscles have a zero activation. In the third column all the muscles are activated of the same activation. Different values of activations are color coded.....67

Figure 3.30: Diagram of the calibration and the online estimation of the major axis of the end-point stiffness ellipse. During the calibration (upper panel) the EMG-to-force matrix ( $H$ ), and consequently its null space ( $N$ ), is calculated from the regression of the recorded EMG signals onto the exerted isometric end-point forces. During the online operation (lower panel) the null space component of the recorded EMG signals, obtained multiplying the EMG signal for  $NT \cdot N$ , is used to estimate the major axis of the end-point stiffness ellipse the subject is exerting. .70

Figure 4.1: The Hi5 system .....73

Figure 4.2: Setup .....74

Figure 4.3: Setup. A. The Hi5 interface. B. Wrist completely extended, the steel bars against which the subject exerted the isometric force are indicated. C. Wrist completely flexed. D. An example of the scene shown by the display. E. Scheme of the setup in which the torque sensor, the motor, and the EMG positioning are indicated.....77

Figure 4.4: Muscles recorded. FCR on the left, ECR on the right .....78

Figure 4.5: Experimental protocol .....79

Figure 4.6: Isometric task.....84

Figure 4.7: Target Position during one tracking trial .....85

Figure 4.8: Tracking task .....85

Figure 4.9: Co-contraction (upper figures) and torques (lower figures) exerted during a time interval in which the target move along a complete sinusoid. The red lines in the Co-contraction panels of the aided sessions indicates the 0.25 threshold above which no torque exertion occurs. ....87

Figure 4.10: Initial maximum voluntary torque of extension (left), and flexion (right), averaged on subjects (mean  $\pm$  std).....89

- Figure 4.11: Initial (grey) and final (black) perceived fatigue of each session based on the RPE CR10 Borg scale.....90
- Figure 4.12: Example of the median frequency of the ECR (up), calculated during all the repetitions of the extension isometric task, and FCR (down), calculated during all the repetitions of the flexion isometric task, of subject 1 ....91
- Figure 4.13: Slope of the regression of the median frequency along the repetitions of the ECR (left) and FCR (right) for each session. Mean  $\pm$  std along subjects.....92
- Figure 4.14: Examples of the task error committed by subject 8 during each repetition and session.....93
- Figure 4.15: Task error committed by each subject during all the repetition of the Baseline session. A consistent decrease between the first and the second repetition was visible. ....94
- Figure 4.16: Mean  $\pm$  std among all subjects and repetitions of the task error for the different sessions.....95
- Figure 4.17: Examples of the energy consumption of subject 8 during each repetition and session.....96
- Figure 4.18: Mean  $\pm$  std among all subjects and repetitions of the energy consumption for the different sessions. ....97
- Figure 4.19: Example of the co-activations calculated from the data recorded during the Control session from subject 8. The red continuous line is the mean among all the repetitions of the co-contraction while the black dashed lines are the mean  $\pm$  the standard deviations of the co-activations. In green the mean co-contraction value.....100
- Figure 4.20: Example of the co-activations calculated from the data recorded during the Baseline session from subject 8. The red continuous line is the mean among all the repetitions of the co-contraction while the black dashed lines are the mean  $\pm$  the standard deviations of the co-activations. ....101
- Figure 4.21: Example of the co-activations calculated from the data recorded during the Proportional (upper), Integral 1 s (middle), and Integral 2 s (lower) sessions from subject 8. The red continuous line is the mean among all the repetitions of the co-contraction while the black dashed lines are the mean  $\pm$  the standard deviations of the co-activations.....103

Figure 4.22: Logistic curve based on the experimental parameters. The red curve represents the curve that should be used for the control of the exoskeleton while the magenta curve represents the original logistic curve. The co-activation is normalized to the maximum voluntary co-contraction. The exoskeleton stiffness is normalized to the maximum stiffness the exoskeleton could exert. .... 105

Figure 5.1: Main categorization of actuators and, in particular, of Variable impedance actuators. .... 108

Figure 5.2: The sub-categorization of the ‘spring preload’ category. .... 111

Figure 5.3: The sub-categorization of the ‘changing transmission between load and spring’ category. .... 115

Figure 5.4: The DLR FSJ actuator. A. The DLR Floating Spring Joint. B. The FSJ mechanism. C. The DLR FSJ technical design. D. Cross section of the FSJ. E. The spring mechanism of the FSJ is located in series between the harmonic drive gear box of the main actuator and the link. F. The FSJ mechanism principle in a flattened view. .... 122

Figure 6.1: Concept of human-exoskeleton interaction with the implementations developed in this thesis. The arm stiffness is estimated as the null space projection of the recorded muscle activation, as described in Chapter 3. The stiffness required by the exoskeleton is related to the estimated arm stiffness with a logistic law, and it is exerted following an Integral 1 s command logic, as described in Chapter 5. The motor commands, that generate the required exoskeleton stiffness, are calculated based on the actuators type (‘preload adjustment of single spring’ actuator) and the exoskeleton design and activate the real actuators (DLR FSJ), as described in Chapter 5. The actions exerted by the exoskeleton and the operator combine to generate the end-point force and stiffness ..... 125

## List of Tables

Table 3.1: Hill muscle parameters got from literature. .... 39

Table 3.2: Distance between the joint centers of rotation and the connection between the muscles and the bones. The origin attach is intended as the distance

---

between the connection of the origin side of the muscle with the bone, while the insertion attach is intended as the distance between the connection of the insertion side of the muscle with the bone (see Figure 3.1). .....	39
Table 3.3: Scaled Hill muscle parameters got from literature.....	41
Table 3.4: Hill muscle parameters get from literature. ....	61
Table 3.5: Distance between the joint centers of rotation and the connection between the muscles and the bones. The origin attach is intended as the distance between the connection of the origin side of the muscle with the bone, while the insertion attach is intended as the distance between the connection of the insertion side of the muscle with the bone (see Figure 3.1). ....	62
Table 3.6: VAF calculated if the stiffness ellipse major axis, the minor axis or the area are approximated as the product of the null space projection of the muscle activation for the regression slope, averaged among end-point positions. The regression is performed for those muscle activations whose activation of each muscles is lower than the selected value in the first column. ....	69
Table 4.1: The Borg RPE CR10 scale.....	82



# Chapter 1

## Introduction to exoskeletons

Even if the first prototypes of robotic exoskeleton appeared few decades ago (late 60s early 70s) a huge number of exoskeletons were developed in the recent years mostly for military or rehabilitation purpose.

Despite the on-going trend in automation and mechanization in industry, 26% of Italian workers reported their work involved carrying or moving heavy loads for at least 25% of the working time, 54% reported their work involves a repetitive hand or arm movement for at least 25% of the working time, and 42% experience tiring or painful position for at least 25% of the working time (EWCS, 2015).

A full-automation would solve all these problems, but in many cases it is not feasible. If, for example, high product mix with a relatively small order size is required, like in the dynamic manufacturing or warehousing environments, a full-automation would be too expensive or even impossible. Furthermore, in this context the observation capacity of the human, together with his ability to decide and adopt the proper action in few seconds, is still required. For this reason coupling a robotic device (i.e. an exoskeleton) with a human operator, might represent an interesting solution (Cavallaro, Rosen, Perry, & Burns, 2006), especially with the increasing of the working age in the industrial field, and the consequent higher percentage of diseased employees whose limitations does not allow them to work on the line.

Therefore, recently the manufacturing field is showing a growing interest for the introduction of exoskeletons in the industrial practice. However, the different acceptance the industrial workers have, lead the application of exoskeleton in the

industrial field to have completely different specifications with respect to the exoskeletons developed for military or rehabilitation field. Since the most common limitations, due to pathologies related with the manufacturing work, regard the wrist, the shoulder, and the elbow, in this thesis, only the upper-limb exoskeleton with industrial applications were considered. In particular, in this thesis, a novel approach was proposed for those exoskeletons whose aim is the modulation of the operator stiffness. Even if this approach was proposed for exoskeletons developed for industrial applications, it could be implemented also in exoskeletons developed for other applications, like exoskeletons for neuro-rehabilitation, prosthesis or tele-operated robots.

The definition and characterizations of exoskeletons are presented together with the limitations of its introduction in the industrial practice, in terms of operator acceptance, actual beneficial effects of its use, and standards regulating the human machine interface in the industrial field. Then, a design of the control logic, based on musculo-tendon models and experimental test, is proposed together with the main characteristics of the exoskeleton components and design.

## **1.1 Exoskeleton definition and generations**

The term ‘exoskeleton’ is taken from the biology, and it identifies an outer cover that shields a creature, enhances its power and allows a sensing and data fusion. An example of a biological exoskeleton is the shell of a crab whose purpose is not the only defense of the body, but it serves also as a surface for muscle connection, a waterproof wall against dehydration, and a sensory interface with the surroundings too (Gopura et al., 2011).

Despite the large number of exoskeleton concepts developed in the last years and their wide application, the definition of ‘exoskeleton’ is still debated (Rosen, Brand, Fuchs, & Arcan, 2001).

The authors of (Rosen et al., 2001) define an exoskeleton as “an external structural mechanism whose joints correspond to those of the human body. It is worn by the human and the physical contact between the operator and the exoskeleton allows direct transfer of mechanical power and information signals”. This implies that a structure, whose joints do not correspond to those of human body, can not be called an exoskeleton, even if it allows information sharing between the operator and the exoskeleton. The authors of (Pratt et al., 2004) extend

the definition to any device, that an user can wear or drive, which permits the user's natural motion and whose interface transmits information both ways from user to machine. The authors of (Rocon et al., 2007) identify the principal exoskeleton characteristics. It is, in the robotic perspective, a wearable robot, a mechatronic system designed to match the shape and functions of the human body, worn by a person in such a way that the physical interface permits a direct transfer of information and mechanical power.

Beyond the differences, the characteristics of exoskeletons all the studies identify are the wearability and the direct human-robot interaction, which implies the flow of information/power both from the robot to the human and from the human to the robot. The transmission of the information from the robot to the human is a result of the intrinsic characteristics of the exoskeleton. The exchange is both cognitive (exoskeleton gives feedback to the operator) and biomechanical (exoskeleton applies controlled forces on the operator) (Rocon et al., 2007). The transmission of the information from the human to the robot, i.e. the control exerted by the user on the machine, can be performed in different ways and defines the exoskeleton generation. Three generations were identified by (Rosen et al., 2001): the user controls the exoskeleton (1) with his/her kinematics, (2) in a dynamic way, and (3) with his neuromuscular signals, recorded with electromyography (EMG). A fourth generation, in which the exoskeleton was controlled by the electrical signal acquired directly from the brain, was identified by (Cavallaro et al., 2006).

(1) First-generation exoskeletons are used to assist human locomotion and to apply a set of predefined joint angle trajectories. An example of a position-based control exoskeleton is the Hardiman (Makinson, 1971) (Figure 1.1), developed for military purposes, which enhances the operator performance.



Figure 1.1: Example of first generation exoskeleton. The Hardiman

(2) In exoskeletons of the second generation, two control strategies are commonly applied (Young & Ferris, 2016). The first involves an open-loop control such that a pre-specified force or torque value is applied based on the position (e.g. the portion of the gait cycle for lower limb exoskeletons). The second strategy consists of a control proportional to the force/torque exchanged between the user and the exoskeleton. Examples are BLEEX (Zoss, Kazerooni, & Chu, 2006) (Figure 1.2A) for load carrying and ALEX (Banala et al. , 2009) (Figure 1.2B) and ARMin (Nef et al. , 2007) (Figure 1.2C) for rehabilitation.

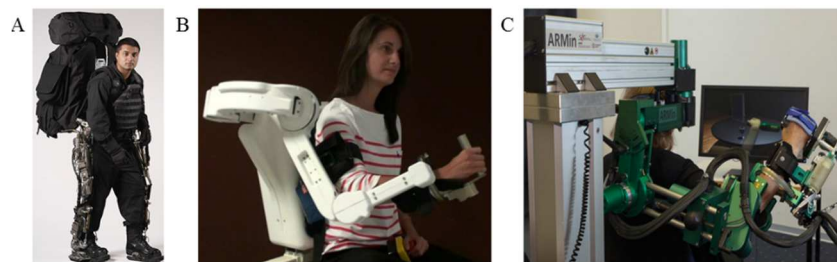


Figure 1.2: Examples of exoskeletons of the second generation. A: The BLEEX. B: ALEX. C: ARMin

(3) An exoskeleton of the third generation was first developed for the upper limb by (Rosen et al., 2001) (Figure 1.3A). Driving the exoskeleton using an EMG signal leads to a movement that feels more natural to the user since it is not necessary to exert an action on the exoskeleton. As a matter of fact, EMG signals appear approximately 20–80 ms prior to the muscles contracting mechanically (Zhou et al., 1995), thus allowing a signal evaluation before the motion. EMG-based exoskeleton was develop for the upper limb (Cavallaro et al., 2006; Kiguchi, Tet al, 2004; Rosen et al., 2001) (Figure 1.3B), for the lower limb (Fleischer & Hommel, 2008; S. Lee & Sankai, 2002) (Figure 1.3C, D), and also for the hand (Lucas et al., 2004; Mulas et al., 2005) (Figure 1.3E, F).

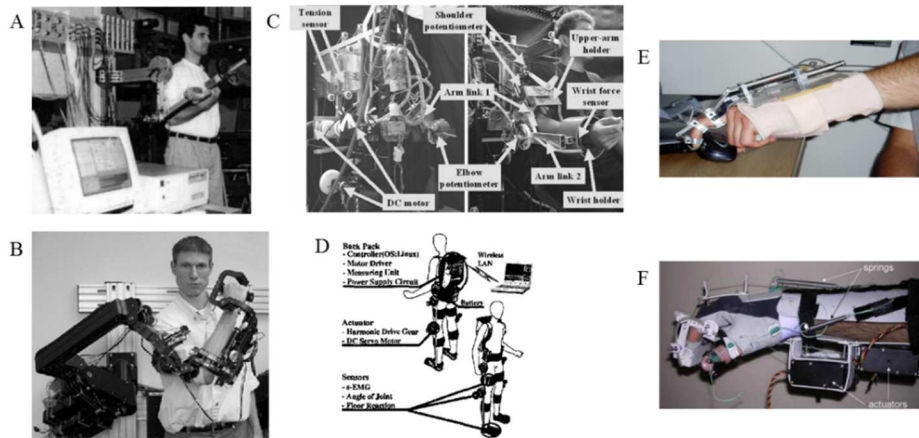


Figure 1.3: Examples of exoskeletons of the third generation. A: Exoskeleton described in (Rosen et al., 2001); B: Exoskeleton described in (Cavallaro et al., 2006); C: Exoskeleton described in (Fleischer & Hommel, 2008); D: Exoskeleton described in (S. Lee & Sankai, 2002); E: Exoskeleton described in (Lucas et al., 2004); F: Exoskeleton described in (Mulas et al., 2005).

(4) In the fourth generation exoskeletons, the device get the signal directly from the brain with non-invasive electroencephalogram or with invasive action measuring directly from the motor cortex. Recently brain-controlled exoskeletons were developed for upper limb (Bhagat et al., 2016; McDaid et al., 2013) (Figure 1.4A), lower limb (Contreras-Vidal & Grossman, 2013; Kilicarslan et al., 2013; S. Wang et al., 2015) (Figure 1.4B,C, D), and hand (Soekadar et al., 2015) (Figure 1.4E). However, by the best of the author knowledge, at present this kind of exoskeletons are solely research devices.

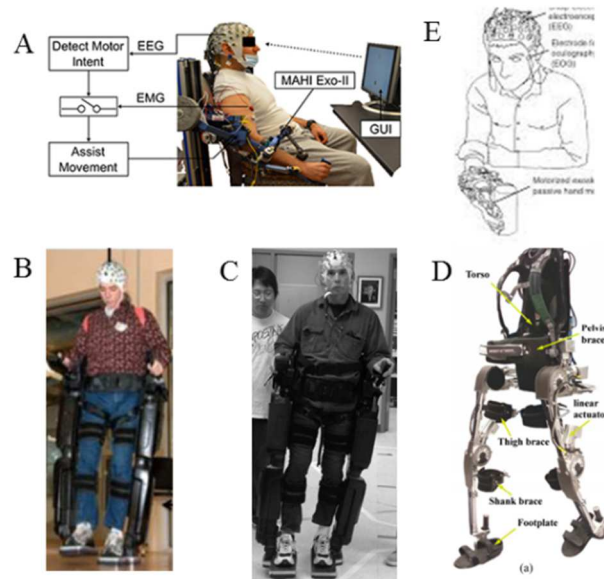


Figure 1.4: Examples of exoskeletons of the fourth generation. A: Exoskeleton described in (Bhagat et al., 2016); B: Exoskeleton described in (Contreras-Vidal & Grossman, 2013); C: Exoskeleton described in (Kilicarslan et al., 2013); D: Exoskeleton described in (S. Wang et al., 2015); E: Exoskeleton described in (Soekadar et al., 2015).

## 1.2 Fields of use of exoskeletons

Exoskeletons are widely applied in different fields. Then, they can be classified according to their field of use (van NINHUIJS et al., 2013).

**Military.** Introducing an exoskeleton on the battlefield that both protects and enhance the performance of his soldier-operator, without reducing his mobility, is a long standing idea. It's not by chance that the first exoskeleton prototype, called Hardiman (Figure 1.5A), was developed for military purposes (Makinson, 1971). Even if this first attempt to build a 'super-soldier' was not completed, due to the weight of its material, more recent exoskeletons were developed for the same purpose. Some examples are the HULC (Human Universal Load Carrier) (Figure 1.5B) and the BLEEX (Figure 1.5C) (Berkeley lower extremity exoskeleton) (Zoss et al, 2006), both developed by the Berkeley Bionics (now called Ekso Bionics), and the Hercule (Figure 1.5D), developed for the French army, with a similar design to the HULC. A novel exoskeleton for the military purpose is Talos (Tactical Assault Light Operator Suit) (Figure 1.5E) that permits the augmentation of the load carrying and incorporates other functions like the termo-regulation and the measurement of the vital functions of the operator (Scataglini et al., 2015).



Figure 1.5: Examples of exoskeletons for military purpose. A: Hardiman. B: HULC. C: BLEEX. D: Hercule. E: Talos.

**Clinical.** While the primary aim of military exoskeletons is to impart increased strength and agility to the user, clinical robotic exoskeletons are being developed in response to other factors: to assist patient rehabilitation following injury and to enhance the mobility or dexterity of the world's aging population (Bogue, 2009). So far, the major number of exoskeletons were developed for rehabilitation and clinical applications (de Looze et al., 2016).

For what concerns the rehabilitation of patients, it was demonstrated that the action of a physiotherapist has positive effects in learning new motor strategy, needed to dare with the disease and give more freedom to the patient (Poulin et al., 2017; Teasell & Kalra, 2004). However, traditional therapies are expensive and the physiotherapist can work with only one patient at a time. The introduction of robotic devices for the rehabilitation would help patients during physiotherapy (Belforte et al., 1997; Nef et al., 2007; Sacco et al., 2011; Veneman et al., 2007) reducing the costs and allowing a more long-term and intense therapy. Moreover robotic devices consent an objective evaluation of the patient disability, the evolution of his/her disease, and the effectiveness of the chosen therapy (Sanger et al., 1994). Positive effects were also detected if the therapy was conducted at home (Holmqvist et al., 2000), then recent studies proposed the tele-rehabilitation using robotic devices (Johnson & Feng, 2007). Advantages of the tele-rehabilitation (Reinkensmeyer et

al., 2002), could be found both in terms of effectiveness of the rehabilitation and in physiotherapist timesaving, because the robotic device could be remotely controlled.

Those exoskeletons, developed to enhance or completely supply the power exerted by patients, like elderly or patients with neuromuscular diseases, would allow their users to gain more freedom in terms of mobility and possibility to execute more daily life tasks. For this reason different groups proposed their devices (Cavallaro et al., 2006; Lee & Sankai, 2002; Pratt et al., 2004) some of which were commercialized. One of the most famous commercial whole body exoskeleton developed for rehabilitation is HAL (Hibrid Assistive Limb) (Lee & Sankai, 2002) (Figure 1.7A), produced by the Cyberdyne Inc.

Enhancing the locomotion independence is the most common purposes of rehabilitation exoskeletons. Then, a huge number of lower limb exoskeletons were developed. While the Honda Motor Company developed different walking assisting device (Figure 1.7B), the Argo Medical Technologies and the Berkeley Bionics have developed two robotic ambulation systems for wheelchair users, respectively the ReWalk (Figure 1.7C) and the “Exoskeleton Orthotic Systems for Individuals with Mobility Disorder” (Figure 1.7D), that represent upright alternatives and improvements of the quality of life for wheelchair users.

Other exoskeleton were developed for the rehabilitation of the upper limb, like the ArmIn (Nef et al., 2007) (Figure 1.7E) and the ABLE (Garrec et al., 2008) (Figure 1.7F), and for the rehabilitation of the hand, like the KMI Hand Mentor (Figure 1.7G).

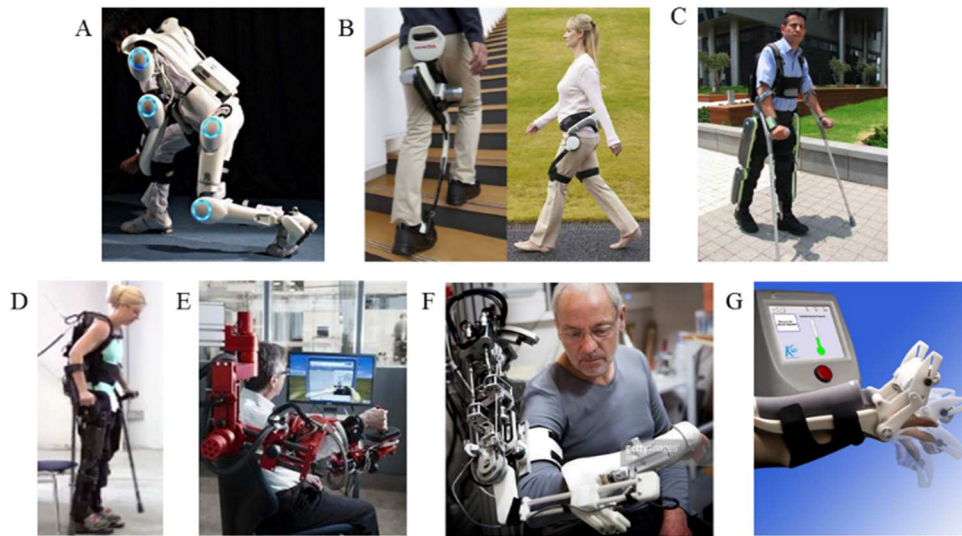


Figure 1.6: Examples of commercial exoskeletons for rehabilitation purpose. A: Hal. B: Honda Motor Company exoskeletons. C: ReWalk. D: RcsO Bionics rehabilitation exoskeleton. E: ArmIn. F: ABLE. G: KMI Hand Mentor.

**Industry.** The industrial field was not addressed by the initial prototypes of exoskeleton. However, the aging of the population and the diseases due to the factory jobs lead to the development of manufacturing exoskeletons whose introduction in the industrial practice would lead to beneficial effects both in reducing fatigue and possible diseases in all workers and in enhancing the force of those workers, like the older ones, whose force is reduced. Beneficial effects in terms of reduced fatigue and enhanced comfort were also demonstrated (see Paragraph 1.1.3) then different groups developed exoskeletons for industrial purposes (Spada et al., 2017; Vorm et al., 2015).

Both active and passive exoskeletons were developed for industrial applications. The active exoskeleton comprises one or more actuators that augments the human power and helps in actuating human joints, while a strictly passive system does not use any type of actuator but rather uses springs, dampers or other materials with the ability to store energy. Due to the legal restrictions in the industrial applications in terms of interaction between human and robots (see Paragraph 1.1.4), the few commercialized upper-body exoskeletons for industrial applications are passive (i.e. not actuated). Their purpose is the balancing of the limb weight performed with a system of springs. Some examples are the X-Ar (Figure 1.7A), developed by Equipois, the Exhaust stronger exoskeleton (Figure 1.7B), which both support the worker's forearm, and the shoulder exoskeleton developed by Levitate technologies (Figure 1.7C). Passive exoskeletons are

developed also for operator's trunk support. Some examples are the PLAD (Figure 1.7D) (Personal Lift Assistive Device), the BNDR (Bending Non-Demand Return), and the Laevo (Figure 1.7E), which supports the operator's trunk. Nevertheless, the positive effects expected by the introduction of active exoskeletons in the manufacturing field leads the Panasonic to develop an actuated exoskeleton specifically for the industrial application, the Power Loader (Figure 1.7F), and the Innophys to develop the Muscle Suit (Figure 1.7G), a powered back support exoskeleton for lifting (Muramatsu et al., 2011). Another industrial application is the Chairless Chair (Figure 1.7H), a lower limb exoskeleton which allows the user to sit whenever and wherever he wants. Some other passive wearable devices, developed for industrial purposes are Zero-G (Figure 1.7I), developed by Equipois, and Fortis (Figure 1.7L), developed by the Lockheed Martin, whose purpose is the support of heavy tools. However, these last two devices may not be properly defined exoskeleton because the joints of the device does not correspond to the operator joints. For an overview of assistive exoskeletons that have specifically been developed for industrial purposes, see (de Looze et al., 2016).



Figure 1.7: Examples of exoskeletons and robotic devices for the industrial field. A: X-Ar. B: Exhaus stronger exoskeleton. C: Exoskeleton developed by Levitate technologies. D: PLAD. E: Laevo. F: Power Loader. G: Muscle Suit. H: Chairless chair. I: Zero-G. L: Fortis.

**Other applications.** Exoskeletons were proposed as supports for agricultural workers during load lifting or a stooping posture (Yagi et al., 2009). The Tokyo University of Agriculture and Technology developed an exoskeleton that is intended to assist less-able farmers with physically demanding tasks such as uprooting crops, tilling the soil and pruning trees (Figure 1.8A). Other exoskeletons were designed for stooped works, like the BNDR, the Happyback (Figure 1.8B) and the Bendezy. For a review see (de Looze et al., 2016). The HAL exoskeleton (Lee & Sankai, 2002) was used to assist nurses in moving patients and a recent development, improved with a suit which protects from radiations, was used by the workers dismantling the crippled Fukushima nuclear plant.

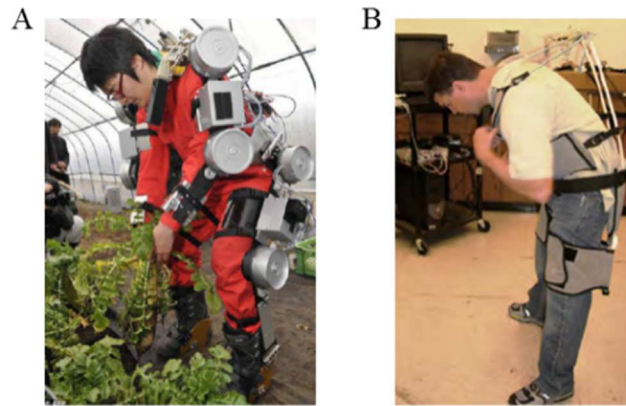


Figure 1.8: Examples of exoskeletons for agricultural purposes. A. The exoskeleton developed at the Tokyo University of Agriculture and Technology. B. The Happy back.

### 1.3 Potential effects of industrial exoskeletons on workers

Consequently, in the last years, different groups investigated the advantages and disadvantages in introducing exoskeleton in the industrial practice. The authors of (de Looze et al., 2016) identified 26 exoskeletons that were developed for industrial purposes (19 active and 7 passive). However, some evaluations of the physical load reductions were performed for only 13 out of the 26 identified.

Several papers analyzed the effects on the operator of the PLAD (Personal Lift Assistive Device), a passive exoskeleton in which elastic elements are situated in parallel to the erector spinae muscles such to permit a load sharing between spine, shoulder, pelvis and lower extremities. The PLAD has been proven to reduce the average peak compressive and shear forces at the lumbar joint during different lifting tasks (Abdoli-Eramaki et al., 2007). The PLAD was also demonstrated to reduce the required muscular effort of the lumbar and thoracic erector spinae muscles during different lifting postures of different weights (Abdoli-Eramaki et al., 2006) and also during asymmetrical lifts (Abdoli-Eramaki & Stevenson, 2008), and it was effective at decreasing the onset and level of back muscular fatigue (Godwin et al., 2009; Lotz et al., 2009). However, not all the operator's muscles were recorded, then the authors of (Frost et al., 2009) questioned whether a decrease of back muscle activity may be accompanied with an increase of the activity of other unrecorded muscles, e.g. the muscles of the legs. This observation was

confirmed by the authors of (Whitfield et al., 2014) who demonstrated that wearing the PLAD does not alter the oxygen consumption, i.e. the total energy that the job demands. Therefore, the PLAD could be concluded to have beneficial effects in term of reducing back muscle activity, but disadvantageous effects on other unrecorded muscles.

A reduction of the muscle activity was reported also during lifting activity for those subjects who were wearing the BNDR (Bending Non-Demand Return), a passive exoskeleton in parallel to the erector spinae muscles, (Toussaint et al., 1995). The BNDR was also observed to reduce torso flexion in stooped lifting (Ulrey & Fathallah, 2013b) and have positive effects on back muscles activity during static trunk bending and spinal loading (Ulrey & Fathallah, 2013a). However a significant increase in lower leg muscle activity is identified (Ulrey & Fathallah, 2013b). Then, the same consideration performed for the PLAD could be done: the BNDR has positive effects in the back muscles activity but enhances the activity of leg's muscles.

The authors of (de Looze et al., 2016) are concerned also about the discomfort associated with wearing passive devices and points out that even a minimal level of discomfort might hinder user's acceptance in the industrial practice. Then, even if some positive effects were observed in the operator who is wearing a passive exoskeleton (like the PLAD or the BNDR), the reported disadvantages may completely prevent its use in the industrial practice.

A recent paper (Theurel et al., 2018) tested the effect of the EXHAUSS stronger exoskeleton, a passive upper-limb exoskeleton, during different tasks (load lifting and lowering, load carrying, and box unstacking and stacking tasks). They noticed postural modifications when wearing the exoskeleton respect with not wearing it. They also noticed an increasing of the cardiac cost during the load-lifting task wearing the exoskeleton and a lengthening of the time required to complete the stacking task. The authors commented the absence of modifications of the task duration and cardiac cost during the load carrying task as a consequence of the upper-limb muscles relieve, exerted by the device, which balances the higher effort needed to carry the additional load of the exoskeleton (approximately 9 kg). However, an exaggerated extension of the arms was noticed during the load-carrying task with a consequent increase of the workload placed in the low back.

In conclusion, the use of passive trunk or upper-limb exoskeletons shows beneficial effects in terms of reducing the activity generated by those muscles that

acts on the limb the exoskeleton is relieving. On the contrary an increase of other muscles activity or postural modification usually vanishes these advantages making the use of passive exoskeleton useless or even negative.

Differently from the passive exoskeletons, the active ones may have larger potential of reducing the loads on many joints throughout the body, due to the action exerted by the active actuators (de Looze et al., 2016).

The authors of (Sylla et al., 2014) tested the effects of wearing the ABLE, an active upper limb exoskeleton (Garrec et al., 2008), in eight subjects who were asked to simulate a drilling task on a surface 2 m high on the floor. They demonstrated a clear reduction of the mechanical energy, intended as the sum of the joint torques, slightly differences between joint angles trajectories, significant modifications of the postural strategy and an increase of the cycle time when using the ABLE exoskeleton. Therefore, they assessed the beneficial effects, in terms of enhanced comfort, the ABLE would have. However, they concerned about the asymmetry in the recorded ground reaction forces, which may be due to the subjects not instructed on how the exoskeleton should be used. This asymmetry might be harmful and lead to postural problems in case of extensive use of the system.

The authors of (Muramatsu et al., 2011) identified that the use of the Muscle Suit, an active exoskeleton of upper limb, led to positive effects on a large number of muscles in the upper extremities during the static holding, dynamic lifting, and holding a weight over the head tasks. However, this exoskeleton unloads its weight on the legs, with a consequent, non-recorded, increase in the leg muscles activity, fatigue and maybe injury occurrence.

Besides the positive effects reported in the literature, the authors of (de Looze et al., 2016) were concerned about the number of exoskeleton joints, each with its actuator and power supply, that will increase the weight. Therefore, additional elements, that will increase the complexity of the design, are required to unload the worker from this constant weight, a shrewdness presents not in all exoskeletons. Therefore, some of the future challenges in the industrial exoskeleton are the reduction of the weight and the investigation on the activation of the leg muscles during a task with and without an exoskeleton, to assess an effective reduction in the overall muscle activation. On the other side, the authors of (Spada et al., 2018) wonder whether the potential benefit of an active exoskeleton, in term of lessen muscle strain, higher comfort rating and dexterity, may compensate the possible

restrictions to movements and work-device interactions in tasks resembling work activities.

## **1.4 Standards and current legislation on collaborative robotics**

Besides the environment around the fourth industrial revolution, also called Industry 4.0 (Lasi et al., 2014), and the consequent proposal about the introduction of exoskeletons in the industrial practice (Munoz, 2017) to achieve human-automation symbiosis work systems related to the Operator 4.0 (Romero et al., 2016), a significant barrier to their use, to date, is the lack of international safety standards for their industrial application. While the ISO 13482 governs exoskeletons used in the context of robot personal care, the standards that governs exoskeletons used in the industrial field are the ones related to robotic devices for collaborative operations.

The concept of collaborative operation was firstly introduced by ISO 10218-1. A collaborative operation happens when purposely designed robots work in direct cooperation with a human within a defined workspace. The collaborative operations are defined by the task, which is what the robot system, composed of the robot device, the end-effector and all its parts, is doing, and the space in which the task is being performed.

Some solutions for securing the area shared between humans and robots were developed and the European standard agencies, the CEN (European Committee for Standardization) and the CENELEC (European Committee for Electrotechnical Standardization), issued a set of standards to evaluate the risks of a specific machine and the related security systems needed to protect the operator. These standards, published on the Official Journal of the European Union, indicated the technical specification to satisfy the directives. Then, a manufacturer, who applies these standards for the certification of his machinery, is presumed to comply with the directives.

The CEN-CENELEC safety standards are classified in four types:

Type A standards deal with the basic concepts and the main general design of all machine standards.

Type B1 standards deal with some security aspects (security distances, temperature, noise etc.).

Type B2 standards deal with the security devices (bimanual controls, interlocking devices, etc.).

Type C standards deal with the safety requirements for particular machine groups (e.g. hydraulic presses, machines at injection).

Component or function safety standards (type B in CEN classification) used in industrial robots sometimes provide very conservative conditions, limiting the cooperation between the human operator and the machine. For example, the type B standard described in the ISO 13855, establishes the minimum distances respect with moving elements, independently from the velocities and the conditions in which they are operating. At the same time the type C standards, described in ISO 10218-2, identifies more flexible cooperative conditions only if these conditions are adequately dealt during all the stages of the risk assessment and the robotic systems are equipped with some technologies to detect a security systems failure (according to ISO 13489). Then, the standards adopted until 2016 completely separated the robot from the operator, through the definition of the robot workspace, in which operators cannot enter if the robot is active, without allowing any possible contact between human and active robots.

In 2016 the previous guidelines of the ISO 10218-2 received a quantitative redefinition in the various modes through the technical specifications ISO/TS 15066, which is a document representing the technical consensus of the committee. Therefore, the ISO/TS 15066 is expected to become soon a standard. One of the major difference of the ISO/TS 15066 respect with the previous ISO 10218-2 regards the safeguarded work volume, which must be calculated a priori and loaded into the robot controller before the startup or during an acknowledge phase made by the operator, according to the ISO 10218-2. This implied that if the working conditions change, the system should be shut down and the new work volumes should be recalculated and reloaded in the robot controller. Due to these regulations, any parametric modification required the reboot of the security-related control system. Alternatively, all conditions must have been introduced a priori, irrespective of their timely invocation. Therefore, this constraint did not allow a real time elaboration of the safe work during the execution of the operations, but it

forced an excessively large safeguarded work volume, which did not allow a man to approach the machine, even in no real danger situations.

The technical specification defined in the ISO/TS 15066, provide four possible human-robot cooperative conditions:

1. Safety-rated Monitored Stop;
2. Hand-Guiding;
3. Speed and Separation Monitoring (SSM);
4. Power and Force Limiting (PFL).

In the **Safety-rated Monitored Stop** type, a stop would occur without the removal of the power when the operator is moving close to the robot, then both the operator and the robot can move in the same volume, but not at the same time. In this condition a direct interaction between the operator and the robot is allowed only if the safety-rated stop condition is active and this occurred before the operator enters in the robot workspace. The drive power remains on when the operator is interacting with the robot and the motion resumes only after the operator leaves the workspace.

In the **Hand-Guiding** condition the robot system is manually controlled by the operator, then both the operator and the robot can move at the same time. The robot needs to be hand-operated and to achieve a safety rated monitored stop, in which the power is on, before the operator enters in the collaborative workspace. The operator grasps the hand-operated device and activates the motion or the operation through an enabling device, which needs to be included too. Non-collaborative operation could be resumed only after the operator leaves the collaborative workspace.

In the **Speed and Separation Monitoring** type the robot system is controlled based on its separation respect with an intrusion. During the Speed and Separation Monitoring type both the operator and the robot can move at the same time, but the robot will slow down upon the human approach and it stops before the impact. In this case, a minimum protective separation distance between the operator and the robot is maintained at all times, but protective devices which determine the operator approach are needed. So far, the same function was already accomplished with external safety devices, like safety laser scanner or safe vision systems.

In the **Power and Force Limited** type, the robot speed, torque, and motion are controlled such that the impact will not hurt or injure the operator. In addition, in

this case both the operator and the robot could move at the same time. The risk assessment would determine the suitability. While the Speed and Separation Monitoring type is designed to avoid the impact between the operator and the robot, this type is designed to reduce the dangerous effect of the impact when it occurs. The contact between the operator and the robot could occur either intentionally or unintentionally, and then the robot needs to be specifically designed to limit the power and the force exerted. Hence, the force exerted by the robot, the end-effector and the handled piece needs to be limited. The robot needs to decrease the power during quasi-static pressures and during transient, or dynamic, actions.

In conclusion, even if specific standards regarding active exoskeletons for industrial purpose still do not exist, the ISO/TS 15066 opens new possibilities in the interaction and collaboration between the human and the robot. Since an exoskeleton could be intended as a hand guided robotic device, the first step towards the introduction of exoskeletons in the industrial practice has occurred. However, still a lot of work is needed before the plenty introduction of exoskeletons in the industrial practice.

## **1.5 Exoskeletons with variable impedance**

During manufactory works, workers interact with environment and a huge number of tools. Sometimes these interactions are instable or high precision is needed, then operators are required increasing their limb impedance. In these operations, the action of an exoskeleton that increases the operator force, may not be required, and it could also be harmful, in particular for high precision operations. On the contrary, an exoskeleton that increases the operator stiffness may represents a better aid. Therefore, even if a large number of exoskeletons that increase the power exerted by the operator were developed so far, considerably less attention was given to exoskeletons that increase operator's stiffness. Even if passive exoskeletons that increase the power exerted by the operator were largely developed, by the best of our knowledge, no passive exoskeletons that modulates their stiffness, based on operator stiffness, in real time were developed. Therefore, in this thesis, active exoskeletons, which act on the upper limb and whose stiffness could be modulated, were studied.

### **1.5.1 Arm impedance**

It is known that limb impedance is achieved co-activating muscles (Hogan, 1984a; Milner, 2002; Milner & Cloutier, 1993) and a huge literature characterizes arm impedance, in term of inertia, damping, and stiffness, during both dynamic tasks (Burdet et al., 2001; Flash, 1987; Franklin et al., 2003; Gribble et al., 2003; Latash, 1992; Wang et al., 2001) and isometric tasks (Artemiadis et al., 2010; Darainy et al., 2004; McIntyre et al., 1996; Perreault, 2002; Shadmehr, 1993).

End-point stiffness is defined as the relationship between externally applied displacements of the hand and the forces generated in response (Hogan, 1984b; Yoshikawa, 1985). End-point stiffness is non-isotropic and can be graphically represented as an ellipse (Mussa-Ivaldi, Hogan, & Bizzi, 1985). The joints stiffness, and consequently the end-point stiffness, depends on the physiological characteristics of the muscles that acts on the joint, on their activation and contraction velocity, and on the joints angle. The muscle patterns that modulate stiffness were also studied both during dynamic (Gribble et al., 2003; Osu et al., 2004) and isometric tasks (Gomi & Osu, 1998; Osu & Gomi, 1999).

### **1.5.2 The real-time impedance control in robotic manipulators**

The ‘impedance control’ identifies an approach, firstly introduced by (Hogan, 1984b), which facilitates stable robot interactions with the environment by replicating soft and passive contacts. The impedance control was mainly applied to reduce the effects of the impact of the robotic manipulator, or one of its elements, with other objects or with humans (Anderson & Spong, 1988; He et al., 2016). The impedance control approach is expected to receive also more attention by the industrial robot designers consequently the definition of the technical specification ISO/TS 15066, which allows cooperative works between humans and robots in the industrial field if ‘Power and Force Limiting’ are implemented (see paragraph 1.4).

However, a unique a-priori definition of the impedance modulation is not enough because if the robotic device is requested to have unknown interactions with the environment, a quick, case-specific impedance modulation is required. Consequently, in the last years, different groups developed robotic devices whose impedance could be real-time modulated based on the impedance of a human operator. The operator impedance was estimated from the EMG signal collected from his muscles. This approach, called tele-impedance (teleoperation with impedance regulation) was firstly developed by the authors of (Ajoudani et al.,

2012), who calculated the operator's limb impedance from the recorded EMG signal and consequently controlled the impedance of an external robot device. The advantages of the tele-impedance is the simple natural control interface, the low cost of sensing EMG signals, and the transparent human-robot interface, avoiding feedback delay. However, a subject-specific and session-specific calibration is required and the noise in the EMG electrode, due to skin-electrode interface, interaction with the electricity frequency, movement artifact, involuntary electrode detachment, cross-talk with other muscles may make the usage of these devices reserved to EMG experts only. Devices based on tele-impedance or similar impedance controls, were developed also by different groups. The authors of (Liang et al., 2014) implemented a robot whose end-point position was commanded with the user position and the impedance was calculated from the EMG signal recorded from the user. The authors of (Ison & Artemiadis, 2015) developed a control of the impedance of a robot based on EMG signal of an operator and tested both isotropic impedance (the same displacement led to the same force independently on the direction of the displacement) and non-isotropic impedance (the same displacement led to different forces depending on the direction of the displacement). The authors of (Smith et al., 2015) developed a robot with a biomimetic control of the stiffness, based on the stiffness of the operator's muscles. This robot presented stable behavior in unstable dynamics with a reduced control effort.

Real-time impedance control, based on EMG signals, was also developed for the modulation of the stiffness of non-industrial devices, in particular it was implemented in upper limb (Blank et al., 2014) and hand (Hocaoglu & Patoglu, 2012) prosthesis.

### **1.5.3 Exoskeletons and impedance**

In the early prototypes the joint impedance obliges the operator to enhance the force he needs to perform a movement. Therefore, its reduction was one of the priority in the exoskeletons design (Pratt et al., 2004). However, in the last years, a trend in developing rehabilitation exoskeletons with variable impedance can be identified in literature. Impedance control in exoskeletons was implemented for rehabilitation purpose to drive the patient during the rehabilitation session, to reduce hand tremor (Rocon et al., 2007) or to reduce the working employment of the therapist on each patient (Peattie et al., 2009; Van Der Kooij et al., 2006; Veneman et al., 2007). The modulation of the joint stiffness was also tested to reduce the angular error of the

subject arm when moving along a reference trajectory. This kind of control, in which the patient/operator has a sensorimotor feedback of the impedance modulation, is called ‘virtual impedance’ (Lee & Sankai, 2005). The authors of (Karavas & Ajoudani, 2013) developed a knee exoskeleton whose stiffness was directly controlled with recorded EMG signal. The authors of (Mghames et al., 2017) implemented a simple model of two antagonist muscles to control the movement, the force exertion and the impedance of an elbow exoskeleton.

However, even if these exoskeletons allowed the modulation of the impedance, they could not be applied in the industrial field, to help workers in reducing the effort they made to stiffen their limb. In fact, the pattern of the impedance of some of the described exoskeleton was set a-priori, with the consequent loss of the advantages deriving from the human operator flexibility. Consequently, only a tele-impedance logic can be implemented on exoskeletons developed for the industrial practice. Rehabilitation exoskeletons is not suitable for industrial application per se. On the other side, recording a reduced number of muscles, as performed by the authors of (Mghames et al., 2017), would led to a drastic reduction in the flexibility achieved by humans, with a consequent limitation in the industrial applicability.

In conclusion, by the best of the author knowledge, no exoskeleton whose impedance could be modulated in real-time based on the EMG signal of the operator, was developed so far for upper-limb, such to allow its introduction in the industrial practice. Consequently, the purpose of this thesis is to propose a concept of an exoskeleton, which would aid the operator during those industrial manipulations in which an impedance modulation is required, without reducing the human natural flexibility. However, the proposed impedance modulation logic is not specific for industrial applications, but it could be implemented also in exoskeletons developed for neurorehabilitation or other robotic devices, like prosthesis or surgery robots.

## Chapter 2

# Exoskeleton concept

### 2.1 Machining classification

Humans possess naturally developed algorithms for control of movement that allows a huge flexibility in achieving tasks. However, the muscle strength limits the forces a human could exert. In addition, muscle strength may decrease with aging, fatigue, or neuromuscular diseases. By contrast, robotic manipulators can perform tasks requiring high forces, but their control algorithms do not provide the flexibility and quality of performance naturally achieved by humans. For this reason, interfacing a human operator with a robotic device would benefit both the human and robotic elements. Exoskeleton are robotic devices that combine the human precision and the robot force.

The growing interest for the introduction of exoskeleton in the industrial practice, led different groups to develop different designs for power enhancing. However, workers may need to perform machining that requires instable interactions with tools. Consequently, an exoskeleton with variable stiffness may have beneficial effects in terms of worker's injury reduction and industry productivity. The machining the variable stiffness exoskeleton is required to perform, could be classified in different ways (Daniele Borzelli, Pastorelli, & Gastaldi, 2017b), mainly based on the task the operator needs to perform and on the perturbation properties.

A classification based on the required task leads to the identification of two main groups:

- **Isometric operations:** the operator is asked to use the device to exert a force. The small shifting or rotations that may occur are along or around the direction of the applied force. The operator could easily support the requested force for the whole duration of the operation, then a force amplification is not needed and

the major contribution of the muscles is in stiffening the joint rather than in exerting a force.

- **Dynamic operations:** the operator is asked to move the device in the space. Small forces may occur along the direction of the movement and are commonly needed to handle the device itself.

Many operations in the industrial practice, in which a joint stiffening is required, can be described as a combination of isometric and dynamic tasks. However, even if during some operations a motion of the device exerting a force is required, usually the limb stiffening compensates instabilities derived from one of the two operations. If we analyze, for example, the use of a screwdriver when the screw is still not guided by the hole (see Figure 2.1), the instability derives from the force exerted by the operator that could be not perfectly coaxial with the screw axis. Then, the use of a screwdriver implies an increase of the arm stiffness to compensate instabilities due to the isometric task, even if a wrist rotation and a shifting of the device (i.e. a dynamic operation) does occur.

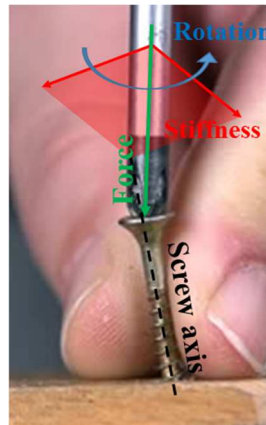


Figure 2.1: Example of the actions exerted during the use of a screwdriver. The operator needs to exert a force (green arrow) and a torque (blue arrow). If the screw axis (black dotted line) is not aligned with the exerted force, the operator needs to increase the stiffness along the directions orthogonal to the force (red arrows and plane) such to avoid the screwdriver to lose contact with the screw.

The separation between isometric and dynamic is not just a classification based on the mechanical properties of the machining but it looks to be a physiological separation implemented in the Central Nervous System, which modifies its motor strategy depending on the task. In fact, although during dynamic tasks the stiffness ellipse aligns with the direction of the instability, as observed for ball-catching

(Lacquaniti, Carrozzo, & Borghese, 1993) and a pointing tasks (Hiroaki Gomi & Kawato, 1996), only small rotations were observed in the end-point stiffness ellipse during isometric tasks (E. J. Perreault, Kirsch, & Crago, 2002; Selen, Franklin, & Wolpert, 2009). Then, different tasks led to different motor behaviors performed by the operator.

A classification of the operations based on the perturbation properties led to the identification of two main groups:

- **Continuous instability:** the displacement that causes the instability persists in time. The operator enhance his arm stiffness because of the sensorimotor feedback of the instability. Different effects may generate the instability: the device itself (e.g., rotational elements of the device's engine), the interaction of the device with another object (e.g., vibration owing to a drilling action), the environment in which the device is used (e.g., a windy environment), the operator's working conditions (e.g., a moving platform), or the operator's physiological tremors (e.g., fatigue).

- **Spiky instability:** the displacement that cause the instability consists in one or more non-periodic short-term perturbations. Then the operator cannot compensate the instability due to its sensorimotor feedback, because the time delay between the feedback and the stiffness increase would lead the system to an imbalance. The operator dares with this kind of instabilities with a preventive enhancing of the joint stiffness based on his experience of the perturbation that may occurs. This behavior identifies a feedforward mechanism implemented in the Central Nervous System (Burdet et al., 2001; Franklin et al., 2003). The effects that generate this behavior may happen: when the work material is non-homogeneous (e.g., ribs on wood), the environment or the tool the operator is using may exert undesired actions (e.g., a drill press may make the object to be drilled escape from the operator's hand), some actions may lead to unstable configurations (e.g., the exertion of a force with a screwdriver non-orthogonal to the plane), or for security reasons (e.g., managing dangerous substances or devices whose incorrect use may lead to injuries). Also the perturbation related to deflective force fields could be ascribed to this category, because the operator has a sensorimotor feedback of the instability only after trajectory deflections, then an a-priori arm stiffening does occur (Burdet et al., 2001).

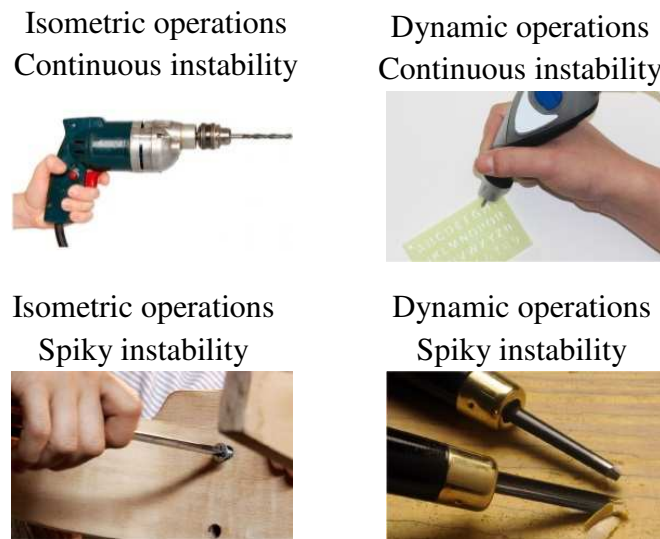


Figure 2.2: Iconic machining of different tasks.

The coupling of the identified classifications based on the task and on the perturbation leads to the identification of different tasks in which the exoskeleton could operate. An iconic machining was identified for each group (see Figure 2.2):

- **Isometric task, continuous instability:** the use of a drill at the initial contact with the plane. The exerted force is needed to start the hole while the instability is generated by the rotation of the drill's motor internal elements. Stiffness modulation is required to reduce vibration generated by the drill's motor.

- **Dynamic task, continuous instability:** engraving a plane with an electric tool. A movement is required and the instability is generated by the rotation of the engraver's motor internal elements. The exerted small forces are required to move the device. Stiffness modulation is required to reduce vibration generated by the engraver's motor.

- **Isometric task, spiky instability:** the use of a screwdriver (when the screw is still not guided by the hole in the plane). The force is required to start the screwing. The instability is due to the coupling between the screw and the plane and it occurs if the exerted force is not orthogonal to the plane. The operator stiffens the arm to prevent deflections due to the exertion of a force non-orthogonal to the plane.

- **Dynamic task, spiky instability:** engraving a plane by hand. A movement is required and the instability derives from the dis-homogeneities of the material of

the plane to be engraved, that the worker predicts by his experience. The exerted small forces, which are needed to be precisely tuned depending on the worker intentions, are required to move the device. Stiffness modulation is required to reduce the effects the inhomogeneity would have

The directions of the stiffening are usually orthogonal to the direction of the force or of the movement (see Figure 2.1). Then, the system needs to select the direction respect with it is necessary to increase the stiffness, while reducing the stiffness along the other directions.

## **2.2 Human-Exoskeleton interface functional blocks**

The development of an exoskeleton, whose purpose is not only the enhancing of the operator's power but also the exertion of stiffness, requires the knowledge of the operator's impedance. Unfortunately, while force transducer's allows the online calculation of operator's end-point force, the mechanical calculation of the end-point stiffness is feasible only after the application of a perturbation, a measure that is not feasible during industrial operations.

Therefore, other means to estimate the operator's end-point stiffness are required, like the one based on the Electromyographic (EMG) signal. Therefore, the knowledge of the action shared between the human operator and the robotic device are needed.

A diagram block of a human-machine interaction between a human operator and an upper limb exoskeleton of the third generation (see Paragraph 1.2), which enhances both the operator stiffness and force, is reported in Figure 2.3. The human and the exoskeleton are considered as two separate entities and the operator controls the robot by the activation of his muscles (i.e. with the EMG signal) and his arm configuration. In the following paragraphs, each block of the presented diagram is described.

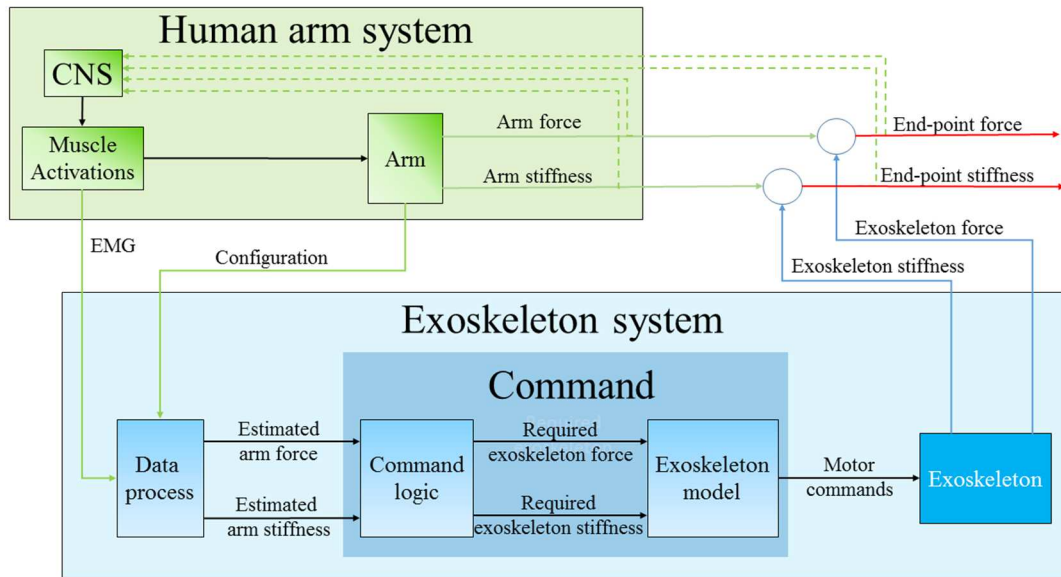


Figure 2.3: Concept of human-exoskeleton interaction.

### 2.2.1 The ‘Human arm system’ block

The ‘Human arm system’ block represents the operator’s arm system and the control laws naturally exploited during a movement.

The ‘CNS’ block represents the computational process and the control laws implemented in the Central Nervous System. The Central Nervous System records the sensorimotor information from the sensory organs, calculates the muscle patterns required to perform the task and sends electrical impulses via the moto-neurons to activate the muscles. The control strategies naturally implemented in the Central Nervous System are still debated (Kutch & Valero-Cuevas, 2012; Tresch & Jarc, 2009). Furthermore, a huge number of parameters, like the learning process, which modifies the muscular behavior in trained subjects (Burdet et al., 2001; Osu et al., 2002; Thoroughman & Shadmehr, 1999), the muscular fatigue, that alternates the recruitment of agonist muscles (Gandevia, 2001; Merletti & Farina, 2016), the muscle pain, that modifies the muscle recruitment (Hodges & Richardson, 1999), psychological factors, and so on influences the control strategies. Therefore, a complete description of the CNS, accepted from the scientific community, does not still exist.

The ‘Muscle activations’ block represents the muscles, which receive the electrical signal from the moto-neuron, and contracts to exert the arm force and

stiffness required. Even if the muscle is a complex system, simple models that calculate the force exerted by each muscle were developed. These models are mainly based on three factors: the muscle activation, the length of the muscle, and the contraction velocity (Kistemaker et al., 2010).

The 'Arm' block represents the operator's arm on which the torques exerted by each muscle act. It generates the force and the stiffness that are combined with the force and stiffness exerted by the exoskeleton to generate the endpoint force and stiffness.

### **2.2.2 The 'Exoskeleton system' block**

The 'Exoskeleton system' block represents the robotic device mechanically connected to the human operator.

Physiological electrical signals from the operator muscles (i.e. the surface EMG signal) are recorded. The EMG signals contain the information about the force and the stiffness the operator wants to exert to achieve / accomplish the task. However, this information needs to be decoded by the exoskeleton command logic. The 'Data Process' block estimates the operator behavior. Since the muscle tension depends not only on the muscle activations but also on the length of the muscles and their contraction velocity, the joint configuration is needed to estimate the force and stiffness the subject intends to exert.

The estimation of the force and the stiffness the subject is intended to exert are processed by the 'Command' block. This consists of the 'Command logic' and the 'Exoskeleton model' blocks. The 'Command logic' block represents the logic that calculates the effort the exoskeleton is expected to exert such to assist the operator. Its purpose is to identify the force and the stiffness the exoskeleton needs to exert based on the force and stiffness exerted by the operator. The 'Exoskeleton model' block converts the force and stiffness the exoskeleton needs to exert on the operator into the activation of the motors. This block has implemented information about the structure of the exoskeleton and the technical information about the motors installed, and it calculates the activation required by the actuators to exert the requested force and stiffness.

The 'Exoskeleton' blocks represent the physical device, whose motors are activated as defined in the 'Command' block, which exerts the force and the

stiffness that combine with the force and the stiffness exerted by the operator to obtain the end-point force and stiffness.

In this thesis, elbow, wrist, and arm models are developed and an estimation of the end-point stiffness, based on the muscle activations, is proposed. Then, a control logic for the modulation of the exoskeleton stiffness, based on the operator stiffening, is tested based on experimental data. Finally, the devices that generate the exoskeleton stiffening is selected.

## Chapter 3

# The upper limb models

In this chapter the problem of the identification of limb stiffness from muscle activation represented in the ‘Data process’ block of human-exoskeleton interaction shown in the Figure 2.3 was addressed.

Two simple models made of 1 joint and 2 antagonist muscles (1J2M), and 2 joints and 6 muscles (2J6M) were proposed. The 1J2M model was developed to approximate the elbow and the wrist joints, while the 2J6M model was developed to approximate the elbow-shoulder joint system. However, these models could also be applied approximate other joints (i.e. the 1J2M can also approximate the knee joint while the 2J6M can approximate the hip-knee joint system) by simply changing the parameters related to the muscle characteristics and geometry.

### 3.1 Musculo-tendon system model

In both the 1J2M and 2J6M models the musculo-tendon system was analytically described based on the Hill model (Hill, 1953). The Hill model is a conventional approximation in computational literature and a valid method for the analysis of feasible mechanical behavior of the limb for which an analogue of musculo-tendons is required (Inouye & Valero-Cuevas, 2016).

The Hill model is composed of two segments that modeled the muscle belly and the tendon actions. The muscle belly is the thicker, fleshy middle part of the skeletal muscles while the tendon is the tough band of fibrous connective tissue that connects the belly to the bones (Figure 3.1).

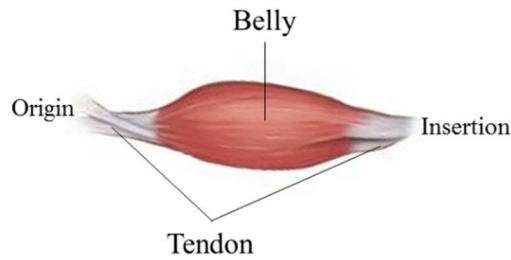


Figure 3.1: Skeletal muscle structure. The belly is the middle thicker part of the muscle while the tendons connect the muscle with the bones. The origin is the attachment to the stationary end of the muscle and the insertion is the attachment to the mobile end of the muscle

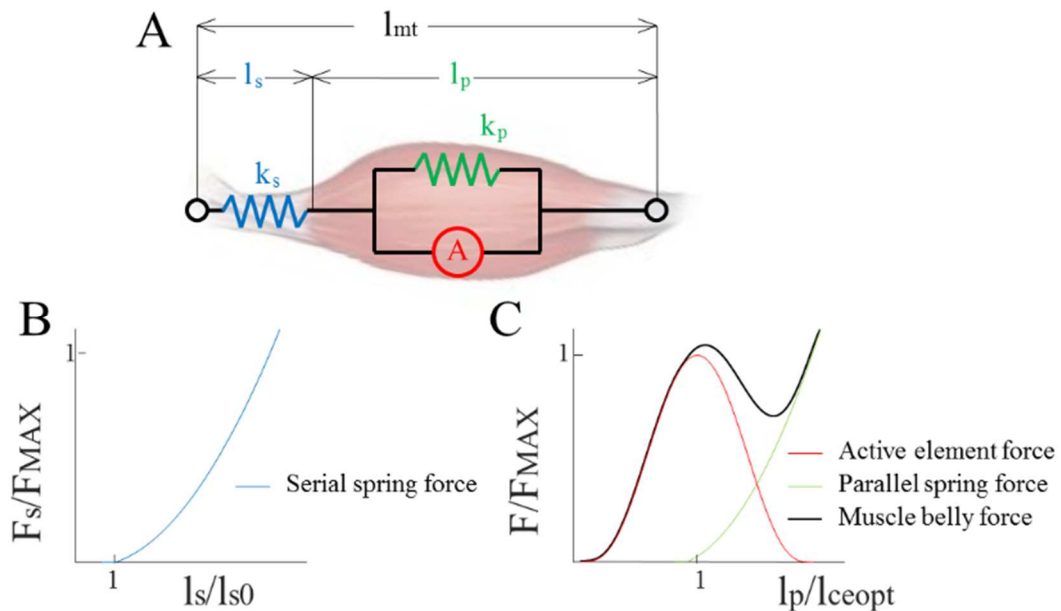


Figure 3.2: The Hill musculo-tendon model. A. The musculo-tendon system is modeled with an active element (A) and a parallel spring ( $k_p$ ), which modulate the action of the muscle belly, and a serial spring ( $k_s$ ) which modulates the tendons action. B. The force exerted by the serial spring, depending on the relative length of the tendons ( $l_s/l_{s0}$ ). C. The force exerted by the muscle belly (black) as the sum of the action exerted by the parallel spring (green) and the active element (red) depending on the relative length of the belly ( $l_p/l_{ceopt}$ ).

The behavior of the muscle belly, whose length is  $l_p$ , is approximated with an active element (A) and a non-linear spring parallel to A. Two tendons connect the muscle belly to the bones at two points: the origin (the proximal side) and the insertion (the distal side). Both tendons are modeled with one segment, whose

length is  $l_s$ , composed of a non-linear spring in series with  $A$ . Commonly, in literature (McMahon, 1984) a damping element in parallel with the active element, is added to model the effect of the contraction velocity on the muscle belly. However, in this study, only the steady state of the isometric force exertion was considered. Therefore, no muscle length variation occur, the contraction velocity is zero, and the damping component was also zero. Hence, the damping element is not modeled in this study.

### 3.1.1 The active element

The active element  $A$ , models the actin and myosin actions that generate the voluntary force in the muscle.

The equation that approximates the force exerted by the active element ( $F_A$ ) given the length of the muscle ( $l_p$ ) is (Kistemaker et al., 2010):

$$F_A = m \cdot F_{MAX} \cdot \left[ -a \cdot \left( \frac{l_p}{l_{ceopt}} \right)^2 + 2a \cdot \frac{l_p}{l_{ceopt}} - a + 1 \right] \quad (3.1)$$

Where:

$l_{ceopt}$  is the optimal length at which the muscle exerts the maximum force  $F_{MAX}$ .  $l_{ceopt}$  and  $F_{MAX}$  are muscle specific and their values, for the muscles used in this study, were obtained from (Holzbaur, Murray, & Delp, 2005) and reported in Table 3.1

$$a = 1/\text{width}^2,$$

$\text{width} = 0.66$  is the muscle width.

The relation between the active isometric force exerted by the muscle and its length depends on the optimal fiber length ( $l_{ceopt}$ ) and it can be approximated with an inverted parabola (Gollapudi & Lin, 2009).

The relation between the active isometric force and the muscle activation  $m$  was linearly modeled (Nazari et al, 2013). The muscle activation was reported as a fraction of the Maximum Voluntary Contraction (MVC), which is the maximum

contraction the muscle could exert. Hence, the muscle activation is between 0 and 1.

Even if the force the muscle active element exerts depends also on the contraction velocity, in this study only the steady state in which the muscle is exerting a constant isometric force was considered. Then, the term for active force that depends on the contraction velocity, was neglected.

In Figure 3.3 the relation between the force exerted by the active element, normalized to the maximum force it could exert, the length of the muscle, normalized to the optimal length, was presented for different muscle activations, normalized to the MVC.

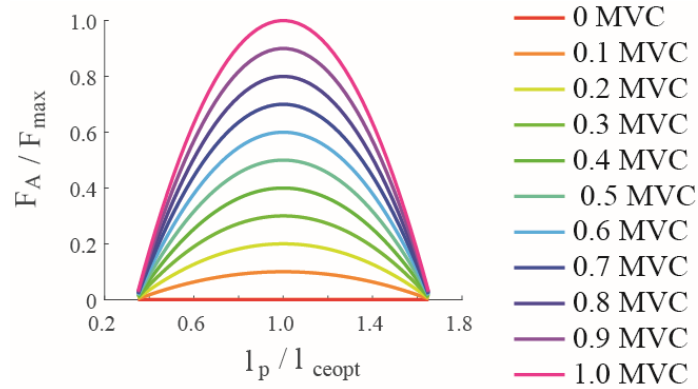


Figure 3.3: The force exerted by the active element depending on the muscle activation and on the length of the belly segment. The force is normalized to the maximum force the muscle active element could exert, the belly length is normalized to its optimal length, and the muscle activation is normalized to the MVC.

### 3.1.2 The parallel spring

The spring, in parallel with the active element, models the behavior of the collagen tissue in the muscle. The relation between the force exerted by the parallel spring and the length of the muscle belly could be approximated with a quadratic fit (Gollapudi & Lin, 2009). The relation between the force exerted by the parallel spring ( $F_p$ ) and the length of the muscle belly is (Kistemaker et al., 2010)

$$F_p = k_p \left[ \max \left( 0, l_{cerel} - \frac{l_{p0}}{l_{ceopt}} \right) \right]^2 \quad (3.2)$$

Where:

$l_{cerel} = \frac{l_p}{l_{ceopt}}$ : length of the muscle, relative to its optimal length,

$k_p$ : stiffness of the non-linear spring in parallel with the active element, which was chosen such that at  $F_p = F_{MAX}$ ,  $l_{cerel} = 1 + width$ ,

$l_{p0}$ : muscle belly relaxation length, which indicates the maximum length of the muscle for which the parallel spring does not exert any passive force. In this study  $l_{p0}$  was set equal to  $l_{ceopt}$  as in (Holzbaur et al., 2005).

In Figure 3.4 the relation between the forces exerted by the passive parallel element, normalized to the maximum force the active element could exert, and its length, which is equal to the muscle length, normalized to the optimal length, was presented.

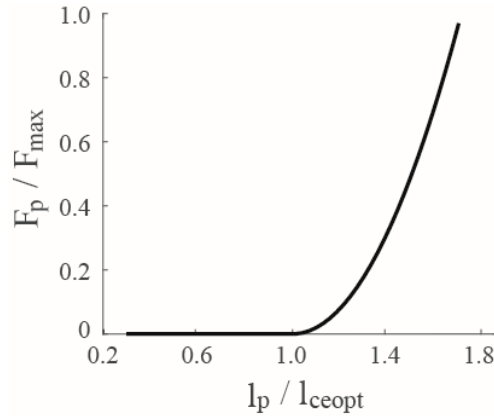


Figure 3.4: The passive parallel spring force, normalized to the maximum force the muscle active element could exert, depends on the length of the belly segment, normalized to its optimal length.

### 3.1.3 The serial spring

The serial spring represents all the tendinous tissue in series with the contractile elements. It behaves like a non-linear spring whose relation could be approximated with a quadratic fit (Magnusson et al., 2001). The relation between the force exerted by the serial spring ( $F_s$ ) and the length of the tendon is (Kistemaker et al., 2010):

$$F_s = k_s [\max(0, l_s - l_{s0})]^2 \quad (3.3)$$

Where:

$k_s$ : tendon stiffness, which was chosen such that at  $F_{MAX}$ ,  $l_s = 1.04 \cdot l_{s0}$

$l_{s0}$ : tendon slack length, that indicated the maximum length of the tendon for which the serial spring does not exert any force.  $l_{s0}$  is muscle specific and its value, for the muscles used in this study, was gotten from literature (Holzbaur et al., 2005).

In Figure 3.5 the relation between the forces exerted by the passive serial element, normalized to the maximum force the active element could exert, and the tendon length, normalized to the tendon slack length, was presented.

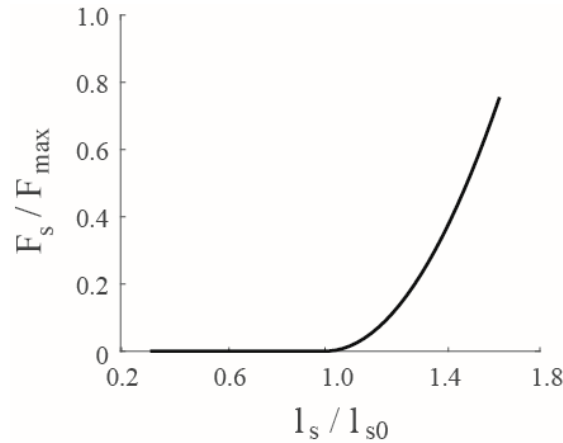


Figure 3.5: The passive serial spring force, normalized to the maximum force the muscle could exert, depends on the length of the tendon, normalized to the tendon slack length.

### 3.1.4 The musculo-tendon system

The actions exerted by the active element and the parallel spring (Equations 3.1, 3.2) could be combined (Figure 3.6 upper) to identify the relation between the force exerted by the muscle belly segment with respect to its length. The force exerted by the musculo-tendon system, depending on its length, can be calculated based on Equations 3.1, 3.2, and 3.3 was reported in Figure 3.6.

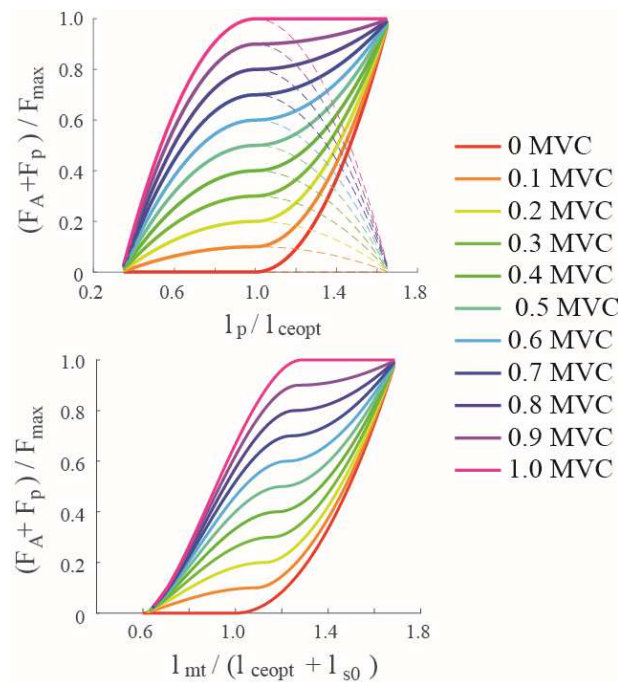


Figure 3.6: Force exerted by the muscle segment (left) in relation to its length at different activations of the active element (color coded and normalized to the MVC). Force exerted by the musculo-tendon system (right) in relation to its length at different activations (color coded and normalized to the MVC).

### 3.2 1J2M: 1 joint and 2 antagonist muscles model

The study of the modulation of the stiffness of one joint was performed with a model made of two antagonist muscles, which reflected the architecture of both the elbow and the wrist (see Figure 3.7).

In the literature, different graphic-based software systems were developed to allow users with low programming experience to perform analysis with a reliable musculo-skeletal model. Some examples are SIMM (Delp & Loan, 1995) and OpenSim (Delp et al., 2007). However, the complexity of these models does not allow a real-time evaluation of the stiffness exerted by the operator. Therefore, a model made of 1 joint and 2 antagonist muscles was developed.

Since agonistic muscles can exert the same action, only one muscle was selected and modeled. The selected muscles were prime movers or synergists muscles. The prime movers are those muscles whose activation cause a movement

to occur, while synergists are those muscles that perform, or help to perform, the same set of joint motion as the prime movers.

The prime movers of the elbow are the Brachialis for the flexion and the Triceps for the extension. However, since the Brachialis is a deep muscle, which cannot be recorded with surface EMG, instead most previous research recorded the Brachioradialis (R Osu & Gomi, 1999), a synergistic muscle. The prime movers of the wrist are the Flexor Carpi Radialis, and the Flexor Carpi Ulnaris, for the flexion, and the Extensor Carpi Radialis Longus, the Extensor Carpi Radialis Brevis and the Extensor Carpi Ulnaris, for the extension.

Hence, in this study, the muscles used to model the behavior of the elbow joint are the Brachioradialis (BRD, muscle 1), that acts as an elbow flexor, and the Lateral head of the Triceps (TriLat, muscle 2) that acts as an elbow extensor. The muscles used to model the behavior of the wrist joint are the Flexor Carpi Radialis (FCR, muscle 1), that acts as a wrist flexor, and the Extensor Carpi Radialis Longus (ECRL, muscle 2) that acts as a wrist extensor.

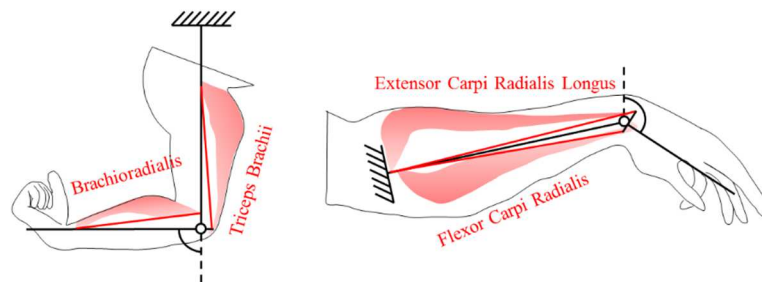


Figure 3.7: The model made of 1 joint and 2 muscles could approximate both an elbow joint (left) and a wrist joint (right).

### 3.2.1 Joint model

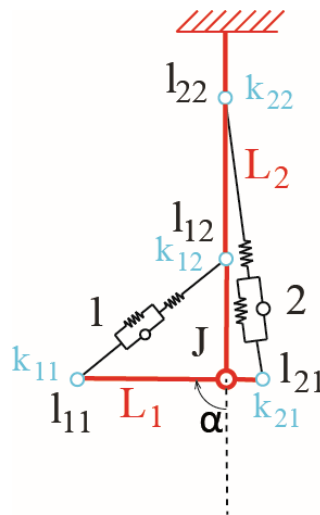


Figure 3.8: Model of human elbow or wrist joints.

The simplified model consists of two rigid segments connected by a single degree of freedom (DOF) hinge joint (see Figure 3.8). If the approximated joint J is the elbow, the hinge joint approximates the elbow (Marieb & Hoehn, 2007) and the links approximate the humerus bone ( $L_1$ ) and radio-ulna bones ( $L_2$ ). If the approximated joint is the wrist, the hinge joint approximates the wrist and the links approximate the radio-ulna bones ( $L_1$ ) and the hand bones ( $L_2$ ).

Two actuators, simulating the actions of antagonist muscles on the joint, and controlling the single DOF. Since muscles can exert only pulling actions, single effect actuators (i.e. wires), one opposed to the other, are used in the model. Hinges make the connections between the links and the actuators ( $k_{ij}$ ,  $i = 1, 2$ ;  $j = 1, 2$ ).

The maximum force exerted by the muscle active element, the optimal belly fiber length, the muscle belly relaxation length and the tendon slack length of the muscles modeled in this study were gotten from literature (Holzbaur et al., 2005) and are reported in Table 3.1.

Table 3.1: Hill muscle parameters got from literature.

	Elbow		Wrist	
	1: flexor (BRD)	2: extensor (TriLat)	1: flexor (FCR)	2: extensor (ECRL)
$F_{MAX}$ (N)	261.33	624.30	73.96	304.89
$l_{ceopt}$ (m)	0.1380	0.1138	0.0628	0.0810
$l_{p0}$ (m)	0.1380	0.1138	0.0628	0.0810
$l_{s0}$ (m)	0.1726	0.0980	0.2440	0.2240

The parameters reported in Table 3.2 represent the distance between the joint's center of rotation and the point of muscle insertion with the bone. The BRD is connected to the Humerus (origin  $l_{11}$ ) and the Radius (insertion  $l_{12}$ ). The TriLat is connected to the Humerus (origin  $l_{21}$ ) and the Ulna (insertion  $l_{22}$ ). The FCR is connected to the Humerus (origin  $l_{11}$ ) and to the Second Metacarpal bone (insertion  $l_{12}$ ). The ECRL is connected to the Humerus (origin  $l_{22}$ ) and to the Second Metacarpal bone (insertion  $l_{22}$ ).

Table 3.2: Distance between the joint centers of rotation and the connection between the muscles and the bones. The origin attach is intended as the distance between the connection of the origin side of the muscle with the bone, while the insertion attach is intended as the distance between the connection of the insertion side of the muscle with the bone (see Figure 3.1).

	Elbow		Wrist	
	1: flexor (BRD)	2: extensor (TriLat)	1: flexor (FCR)	2: extensor (ECRL)
<b>Origin attach (m)</b>	0.130	0.022	0.250	0.250
<b>Insertion attach (m)</b>	0.200	0.190	0.020	0.007

The elbow angle is set to zero when the forearm is aligned with the humerus and it increases with the flexion of the elbow. The wrist angle is set to zero when the hand is aligned with the forearm, it is negative when the wrist is extended and positive when the wrist is flexed.

However, the musculoskeletal model parameters were identified and approximated the muscle with a complex geometry that cannot be fit with a mere wire (see Figure 3.9). In particular, one of the major discrepancies is due to the different lengths the modeled muscle assume for a particular joint angle with respect to the real one. Then, the optimal belly fiber length, the muscle belly relaxation length and the tendon slack length are scaled by the same parameter, specific to the muscle, to reduce the discrepancy between the length of the model from which the parameters were identified from and the model developed in this study. The parameter was chosen such that the peak force generated by both muscle models occur at the same joint angle. The musculo-tendon model identified to define the scaling parameter was the one implemented in the OpenSim® project, a software of musculo-skeletal simulation which could be freely downloaded from the SimTK platform (<https://simtk.org/>). The scale factor and the scaled parameters, used in this study, were reported in Table 3.2, together with the stiffness of the parallel and the serial springs (see Equations 3.2 and 3.3). The comparison between the joint torques exerted by the BRD, for different joint angles and muscle activations, simulated with OpenSim and the model developed in this thesis, was reported in Figure 3.10.

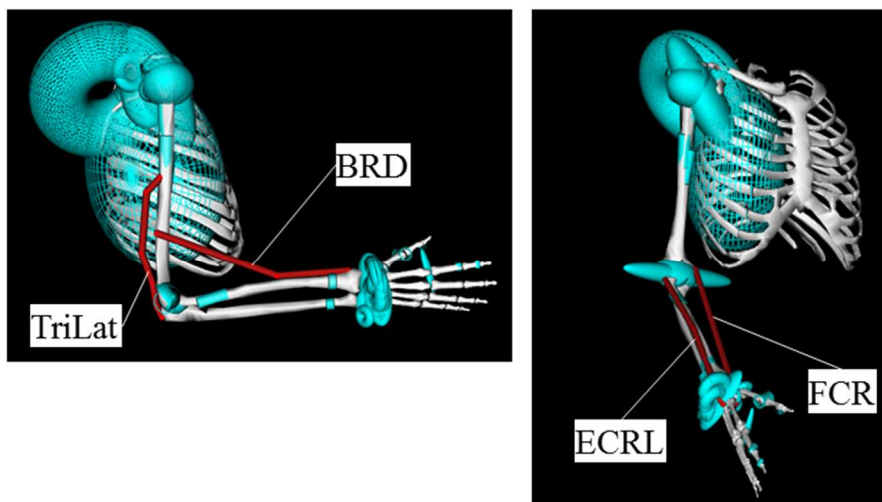


Figure 3.9: The muscle model implemented in the Simulink software. Left: the elbow model in which the only BRD and TriLat muscles are displayed. Right: the wrist model in which the only FCR and ECRL muscles are displayed.

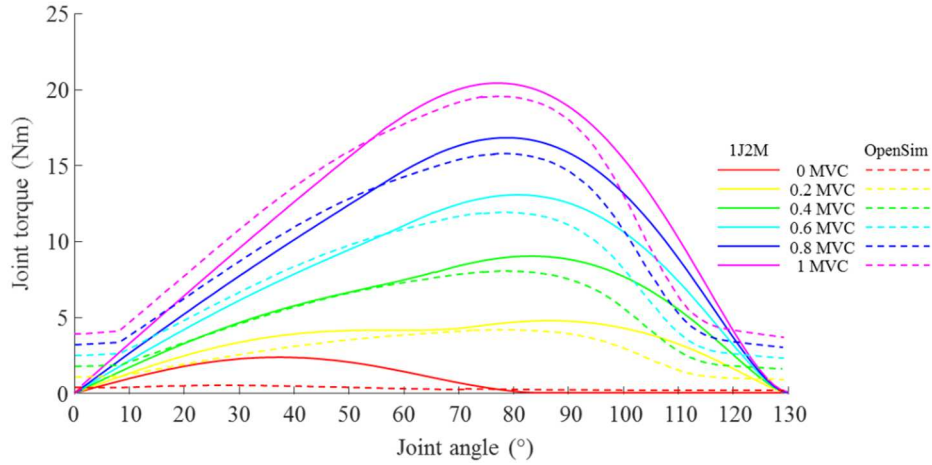


Figure 3.10: Comparison between the muscle torque-joint angle curves of the BRD (muscle 1) calculated with the model presented in this chapter (continuous line) respect with the one calculated with the musculo-skeletal modeling software OpenSim (dotted line) for different muscle activations.

Table 3.3: Scaled Hill muscle parameters got from literature.

	Elbow		Wrist	
	1: flexor (BRD)	2: extensor (TriLat)	1: flexor (FCR)	2: extensor (ECRL)
Scale factor	0.85	0.85	0.81	0.92
Scaled $l_{ceopt}$ (m)	0.1173	0.0967	0.0509	0.0745
Scaled $l_{p0}$ (m)	0.1173	0.0967	0.0509	0.0745
Scaled $l_{s0}$ (m)	0.1467	0.0833	0.1976	0.2061
$k_p$ (N/m)	600	1433	170	700
$k_s$ (N/m)	$163 \cdot 10^3$	$390 \cdot 10^3$	$46 \cdot 10^3$	$191 \cdot 10^3$

### 3.2.2 Equations for force balancing

The two antagonist muscles are able to generate two torques in opposite directions that may compensate each other, thereby enhancing the joint stiffness. Then, if both muscles are activated, both torque and rotational stiffness may be exerted by the joint depending on the muscle activations. Therefore, any

combination of muscle activation can be separated into a component that generates torque (related to the higher torque one of the two antagonist muscles exerts) and another that generates rotational stiffness (related to the equal amount of torque generated by both muscles). In this study we analyzed the only component that generates the rotational stiffness. In other words, the system is in equilibrium and the joint torque is zero.

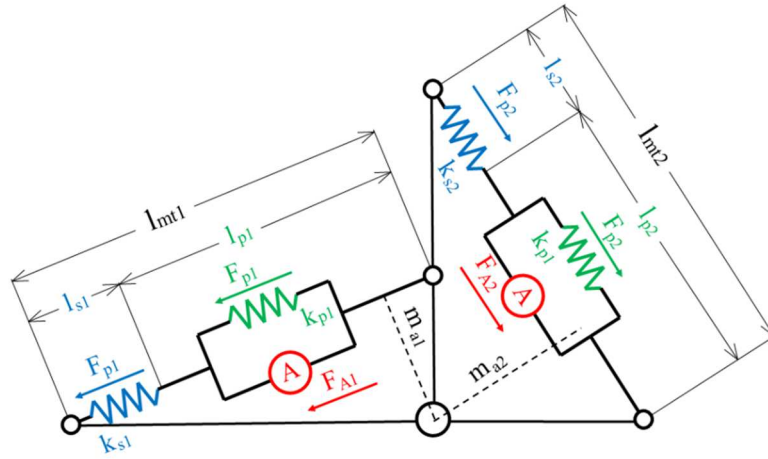


Figure 3.11: The forces exerted by the two muscles

The equations that describe the equilibrium (Figure 3.11) among the internal forces shared between the serial spring ( $F_{s_i}$ ), the parallel spring ( $F_{p_i}$ ), and the active element ( $F_{A_i}$ ), for the muscle  $i$ , where  $i$  could be 1 or 2, and among the torques exerted by the antagonist muscles are (Borzelli et al., 2016, 2017a; Borzelli et al., 2017b):

$$\begin{cases} F_{s1} = F_{p1} + F_{A1} \\ F_{s2} = F_{p2} + F_{A2} \\ m_{a2}(F_{p2} + F_{A2}) = m_{a1}(F_{p1} + F_{A1}) \end{cases} \quad (3.4)$$

Where  $m_{a_i}$  is the moment arm of the muscle  $i$ . The force equations are coupled with the geometrical equations that defined the length of the muscle  $l_{mti}$  and its moment arm based on the lengths of each segment, the joint angle, and their attachments on the bones:

$$\begin{cases} l_{mti} = l_{pi} + l_{si} \\ l_{mti} = \sqrt{l_{i1}^2 + l_{i2}^2 - 2 \cdot l_{i1} \cdot l_{i2} \cdot \cos \beta} \\ m_{\alpha_i} = \frac{2}{l_{mti}} \sqrt{\frac{P_i}{2} \left(\frac{P_i}{2} - l_{i1}\right) \left(\frac{P_i}{2} - l_{i2}\right) \left(\frac{P_i}{2} - l_{mti}\right)} \end{cases} \quad (3.5)$$

Where  $P_i$  is the perimeter of the triangle whose sides are  $l_{i1}$ ,  $l_{i2}$ , and  $l_{mti}$ ,  $l_{i1}$  is the origin attachment of the muscle to the bone,  $l_{i2}$  is the insertion attachment of the muscle on the bone.  $\beta$  is equal to  $\pi - \alpha$  for muscle 1 and to  $\alpha$  for muscle 2; where  $\alpha$  is the joint angle defined such that  $\alpha = 0 \text{ rad}$  when the elbow joint is completely extended or the wrist joint is in a neutral position. The system, is composed of geometric and force equations, together with the equations for the evaluation of the forces exerted by the muscle elements, was implemented in Matlab®. Physiological range of the elbow angle was set from  $0^\circ$  to  $130^\circ$  and physiological range of the wrist angle was set from  $-70^\circ$  to  $75^\circ$  (Iannotti & Parker, 2013).

### 3.2.3 The elbow model

#### 3.2.3.1 Musculo-tendon system characteristics

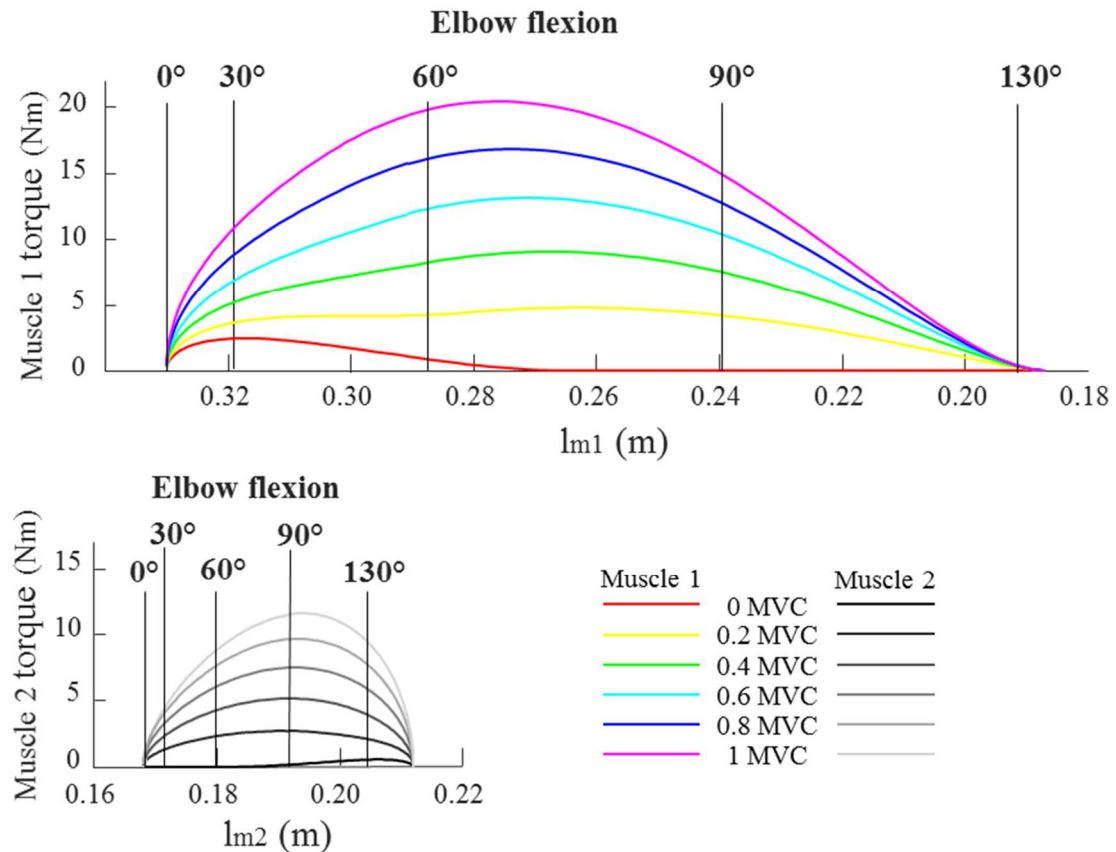


Figure 3.12: Intersections between the characteristics of the torque, related to the musculo-tendon length, exerted by the two muscles for different elbow flexion, at different level of activation of muscle 1 (BRD, colored) and 2 (TriLat, gray scale).

The two antagonist muscles were observed to exert torque along different range of length (between 0.187 and 0.330 m for muscle 1 and between 0.168 and 0.212 m for muscle 2, see Figure 3.12). However, the elbow geometry (intended to be the position of the muscle attachment on the bones, see Table 3.2) permits the two muscles to apply a torque along a similar range of joint angles (between 0° and 128.2°).

### 3.2.3.2 The muscle torque-elbow angle curves

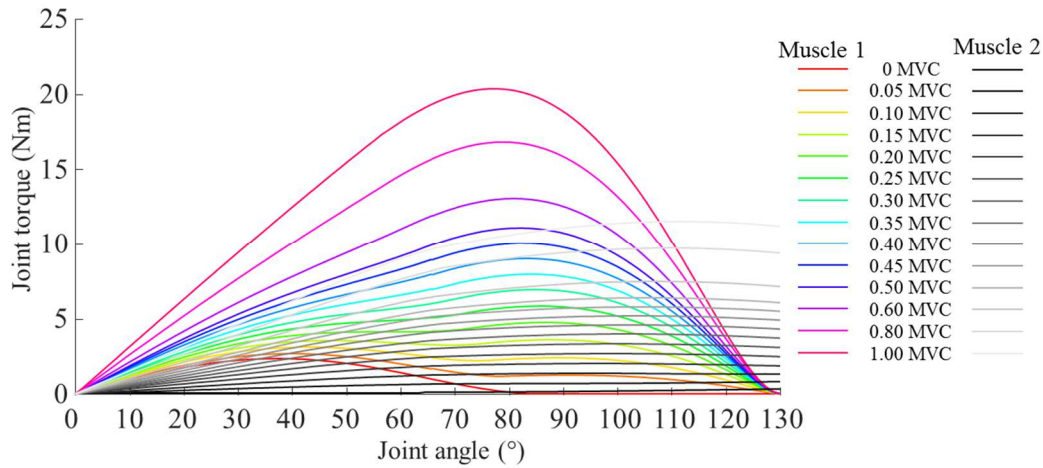


Figure 3.13: Relation between the torque related to the elbow flexion, exerted by the two antagonistic muscles, at different level of activation of muscle 1 (colored) and 2 (gray scale). Muscle activations are not equally spaced.

Once the muscle geometry and parameters are known and the muscle activation is defined, a characteristic curve which relates the torque exerted by each muscle for different joint angle can be identified based on the length the muscle assumes at that particular joint angle (Figure 3.13). The task required by this study, for which the system does not generate any force, i.e. modulates the stiffness, is satisfied only if the two antagonist muscles exert the same torque. In other words the joint stiffness can be modulated only if the muscle torque-joint angle curves of the two antagonist muscles intersect.

The approximation performed by the model presented in this study has some differences in the muscle torque-joint angle curve with respect to the physiological joint. No intersections occur for joint angles higher than  $128.2^\circ$ . This means that the model permits the exertion of only extension torques, generated by the TriLat muscle, and does not permits the stiffness modulation if the joint angle is higher than  $128.2^\circ$ . This is in contrast with literature which identified that both flexion and extension torque, and consequently the stiffness modulation, could occur for elbow angles lower or equal to  $130^\circ$  (Iannotti & Parker, 2013). However, the discrepancy is small ( $1.8^\circ$ ) and we can then affirm that it does not nullify the model.

This model does not allow the exertion of torque if the elbow is completely extended (i.e. during the geometrical singularity for which  $\alpha = 0^\circ$ ) or is hyper-extended ( $\alpha < 0^\circ$ ). However the described model is developed for exoskeleton for industrial application in which such elbow configurations are not recommended.

If the joint angles are closer to the physiological boundaries the proposed model allows only the exertion of small torques when compared to the torques exerted along other joint angles. This behaviour is a consequence of the approximation of muscles with wires. In fact, a complex model, composed of more segments, like the one implemented in the OpenSim® project (Holzbaur et al., 2005), a quasi-constant torque could be detected around the joint angle boundaries (see figure 3.11 for the BRD). However, the presented model was used only to identify a relation between muscle activation components and joint stiffness, for which a precise model around the joint boundaries is not required.

### 3.2.3.3 Antagonist muscle activation

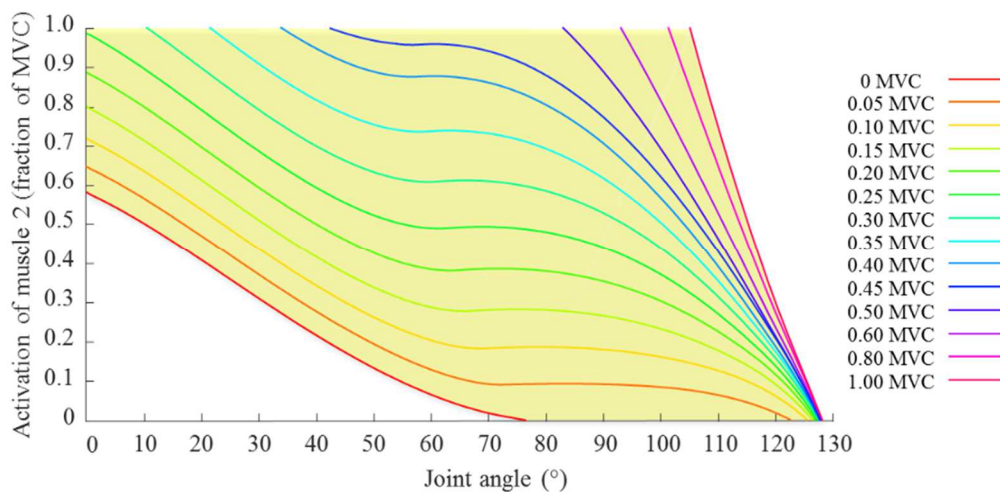


Figure 3.14: Activation of muscle 2 necessary to balance the torque exerted by muscle 1, for different elbow flexions. The different level of muscle 1 activations are reported with different colors. Muscle 1 activations are not equally spaced. In light yellow the surface in which stiffness could be modulated is identified.

In Figure 3.14 the activation of muscle 2, which generates the same joint torque amplitude with respect to the one generated by muscle 1, was represented at different elbow configurations and muscle 1 activations. Curves related to low

activation of muscle 1 are more sparse with respect to curves related to high activation of muscle 1. For this reason, the step from muscle 1 activation is not constant in Figures 3.13 and 3.14. Activating muscle 2 is always necessary for elbow flexions lower than  $76^\circ$  to compensate the force exerted by the passive element of muscle 1.

The torque exerted by muscle 1 cannot be compensated by the torque exerted by muscle 2 in all possible elbow flexions. In practice, higher activations of muscle 1 are balanced by muscle 2 only for elbow flexions higher than  $104^\circ$ . Lower activations of muscle 2 are balanced by muscle 1 only for elbow flexions higher than  $78^\circ$ . These boundaries defined a range of muscle activations for this model in which only stiffness modulation is possible without exerting an elbow torque (yellow surface of Figure 3.14).

### 3.2.3.4 Elbow rotational stiffness

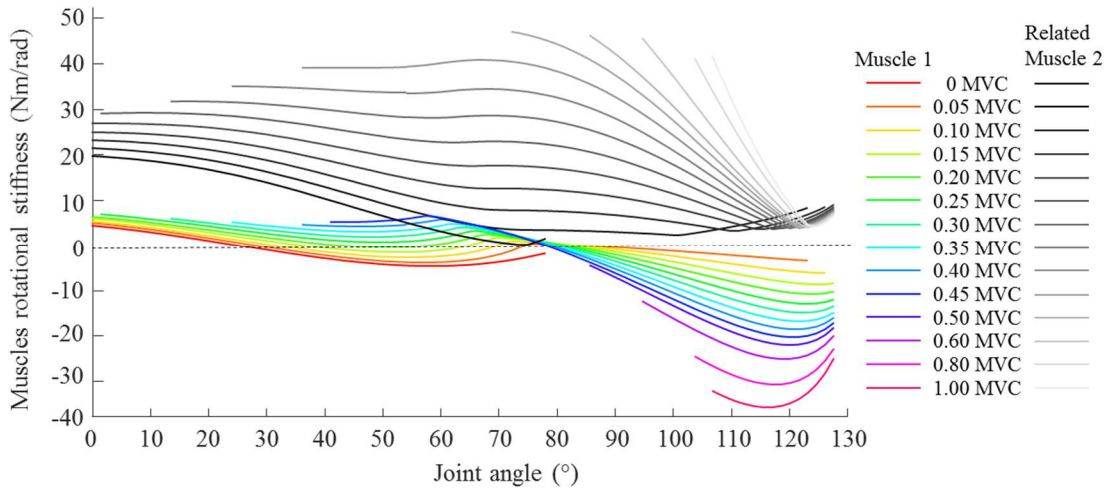


Figure 3.15: Rotational stiffness of the muscles. The stiffness of muscle 1 is represented with a colored scale, each muscle 1 activation is represented with a different color. The stiffness of muscle 2 is represented with a gray scale, the muscle 2 activation, whose torque balanced the torque exerted by muscle 1, is represented with a different level of gray.

The rotational stiffness of the musculo-tendon system is defined as the derivative of torque  $\tau_i$  caused by imposed displacement:

$$K_i = \frac{\partial \tau_i}{\partial \alpha} = \frac{\partial (m_{a_i} \cdot (F_{pi} + F_{Ai}))}{\partial \alpha} = m_{a_i} \frac{\partial (F_{pi} + F_{Ai})}{\partial \alpha} + (F_{pi} + F_{Ai}) \frac{\partial m_{a_i}}{\partial \alpha} \quad (3.6)$$

Once the arm configuration was set, a virtually infinite set of muscle combinations, which does not generate any end-point forces, could be obtained. The differences in these solutions depend on the level of co-contraction, i.e. the simultaneous activation of antagonist muscles. Since the muscle activation is related to the muscle stiffness (Burdet et al., 2013), the co-contraction is related to the joint rotational stiffness. In this study, the activation of the muscle 1 was fixed and the activation of the muscle 2 was simultaneously calculated, for each elbow angle, hence, solving the system of equation 3.4 and 3.5.

Following the typical paradigm for the experimental arm stiffness measurement (Mussa-Ivaldi et al., 1985), a small deflection ( $\partial\alpha = 0.1^\circ$ ) (Hu et al., 2011) was applied to the elbow joint in both positive and negative directions. The deflection resulted in muscle length variation, while the muscle activations were kept constant. Since the torque exerted by each muscle depends on its length, the deflection led to a variation in the torque exerted by each muscle. Since the deflection was small, a linearization of the elbow angle-torque relation around the unperturbed configuration was possible, and the related slopes are the stiffness of the muscles (Figure 3.15).

When the stiffness of muscle 2, is non-negative, the stiffness of muscle 1 may assume negative values. This behavior is physiological and due to the negative slope of the elbow flexion-torque relation curve. Muscle 1 negative stiffness means that, if the joint is displaced, the torque that the muscle exerts is reduced. The effects of stiffness negativity are compensated in a real muscle with the stretch reflex, or myotatic reflex, which consists of a muscle contraction in response to a muscle stretching (Crago et al., 1976). Muscle stiffness equal to zero means that there are no changes in the torque exerted by the muscle when the displacement was applied.

The joint rotational stiffness of the elbow was calculated as the difference between the slopes of the elbow angle-torque curves of muscle 2 with respect to muscle 1 (Figure 3.16).

The joint rotational stiffness showed an increase with the muscle activation for each elbow angle. Two peaks can be found, due to the passive and active elements of muscle 1. Since balancing of the torque exerted by high activation of muscle 1 is possible only for some joint angles, the stiffness of higher muscle activations can be computed only for these angles.

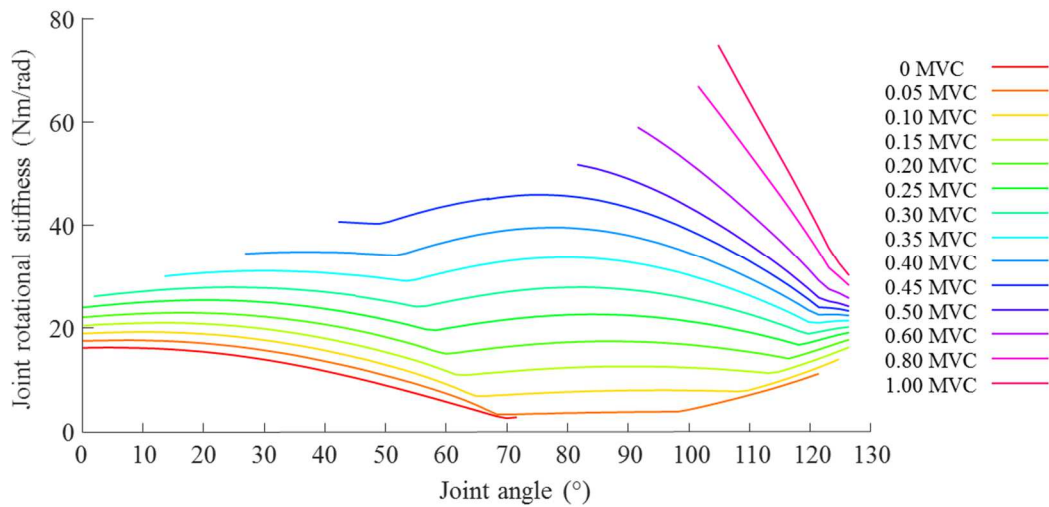


Figure 3.16: Stiffness of the elbow at different elbow flexions and muscle 1 activations, are reported with different colors.

### 3.2.4 The wrist model

In this paragraph, the same 1J2M model was implemented for a wrist joint (see Figure 3.17). The differences with respect to the elbow joint were related to geometrical characteristics (i.e. the attachment of muscles on bones and the joint angle range) and to the Hill model parameters.

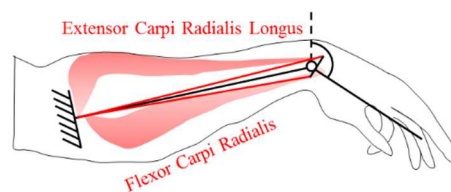


Figure 3.17: The 1J2M modeled as a wrist.

### 3.2.4.1 Musculo-tendon system characteristics

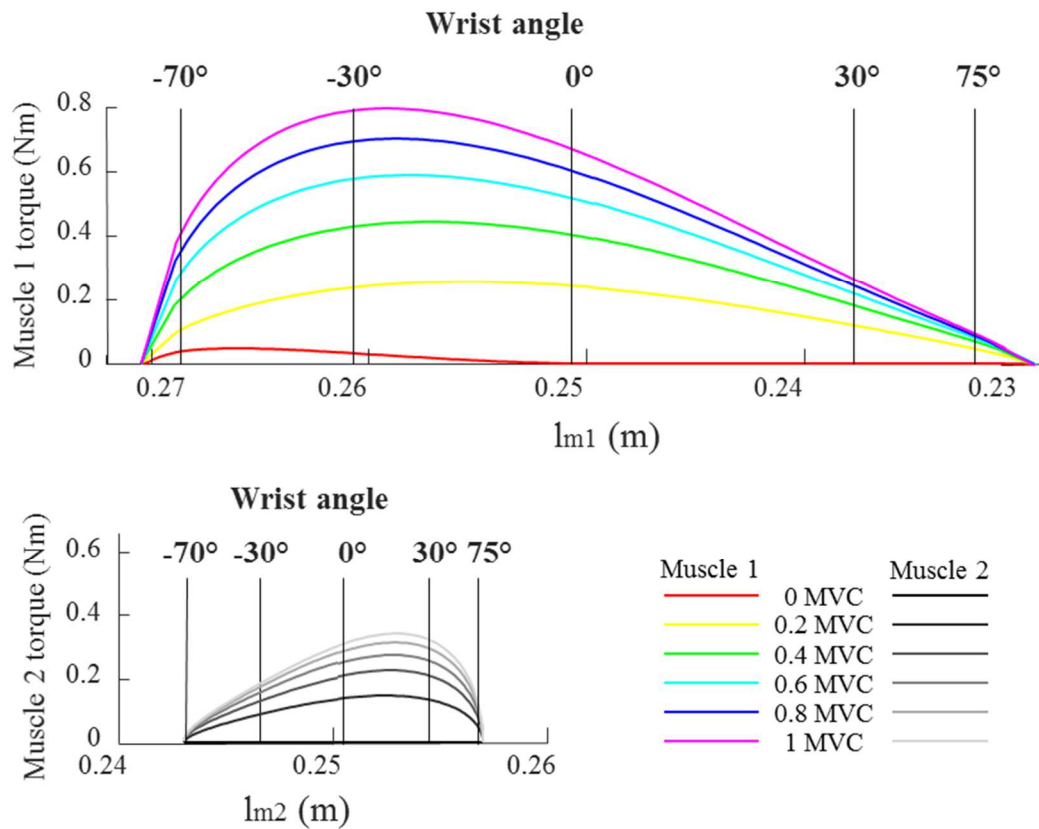


Figure 3.18: Intersections between the characteristics of the torque, related to the musculo-tendon length, exerted by the two muscles for different wrist flexion, at different level of activation of muscle 1 (colored) and 2 (gray scale).

The characteristic curve of the muscle length-torque behavior of one muscle with respect to the other, as presented for elbow joint in Paragraph 3.2.3.1, is shown in Figure 3.18. We may observe that this shifting permits the two muscles to apply a torque along the same range of joint angles (between  $-70^\circ$  and  $75^\circ$ ), even if they exert force along different range of length (between 0.23 and 0.27 m for muscle 1 and between 0.243 and 0.256 for muscle 2).

### 3.2.4.2 The muscle torque-wrist angle curves

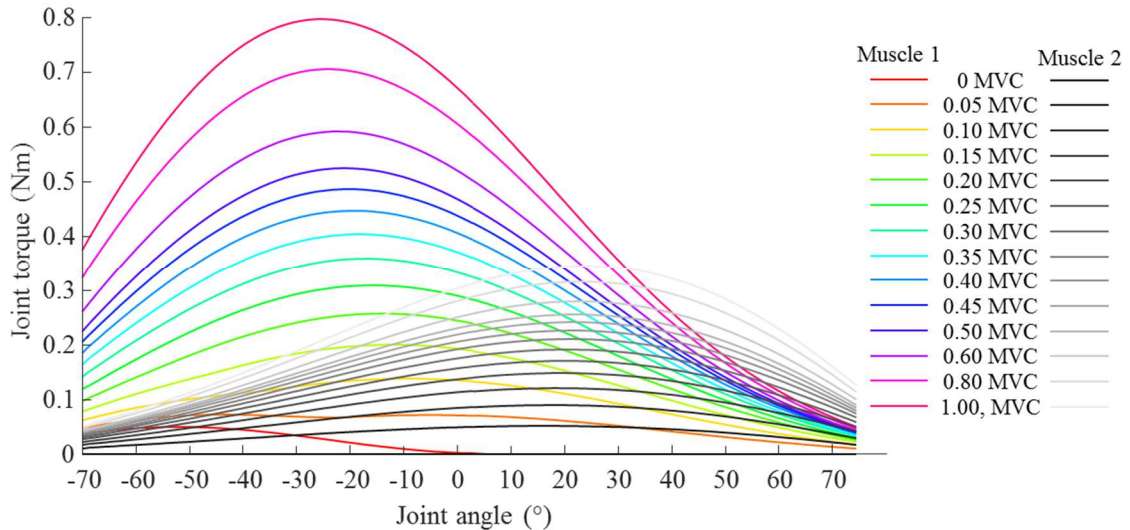


Figure 3.19: Relation between the torque related to the wrist flexion, exerted by the two antagonistic muscles, at different level of activation of muscle 1 (colored) and 2 (gray scale). Muscle activations are not equally spaced.

The characteristic curve which relates the torque exerted by the muscle at different joint angles (Figure 3.19) was identified, as it was done for the elbow joint model (see Paragraph 3.2.3.2) based on the length the muscle assumes at that particular joint angle.

The limitations in the joint boundaries, identified for the elbow joint, were not present for the wrist joint. In fact the described model could span the whole physiological range of movement (between  $-70^\circ$  and  $75^\circ$ , (Iannotti & Parker, 2013)). Stiffness modulation is feasible also for small hyper-extension ( $\alpha < -70^\circ$ ) or hyper flexion ( $\alpha > 75^\circ$ ) because the wrist flexion-muscle torque characteristic curves of the two antagonist muscles intersect also if joint angles exceed the physiological wrist boundaries..

### 3.2.4.3 Antagonist muscle activation

In Figure 3.20 the activation of muscle 2, that assures the equilibrium at the wrist, was represented at different wrist configurations and muscle 1 activations. Curves relating low activation of muscle 1 are more sparse with respect to curves relating high activation of muscle 1. Therefore, the step between muscle 1 activation is not constant in Figures 3.19 and 3.20. Indifferent equilibrium is possible for angles higher than  $0^\circ$ , maintaining both muscles with no activation. Activating muscle 2

is always necessary for wrist flexions lower than  $0^\circ$  to compensate the force exerted by the passive element of muscle 1.

Not all possible wrist flexions and muscle 1 activations are feasible together. In particular, higher activations of muscle 1 are balanced by muscle 2 only for higher values of elbow flexion. Lower activations of muscle 2 are balanced by muscle 1 only for lower values of elbow flexion. These boundaries defined a range of muscle activations in which the stiffening of the elbow, without exerting a torque, is possible (yellow surface in Figure 3.20).

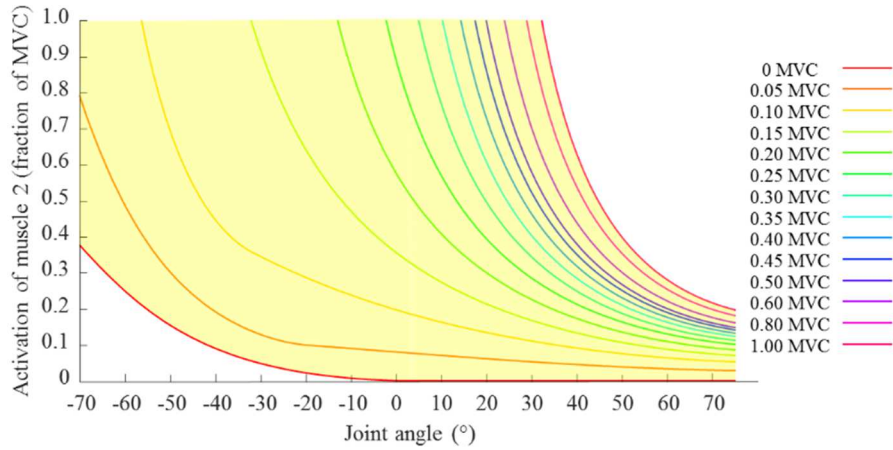


Figure 3.20. Activation of muscle 2 necessary to balance the torque exerted by muscle 1, for different wrist angles. The different level of muscle 1 activations are reported with different colors. Muscle 1 activations are not equally spaced.

#### 3.2.4.4 Wrist rotational stiffness

The rotational stiffness of the musculo-tendon system is defined as the derivative of displacement caused by imposed torque  $\tau_i$ :

$$K_i = m_{a_i} \frac{\partial(F_{p_i} + F_{A_i})}{\partial \alpha} + (F_{p_i} + F_{A_i}) \frac{\partial m_{a_i}}{\partial \alpha} \quad (3.6)$$

Once the wrist configuration was set, a virtually infinite set of muscle combinations can be obtained. The differences in these solutions depend on the level of co-activation of antagonist muscles, which is related to the rotational stiffness. In this study, as performed for the elbow joint in Paragraph 3.2.3.4 the activation of the muscle 1 was fixed and the activation of the muscle 2 was

simultaneously calculated, for each wrist angle, solving the system of Equations 3.4 and 3.5.

Following the typical paradigm for the experimental arm stiffness measurement (Mussa-Ivaldi et al., 1985), a small deflection ( $\partial\alpha = 0.01^\circ$ ) (Hu et al., 2011) was applied to the wrist joint in both positive and negative directions, while the muscle activations are constant. The force exerted by the muscle depends on its length, and a corresponding torque is exerted at the wrist joint. The wrist angle-torque relation can be linearized around the unperturbed configuration, and the slope represents the stiffness of the muscles (Figure 3.21). The rotational stiffness of the wrist is the difference between the slopes of the wrist angle-torque curves of muscle 1 with respect to muscle 2 (Figure 3.22). The stiffness of both muscle 1 and 2 can assume negative values. This behavior can be physiological and due to the negative slope of the elbow flexion-torque relation curve.

The joint stiffness shows an increase with the muscle activation for each wrist angle. Two peaks can be found, due to the passive and active elements of muscle 1. Since balancing of the torque exerted by high activation of muscle 1 is possible only for some joint angles, the stiffness of higher muscle activations can be computed only for these angles. Since there exist some wrist angles at which both muscles are not activated, a range of angles at which the stiffness is null can be found.

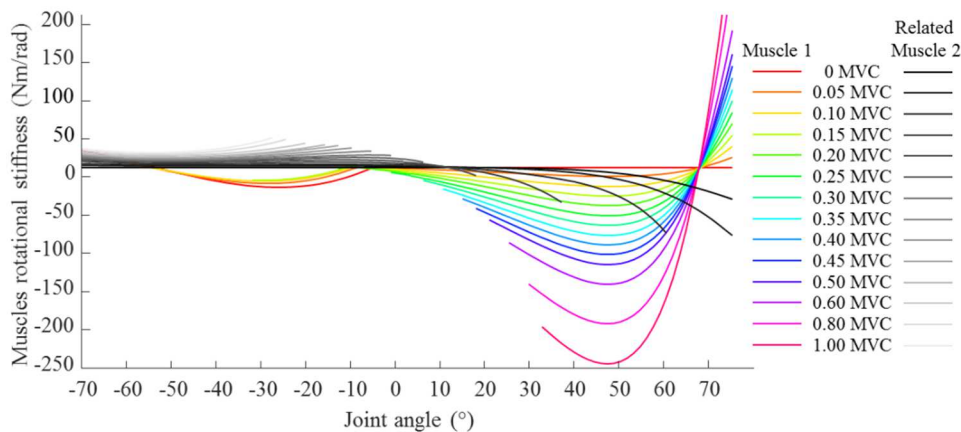


Figure 3.21: Rotational stiffness of the muscles. The stiffness of muscle 1 is represented with a colored scale, each muscle 1 activation is represented with a different color. The stiffness of muscle 2 is represented with a gray scale, the muscle 2 activation, whose torque balanced the torque exerted by muscle 1, is represented with a different level of gray.

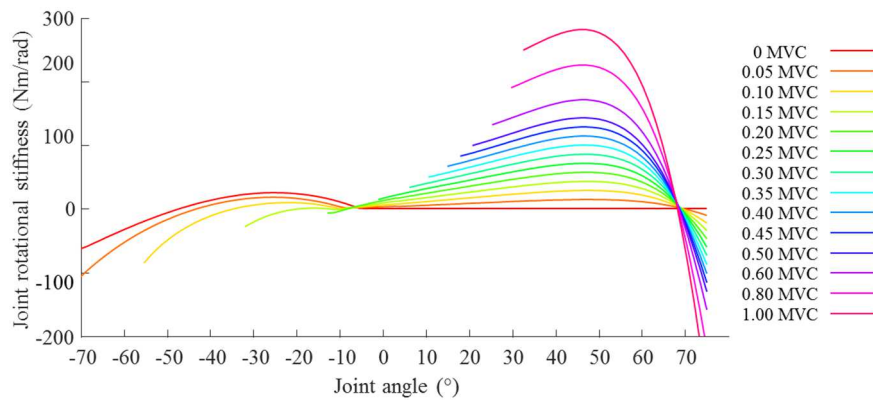


Figure 3.22. Stiffness of the wrist at different elbow flexions and muscle 1 activations, are reported with different colors.

### 3.3 2J6M: 2 joints and 6 muscles model

The model composed of 1 joint and 2 muscles, presented in Paragraph 3.2, could approximate those joints in which an agonist and antagonist prime movers could be identified. However, the approximation of the huge number of muscles acting on the same joint with a couple of muscles reduces the redundancy of the musculo-skeletal system. On the other hand, if more joints are required to be modeled, the action of bi-articular muscles, i.e. those muscles that cross two joints instead of one, may be required. For this reason, in this chapter, a model composed of 2 joints and 6 muscles was described and a simple method to estimate the end-point stiffness for a redundant system was discussed.

#### 3.3.1 Implications of muscle redundancy

A geometrical space could be defined by setting on each axis the activation of one of the recorded muscles. Therefore, each muscle activation can be interpreted as a vector in the muscle space. Then, the *muscle space* is defined as the orthogonal space whose coordinates are the activations of each recorded muscle (Borzelli et al., submitted). Therefore, its dimensionality is equal to the number of EMG signals and each vector represents the muscle activation recorded at a particular sample time.

If we define any matrix  $H$  as the matrix which maps the muscle activation vector  $\mathbf{m}$  into a vector of another space  $F$ , whose dimensionality is lower than the muscle space, each  $\mathbf{m}$  can be decomposed into two orthogonal vectors (Anton,

2010; Strang, 1993). Those two vectors are obtained by projecting  $\mathbf{m}$  onto two orthogonal subspaces: the *null space* of  $H$ , whose elements are mapped by the  $H$  matrix onto zero vectors of the space  $F$ , and the row space of  $H$ , whose elements are the minimum norm vectors the  $H$  matrix maps onto non-zero vectors of the space  $F$ . Any muscle activation vector can be thus uniquely decomposed into two orthogonal vectors by projection onto these two subspaces.

If  $H$  is defined as the specific matrix that maps the muscle activation  $\mathbf{m}$  (i.e. the recorded EMG signal) into the end-point force space  $F$ , so as to satisfy the relation:

$$\mathbf{f} = H(\mathbf{m}, \mathbf{p}, \mathbf{g}) \cdot \mathbf{m} \quad (3.7)$$

Where  $\mathbf{f}$  is the end-point force generated by the muscle activation  $\mathbf{m}$ ,  $\mathbf{p}$  is the limb configuration and  $\mathbf{g}$  its geometry, intended as muscle attachments, the muscle vector  $\mathbf{m}$  could be decomposed into the two orthogonal vectors previously described. The projection of  $\mathbf{m}$  into the row space of  $H$  represents the minimum norm of the muscle activation that generates the required end-point force  $\mathbf{f}$ , while the projection of  $\mathbf{m}$  onto the null space of  $H$  represents the component of muscle activation that does not generate any end-point force.

The identification of the null and row spaces of the  $H$  matrix could be easily done on the 1 joint and 2 antagonist muscles model described in chapter 3. If for example we assume the joint is flexed at  $90^\circ$  (see Figure 3.22), the  $H$  matrix is:

$$H = \begin{bmatrix} -1 & 1 \\ 0 & 0 \end{bmatrix} \quad (3.8)$$

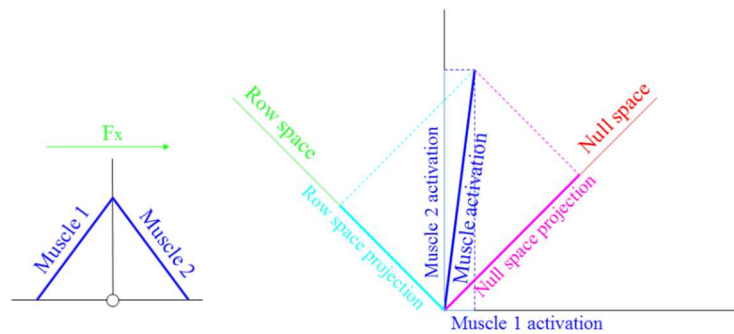


Figure 3.23: Example of the identification of the projection of the muscle activation onto the row and the null spaces. Left: model made of one joint and two identical antagonist muscles ('Muscle 1' and 'Muscle 2', blue lined). The positive direction of the force is represented as a green arrow ( $F_x$ ). Right: The muscle space on whose axes are reported the muscle activations (Muscle 1 on the x axis and Muscle 2 on the y label). The

null (red) and row (green) spaces are identified. An example of muscle activations ([0.1 0.8], blue) together with its projection on the null (magenta) and the row (cyan) spaces are reported.

The null space  $N$ , computed with the Matlab function *null*, and the row space  $H^+$ , computed as the pseudo-inverse of the  $H$  matrix ( $H^+$ ) with the Matlab function *pinv* (only one component was considered, the other was  $[0 \ 0]^T$ ), are:

$$N = \begin{bmatrix} 0.71 \\ 0.71 \end{bmatrix} \quad (3.9)$$

$$H^+ = \begin{bmatrix} -0.71 \\ 0.71 \end{bmatrix} \quad (3.10)$$

Since the muscle space is bi-dimensional and the row space is mono-dimensional, the null space, whose dimensionality is the difference between the muscle space and the row space dimensionalities, is mono-dimensional too and, by definition,  $N$  and  $H^+$  are orthogonal.  $N$  represents the simultaneous and equal activation of both muscles. A modulation of the muscle activation on the only null space led to the modulation of the end-point stiffness with the fixed end-point force, then the null space projection of the muscle activation, in this case, is strictly related to the stiffness. Therefore, in this case, the null space is coincident with the muscle subspace that generates only stiffness (i.e. the stiffness space).

The projection of a muscle activation vector onto the row space would lead to a muscle activation in which at least one component is negative. Since the non-negativity is a physiological condition, we can conclude that any muscle activation, except the case in which no muscle was activated, must have a necessary component of null space required to satisfy the non-negativity condition. This observation is true also if only one of the two antagonistic muscles are activated. Therefore, any physiological activation lead to a modulation of the null space, with a consequent modulation of the stiffness, as noticed in the literature (Burdet et al., 2013).

If a third muscle, whose action is parallel to one of the others (e.g. the flexor), is added to the model (Figure 3.23), the muscle space become tri-dimensional and the  $H$  matrix become:

$$H = \begin{bmatrix} -1 & -1 & 1 \\ 0 & 0 & 0 \end{bmatrix}$$

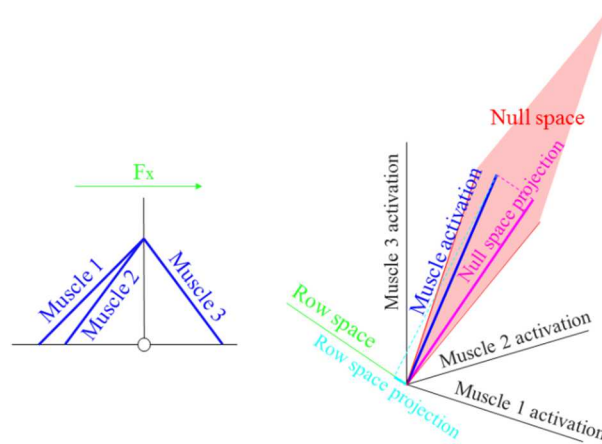


Figure 3.24: Example of the identification of the projection of the muscle activation onto the row and the null spaces. Left: model made of one joint and three muscles two muscles ('Muscle 1' and 'Muscle 2', blue lined) antagonist to a third one ('Muscle 3'). The positive direction of the force is represented as a green arrow ( $F_x$ ). Right: The muscle space on whose axes are reported the muscle activations (Muscle 1 on the x axis, Muscle 2 on the y label, and Muscle 3 on the z label). The null (red plane) and row (green line) spaces are identified. An example of muscle activations ( $[0.1 \ 0.4 \ 0.8]$ , blue) together with its projection on the null (magenta) and the row (cyan) spaces are reported.

The force space remains mono-dimensional, because the force could be exerted along only one axis, and the force vector becomes  $H^+ = \begin{bmatrix} -0.58 \\ -0.58 \\ 0.58 \end{bmatrix}$ . The dimensionality of the null space grows from 1 to 2 and its components are:  $n = \begin{bmatrix} -0.58 & 0.58 \\ 0.79 & 0.21 \\ 0.21 & 0.79 \end{bmatrix}$ . However, since the stiffness space is still mono-dimensional, because the only stiffening around the single joint, that is the stiffening along the x component, is possible, we could decompose the null space into a component that generates the stiffness (stiffness space) and a component that does not generate neither the stiffness nor the force.

However, the stiffness space, or in this case the stiffness vector, is not easy to be mathematically discriminated in the muscle space. On the other hand, the null space, and consequently the projection of the muscle activation onto the null space, can be easily determined based on the  $H$  matrix. Therefore, the question of this chapter is how the projection of the muscle space into the null space may approximate the exerted stiffness, or, in other words, how much is the contribution of those components that does not generate neither force nor stiffness.

The  $H$  matrix, otherwise called EMG-to-force matrix, describes the combination of different effects.

- $\boldsymbol{\mu} = \alpha \cdot \boldsymbol{m}$ , describes the relation between the activation  $\boldsymbol{m}$  of a muscle and force  $\boldsymbol{\mu}$  it exerts, where  $\alpha$  is the scalar. This relation is non-linear and  $\alpha$  depends on the muscle length, the muscle activation, and the contraction velocity, as described in the paragraph 3.1.1.
- $\boldsymbol{\tau} = J_{\mu}^T \cdot \boldsymbol{\mu}$ , describes the relation between the force  $\boldsymbol{\mu}$  exerted by each muscle and the joint torques  $\boldsymbol{\tau}$ , where  $J_{\mu}^T$  is the transpose of the Jacobian matrix. This relation is non-linear and the Jacobian of the muscles depend on the joint configuration, on the attachment of muscles on the bones and on the muscles geometry.
- $\boldsymbol{f} = (J^T)^+ \cdot \boldsymbol{\tau}$ , describes the relation between the joint torques  $\boldsymbol{\tau}$  and the required end-point force  $\boldsymbol{f}$ , where  $(J^T)^+$  is the pseudo-inverse of the transpose of the Jacobian matrix. This relation is non-linear and the Jacobian depends on the limb configuration.

Therefore, the EMG-to-force matrix is the combination of three different non-linear functions:

$$H = (J^T)^+ \cdot J_{\mu}^T \cdot \alpha \quad (4.2)$$

However, even if the relation between the muscle activations and the end-point force is not linear, in literature it was commonly approximated to be linear for low muscle activations during isometric tasks (Borzelli et al., 2013; Osu & Gomi, 1998; Valero-Cuevas et al., 2009).

In this paragraph the projection of the muscle activation onto the null space of  $H$ , is calculated and a linear relation between the end-point stiffness and the null space projection of the muscle activation is tested.

### 3.3.2 The model of 2 joints and 6 muscles

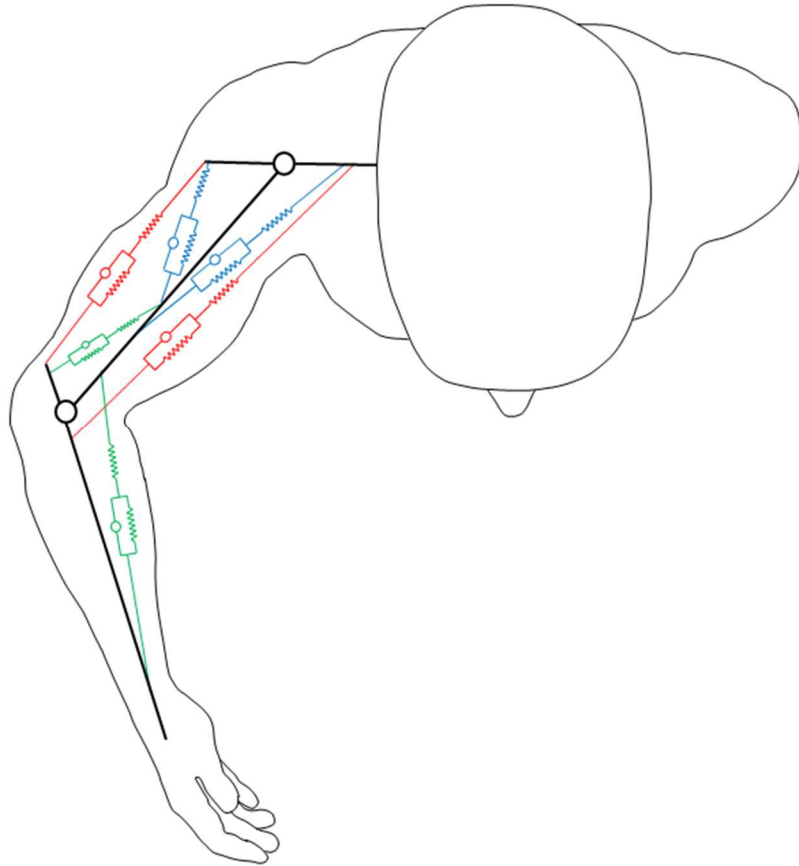


Figure 3.25: Elbow shoulder system approximated with a 6M2J musculoskeletal model. The muscles (shoulder mono-articular in blue, elbow mono-articular in green and bi-articular in red) are approximated with Hill muscle model.

The model presented in this chapter is composed of two joints on which six muscles acts on. In this study, the parameters were selected to approximate the arm limb, but the same model and different parameters could approximate other limbs like the ankle-knee joints and the knee-hip joints.

The 6 muscles (Figure 3.25) were selected as in (Osu & Gomi, 1999) and are two mono-articular, only acting on the elbow joint (brachioradialis, BRD, as a flexor and the lateral head of triceps brachii, TriLat, as an extensor), two mono-articular, only acting on the shoulder joint (pectoralis major sternal, PecMaj, as a flexor and the posterior deltoid, DeltP, as an extensor), and two bi-articular, acting both on the shoulder and elbow joints (biceps brachii short head, BB, as a flexor and the long head of triceps brachii, TriLong, as an extensor) (Figure 3.26). Muscles are modeled with the Hill musculo-tendon model (see Paragraph 3.2). The

Hill model parameters of the mono-articular muscles acting on the elbow joint are reported in Table 3.1, and their attachments on the bones are reported in Table 3.2. The Hill model parameters, gotten from literature (Holzbaur et al., 2005) for the mono-articular muscles acting on the shoulder joint and of the bi-articular muscles are reported in Table 3.3, and the attachments on the bones are reported in Table 3.4. The PecMaj origin attach is in the sternal half of the clavicle and the insertion attach on the humerus. The DeltP origin attachment is in the scapula and the insertion attachment on the humerus. The Biceps brachii short head origin attachment is a coracoid process of the scapula and the insertion attachment on the radial tuberosity of the radius. The TriLat origin attach is in the scapula and the insertion attach on the ulna. The length of the humerus was set to be 0.30 m, while the forearm is set to be 0.25 m length. Both the humerus and forearm lengths were obtained from the Stanford VA Upper limb model developer for OpenSIM®, which used the muscle characteristics reported in (Holzbaur et al., 2005) and used in this study.

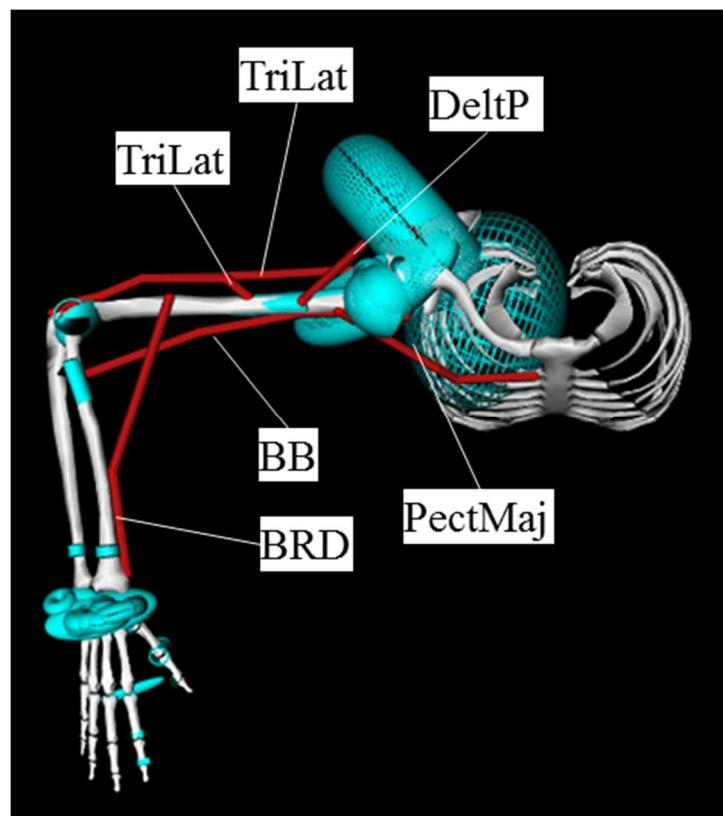


Figure 3.26: The elbow-shoulder system and the modeled muscles.

The muscle space dimension of this model is 6 DOF because 6 muscles were modeled. The shoulder is abducted at  $90^\circ$  and the model could exert forces only along the horizontal plane, then the force space was 2 DOF. Consequently, the null space was 4 DOF (6 muscle space DOF – 2 force space DOF), 3 of which were the dimension of the stiffness space. Therefore, in this case, the dimensionality of the component of null space that does not exert any stiffness is 1 DOF (4 null space DOF – 3 stiffness DOF). The arm was imagined lying on a surface, therefore no muscle action for gravity compensation are required.

Table 3.4: Hill muscle parameters get from literature.

	Mono-articular muscles acting on shoulder		Bi-articular muscles	
	1: flexor (PecMaj)	2: extensor (DeltP)	1: flexor (BB)	2: extensor (TriLong)
$F_{MAX}$ (N)	364.41	259.88	435.56	798.52
$l_{ceopt}$ (m)	0.1442	0.1367	0.1157	0.1340
$l_{p0}$ (m)	0.1442	0.1367	0.1157	0.1340
$l_{s0}$ (m)	0.0028	0.0038	0.1923	0.1430
Scale factor	0.90	0.70	0.95	0.95
Scaled $l_{ceopt}$ (m)	0.1298	0.0957	0.1099	0.1273
Scaled $l_{p0}$ (m)	0.1298	0.0957	0.1099	0.1273
Scaled $l_{s0}$ (m)	0.0025	0.0027	0.1827	0.1358
$k_p$ (N/m)	600	1433	170	700
$k_s$ (N/m)	$163 \cdot 10^3$	$390 \cdot 10^3$	$46 \cdot 10^3$	$191 \cdot 10^3$

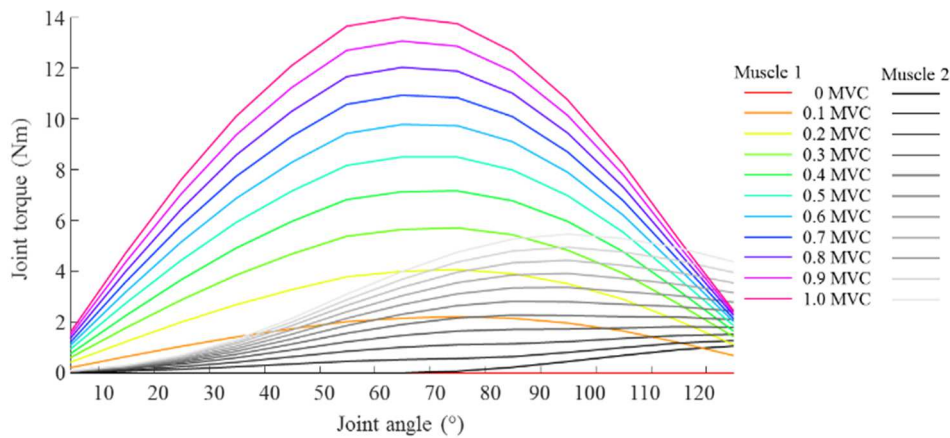


Figure 3.27: Relation between the torque related to the elbow flexion, exerted by the two antagonistic muscles, at different level of activation of muscle 1 (colored) and 2 (gray scale). Muscle activations are not equally spaced.

Table 3.5: Distance between the joint centers of rotation and the connection between the muscles and the bones. The origin attach is intended as the distance between the connection of the origin side of the muscle with the bone, while the insertion attach is intended as the distance between the connection of the insertion side of the muscle with the bone (see Figure 3.1).

	Mono-articular muscles acting on shoulder		Bi-articular muscles	
	1: flexor (PecMaj)	2: extensor (DeltP)	1: flexor (BB)	2: extensor (TriLong)
<b>Origin attach (m)</b>	0.042	0.110	0.037	0.010
<b>Insertion attach (m)</b>	0.071	0.056	0.039	0.041

### 3.3.3 Model simulations

The arm limb motion is only on the horizontal plane. The elbow  $0^\circ$  is set when the forearm and the arm are aligned, and higher angles are achieved with higher elbow flexions, as defined in Paragraph 3.2.1. The shoulder  $0^\circ$  is set when the arm and the shoulders are aligned, and higher shoulder angles are achieved with higher shoulder flexions.

The physiological ranges of the motion of the elbow and shoulder joints were reported in literature (Iannotti & Parker, 2013): the elbow range is between  $0^\circ$  and  $130^\circ$  and the shoulder range between  $-40^\circ$  and  $125^\circ$ . However, the model cannot be used for the whole range of motion because of some intrinsic limitations. In fact, if one of the joint is completely extended, the modeled mono-articular muscles, acting on it, cannot exert any force, because the moment arm is zero. However, in literature, a force could be exerted also for joint angles close to the boundaries, because the moment arm never goes to zero due to the real shape of the muscles. Furthermore, the presented model cannot approximate the forces exerted by the shoulder joint for negative angles. Thus, the elbow and shoulder angles are reduced with respect to the values found in literature. The elbow and shoulder joint angles range of motion are fixed both to be between  $5^\circ$  and  $125^\circ$ . However, the range of motion of this model span, fit the joint angle range in which manufacturing workers are recommended to operate, so as to avoid uncomfortable and non-ergonomic positions. Both the elbow and shoulder joint work-spaces are subdivided into 13 steps of  $10^\circ$ , then the model is displaced in 169 end-point configurations (Figure 3.28).

The activation of each muscle was set to assume a value equal to 0, 0.1, 0.2, 0.3, 0.4, 0.5, 0.6, 0.7, 0.8, 0.9, or 1.0 times the Maximum Voluntary Contraction (MVC). All the possible combinations of muscle activations (1771561) were tested when the limb is displaced in any of the 169 end-point configurations.

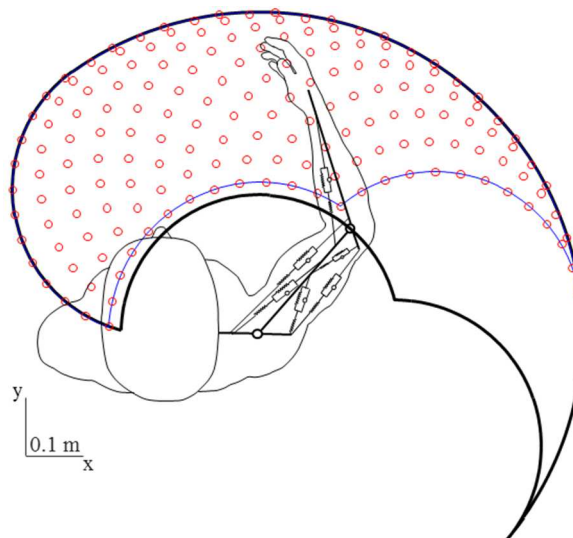


Figure 3.28: Workspace of the upper limb model. The physiological workspace (black line) and the workspace of the model (blue line) are plotted. The positions in which the endpoint stiffness is calculated are reported (red circles).

### 3.3.4 Equations for end-point force calculation

The force exerted by each muscle was calculated from the muscle-tendon length  $l_m$ , estimated from the joint angles, the attached muscle, and the activation  $m$  based on equations (3.1-5).

The equations for the determination of the length of the mono-articular muscles are given in equation (3.5), while the length  $l_{m_b}$  and the moment arm of the bi-articular muscles with respect to the elbow ( $m_{elbow}$ ) and shoulder ( $m_{shoulder}$ ) joints are calculated as:

$$\left\{ \begin{array}{l} l_{m_b} = \sqrt{(l_{i2} \cdot \cos(\gamma) - l_H \cdot \cos(\beta_1) + l_{i1})^2 + (l_H \cdot \sin(\beta_1) - l_{i2} \cdot \sin(\gamma))^2} \\ m_{elbow} = l_{i2} \cdot \sin \alpha_1 \\ m_{shoulder} = l_{i1} \cdot \sin \delta \end{array} \right. \quad (3.7)$$

Where  $l_H$  is the length of the humerus,  $l_{i1}$  and  $l_{i2}$  are respectively the origin and the insertion attachment of the muscle on the bone,  $\gamma$  is equal to the sum of the elbow ( $\alpha$ ) and the shoulder ( $\beta$ ) angles for the BB muscle and to the sum of their supplementary for the TriLat muscle, and  $\beta_1$  is equal to the shoulder angle for the BB muscle and to its supplementary for the TriLat muscle,

$$\delta = \text{asin}\left(\frac{l_H \cdot \sin \beta}{c}\right) + \text{asin}\left(\frac{l_{i2} \cdot \sin\left(\alpha - \text{asin}\left(\frac{l_{i1} \cdot \sin \beta}{c}\right)\right)}{\sqrt{c^2 + l_{i2}^2 - 2c \cdot l_{i2} \cdot \cos\left(\alpha - \text{asin}\left(\frac{l_{i1} \cdot \sin \beta}{c}\right)\right)}}\right)$$

$$\alpha_1 = \alpha + \beta + \delta - \pi$$

$$c = \sqrt{l_{i1}^2 + l_H^2 - 2 \cdot l_{i1} \cdot l_H \cdot \cos \beta}.$$

### 3.3.5 Equations for end-point stiffness calculation

Even if the paradigm, commonly performed in literature to experimentally measure the end-point stiffness, consists of a displacement of the end-point and the measure of the consequent exerted force (Hogan, 1985), in this simulation the displacement was applied to the joints and not to the end-point. Since the angular deflection applied to the joints was assumed small enough to approximate the angle-muscle torque curve with a linear relation (see Paragraph 3.2.3.4), this discrepancy with the

literature is expected to have no influence on the calculation of the end-point stiffness. On the other hand, displacing the joints instead of the end-point leads to a reduction of the calculation time.

The end-point stiffness  $K$  was calculated as the ratio between the end-point force variation  $\Delta F$  with respect to the end-point displacement  $\Delta \varepsilon$ :

$$K = \frac{\Delta F}{\Delta \varepsilon} \quad (3.8)$$

The force variation  $\Delta F$  was calculated as the difference between the end-point force exerted during the deflected displacement with respect to the one exerted during the un-deflected displacement. However, in this study, the component of end-point force generated by the passive elements are neglected and the force variation  $\Delta F$  was calculated as the difference between the force generated by only active elements of the muscles, exerted during the deflected displacement respect with the one exerted during the un-deflected displacement. Since the torque exerted by passive elements depends on their length, and the applied deflection is small, small changes in the passive elements length was expected. Then, approximating the force exerted by passive element with constant values during deflected and un-deflected conditions is expected to have no influence on the calculation of the end-point stiffness.

The equation for the description of an ellipse, centered in the origin is:

$$\frac{x_1^2}{a^2} + \frac{y_1^2}{b^2} = 1 \quad (3.9)$$

Where  $a$  and  $b$  are the major and minor axes of the ellipse, and  $x_1$  and  $y_1$  are the axes, rotated of an angle  $\alpha$ :

$$\begin{cases} x_1 = y \cdot \sin \alpha + x \cdot \cos \alpha \\ y_1 = y \cdot \cos \alpha - x \cdot \sin \alpha \end{cases} \quad (3.10)$$

Therefore, a rotated ellipse centered in the origin is univocally defined by three points that identify the major and the minor axes and their rotation with respect to the reference system.

Three end-point deflections were applied to calculate the stiffness ellipse parameters. The deflections were defined as three different combinations of elbow and shoulder angular deflections that are:

- deflection applied to the elbow joint:  $0.01^\circ$ , deflection applied to the shoulder joint:  $0.01^\circ$ ;
- deflection applied to the elbow joint:  $-0.01^\circ$ , deflection applied to the shoulder joint:  $-0.01^\circ$ ;
- deflection applied to the elbow joint:  $0.01^\circ$ , deflection applied to the shoulder joint:  $-0.01^\circ$ .

Muscle activations are kept constant.

The stiffness ellipse is calculated for each of the 169 upper limb postures and each of the 1771561 muscle activations.

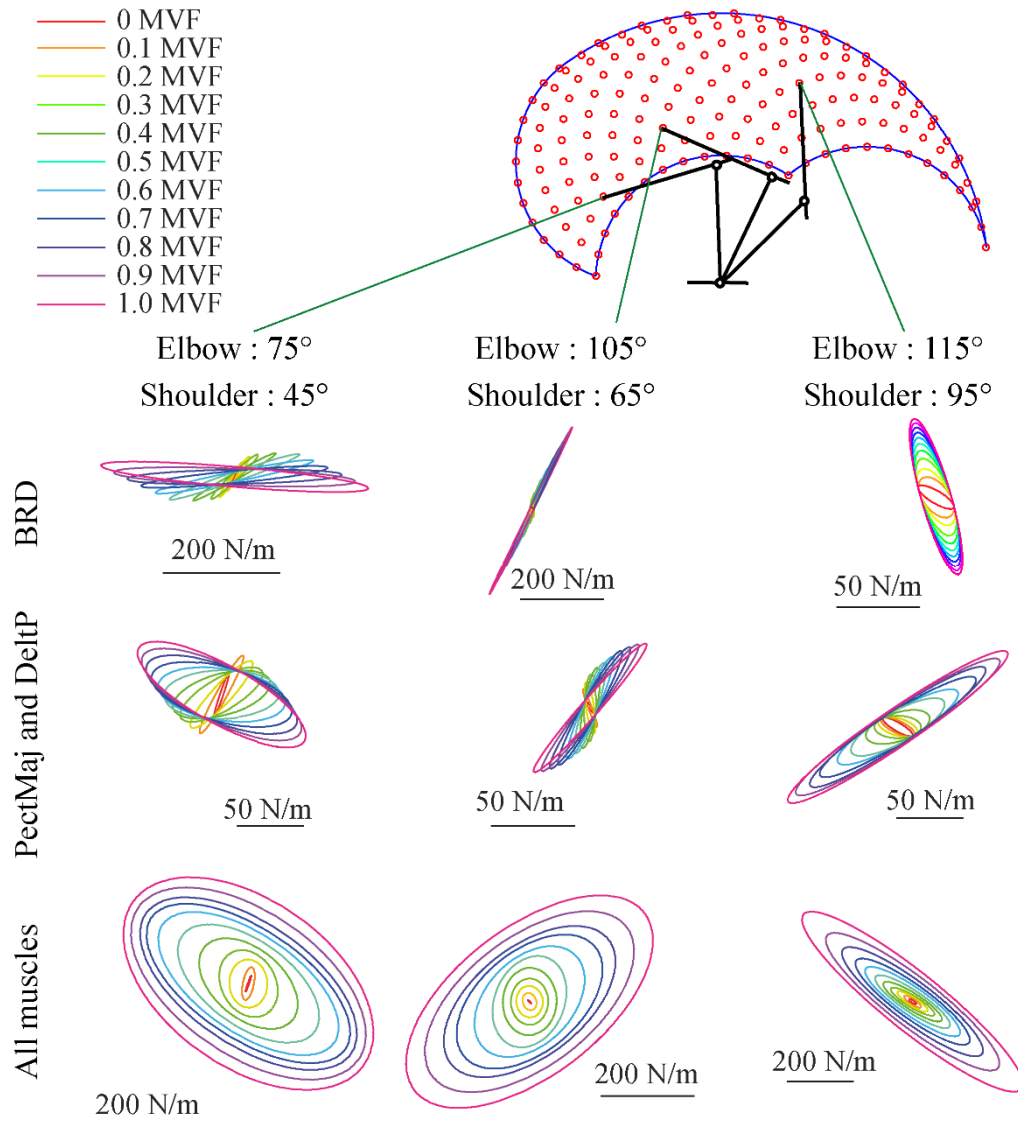


Figure 3.29: Examples of end-point stiffness calculated for different arm configurations and muscle activations. In the first column, the only BRD muscle is activated at different levels, while all the other muscles have a zero activation. In the second column, both the PectMaj and the DeltP are activated of the same value, while all the other muscles have a zero activation. In the third column, all the muscles are activated of the same activation. Different values of activations are color coded.

### 3.3.6 The projection of the muscle activation onto the null space

The matrix  $H$ , which maps the muscle activation onto the end-point force, was calculated as the regression of the muscle activation onto the end-point force, using

the Matlab function *regress*. Since the matrix depends on the joint configuration, an H matrix was calculated for each unperturbed limb configuration.

The regression was computed based on the only muscle activations in which any of the muscle activation are equal or lower than  $i$ , where  $i = 0.1, 0.2, 0.3, 0.4, 0.5, 0.6, 0.8, \text{ or } 1.0$ .

The null space  $N$  of the H matrix, was calculated with the Matlab function *null* and the projection  $n$  of the muscle activation onto the null space was calculated for each muscle activation as:

$$n = N^T \cdot N \cdot m \quad (3.10)$$

The value of  $n$  coincides with the component of the muscle activation that generates the end-point stiffness only if the component of  $n$  which does not generates any end-point stiffness is zero.

### 3.3.7 The stiffness ellipse fitting

The linear relation between the projection of the muscle activation onto the null space, with respect to the major axis and the minor axis of the stiffness ellipse, calculated from the end-point force exerted by muscles, was tested. Since the null space could be related both to the major axis and minor axis, which are independent, the linear relation between the projection of the muscle activation onto the null space with respect to the end-point stiffness ellipse area (i.e. the product of the major and the minor axes, scaled by  $\pi$ ), was tested.

The slope of the regression of the projection of the muscle activation onto the null space with respect to the axes of the stiffness ellipse and its area were calculated. The Variance Accounted For (VAF) tested the reconstruction of the major axis, minor axis and area of the stiffness ellipse with respect to the projection of the muscle activation onto the null space, scaled by the regression slope.

The linear relations are performed on the null space projection of those muscle activations where the muscle has an activation lower than the threshold  $i$ , where  $i = 0.1, 0.2, 0.3, 0.4, 0.5, 0.6, 0.7, 0.8, 0.9, \text{ or } 1$  (see Table 3.5).

Table 3.6: VAF calculated if the stiffness ellipse major axis, the minor axis or the area are approximated as the product of the null space projection of the muscle activation for the regression slope, averaged among end-point positions. The regression is performed for those muscle activations whose activation of each muscles is lower than the selected value in the first column.

Maximum activation of each muscle	VAF, muscle stiffness ellipse		
	Major axis	Minor axis	Area
<b>0.1</b>	0.7618	0.4866	0.4510
<b>0.2</b>	0.7470	0.4136	0.3552
<b>0.3</b>	0.7412	0.4011	0.3075
<b>0.4</b>	0.7277	0.4103	0.2791
<b>0.5</b>	0.7261	0.4252	0.2708
<b>0.6</b>	0.7250	0.4394	0.2581
<b>0.7</b>	0.7251	0.4491	0.2522
<b>0.8</b>	0.7297	0.4522	0.2499
<b>0.9</b>	0.7258	0.4519	0.2419
<b>1.0</b>	0.7242	0.4510	0.2195

The discrepancies between the end-point stiffness and the null space projection of the muscle activation could not be ascribed only to the null space component that does not generate end-point stiffness, but also to the end-point stiffness component generated by the force exerted by the parallel passive element.

The high values of VAF ( $> 0.7$ ) was identified only for the reconstruction of the major axis of the ellipse, but this model could not estimate the minor axis nor the area of the ellipse.

In conclusion, the proposed method consists in an initial calibration. The operator, who wears the exoskeleton, was asked to assume a set of defined poses. When the operator is assuming one of the requested poses, the exoskeleton stiffens to allow the operator to exert isometric end-point forces. The EMG-to-force matrix was calculated as the regression of the recorded EMG signals to the end-point forces. The null space of the EMG-to-force matrix was then calculated.

The calibration will be used to approximate the end-point stiffness ellipse major axis with the real-time projection of the muscle activation into the EMG-to-force matrix null space. This method can be implemented to the exoskeleton real-time estimate of the end-point stiffness the operator is exerting, without applying the common paradigm for which an end-point displacement is needed.

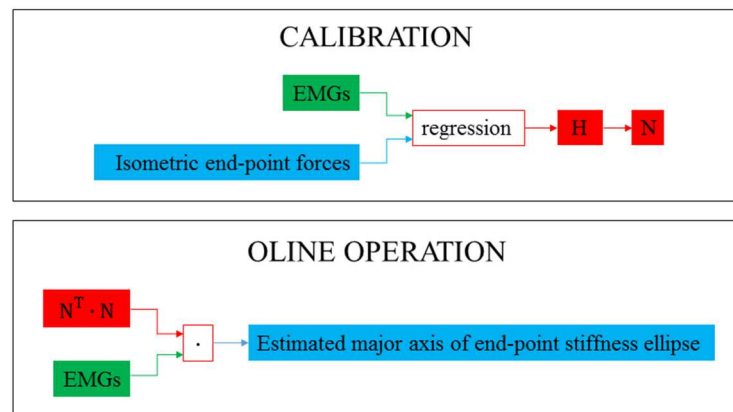


Figure 3.30: Diagram of the calibration and the online estimation of the major axis of the end-point stiffness ellipse. During the calibration (upper panel) the EMG-to-force matrix ( $H$ ), and consequently its null space ( $N$ ), is calculated from the regression of the recorded EMG signals onto the exerted isometric end-point forces. During the online operation (lower panel) the null space component of the recorded EMG signals, obtained multiplying the EMG signal for  $N^T \cdot N$ , is used to estimate the major axis of the end-point stiffness ellipse the subject is exerting.

## Chapter 4

# The exoskeleton command logic

The musculo-skeletal model developed in Chapter 3 validated the approximation of the end-point stiffness exerted by the operator with the null space component of the muscle activations. In this chapter, the stiffness the operator intends to exert is assumed to be known, therefore, the behavior of the exoskeleton is proposed.

Since the human arm is a redundant system both in terms of exerted force (intended as the force exerted during isometric tasks or the force that generates a movement during dynamic tasks) and exerted stiffness, the same end-point force and stiffness could be achieved with a virtually infinite different combination of muscle activations (see Paragraph 3.3.1). Thus, even if the action the operator is exerting is known, the muscles activation that generate it cannot be uniquely estimated.

Different models for the muscle recruitment were proposed, based on the minimization of the global muscle activation (Fagg et al., 2002; Todorov & Jordan, 2002) on the recruitment of fixed groups of muscles, independent from the task (i.e. muscle synergies or motor primitives model) (Bizzi & Cheung, 2013; Overduin et al., 2008), or on the recruitment of groups of muscles depending on the task (the uncontrolled manifold model) (Latash et al., 2002). However, this argument is still debated (Tresch & Jarc, 2009) and the scientific community still do not agree on the model that describes the CNS laws for muscle pattern recruitment. On the other hand, the actions the exoskeleton exerts may modify the operator muscular recruitment. For these reasons a model of the logics implemented by the operator to recruit his muscles, cannot be developed. Therefore, the identification of the best logic to control the exoskeleton (i.e. the ‘Command logic’ block in Figure 2.2) cannot be identified on a model but must be experimented on human subjects.

The arm is a complex system composed of four degree of freedom (3 of the shoulder and 1 of the elbow) with more than 20 muscles acting on them, some of which are deep muscles whose activation cannot be recorded with surface EMG.

Therefore, the musculo-skeletal high redundancy makes the most efficient control logic of the exoskeleton proposed in this thesis, hard to be identified, because of the huge number of uncontrolled variables. Therefore, a joint whose redundancy is lower with respect to the arm (i.e. the wrist) was considered in the experimental session, extending the obtained results to other more complex limbs, like the arm. The identification of the best command logic was performed based on more different kind of parameters, which were both subjective and objective and were calculated during both dynamic and static tasks. Consistent results among different analysis may let us to expect the results obtained with the wrist may be extended to other joints, even if future works are required.

Based on the classifications described in the Paragraph 2.1, the experimental paradigm may regard an isometric or dynamic task on which spiky or continuous instabilities perturb the system. The main disadvantage of an isometric task is that it allows the investigation on a finite number of discrete joint displacements only, while a dynamic task allows the continuous span of the whole space work. Therefore, a dynamic task was selected for this purpose.

Since the operator compensates spiky instabilities based on his experience on the amplitude and occurrence of the perturbation, a paradigm with spiky perturbations would be highly affected by the learning process of the operator. Thus, a continuous instability was introduced to perturb the system.

Therefore, an experimental paradigm was designed in which the subject was asked to perform a tracking task with his wrist, connected to a torque sensor, while a continuous torque disturbance was applied. Different control logic for reducing the disturbance were tested to identify the best logic the exoskeleton should have implemented to help the operator during a stiffening task.

## **4.1 The Hi5**

The test bench, on which the command logics of the exoskeleton were tested, was the Hi5 aptic interface, developed by the Department of Bioengineering of the Imperial College of London. The Hi-5 device was described in detail in (Melendez-Calderon et al., 2011). In this paragraph, the major characteristics were reported.

The system (Figure 4.1) consists of a wrist interface fixed to a table on which the subject place his arm, holds a handle and interacts with wrist flexion/extension

movements. The interface is equipped with a DC motor that allows the experimenter to impose external torques to the wrist joint.

A 22" monitor was placed in front of the device to provide a visual feedback to the subjects. Depending on the experimental requirements, the subjects can be provided with visual cues indicating their wrist position, the applied force, movement performance or muscle activity during the task.



Figure 4.1: The Hi5 system.

#### 4.1.1 Mechanical specifications

Direct drive actuation was selected to achieve backdriveability and a torque of 10Nm was considered to be sufficient for the studies implemented on this setup, based on (Delp et al., 1996).

A DC motor (MSS8, Mavilor) capable of producing a peak torque of 15Nm ( $T_{max}$ ) was chosen for the system. The motor is current-controlled using a DC brush motor amplifier (413C, Copley). The interface is equipped with a 5000 cpr (cycles per revolution) differential encoder (RI 58-O, Hengstler). A torque sensor (TRT-100, Transducer Technologies) with a measuring range of 100 in-lbs (11.29Nm) is mounted between the rotating shaft and the handle (Figure 4.2).

High-quality ABEC-5 ball bearings were selected to minimize friction and backlash in the system.

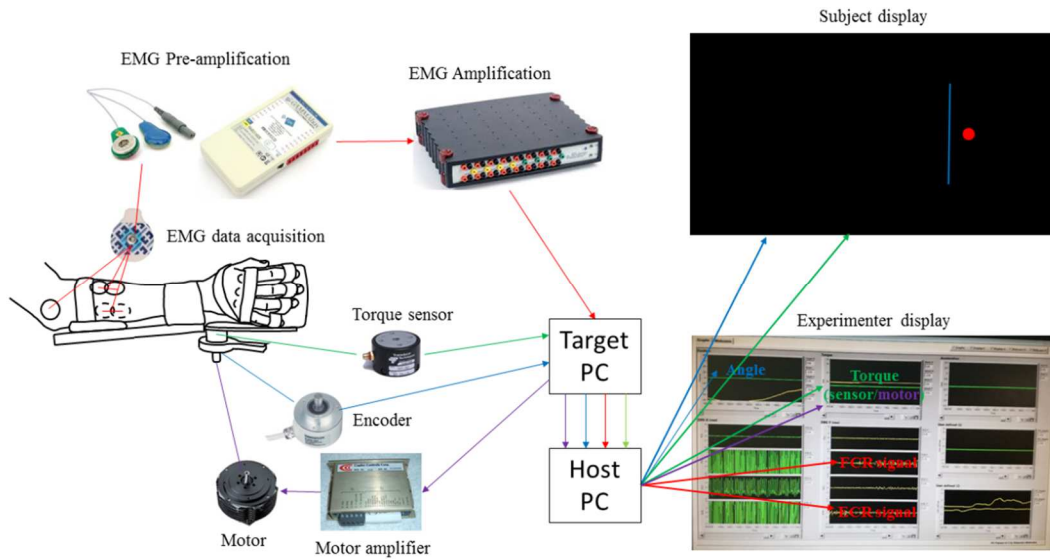


Figure 4.2: Setup.

#### 4.1.2 Software and control

The system is controlled using Labview Real-time v11.0. A dedicated computer (target PC) running on a Real-Time OS reads the sensor inputs, processes them, and sets the outputs (motor command to the servo amplifier, emergency latch) through a data acquisition card (DAQ-PCI-6221, National Instruments) under a 1kHz loop. Data can be saved at either 1kHz or at a selected lower frequency in the target PC. A graphical user interface, on which the experimenter monitors the subjects' performance, is implemented on a second computer (host PC) that runs Windows 7. Data is sent from target to host PC at 66.6 Hz via an Ethernet network. The host PC is equipped with a two dual-graphics cards (NVIDIA Quadro NVS 295) that allows independent control up to four displays (two for the experimenter one for the participant that uses the interface and the last for a possible other participant that uses the twin interface).

The system is implemented with predefined functions to facilitate the programming of customized experimental protocols. These functions include automatic normalization of EMG signals based on maximal voluntary contraction/torque; automatic torque sensor calibration; inertia compensation; predefined control modalities such as position, impedance, torque; friction compensation; and modifiable safety parameters.

### **4.1.3 Ergonomic aspects**

The handle position could be adjusted in order to align either the wrist or the fingers with the mechanism's center of rotation, letting the same device to be used as an aptic interface both of the wrist and of the fingers. The handle used during experiments on the wrist, is designed with an ergonomic finger shape such to minimize finger contractions when stiffening the wrist joint and, consequently, minimizing artifacts in the EMG recordings due to cross-talk with finger muscles. Therefore, the handle shape constrains the subject's hand to assume a slightly flexed and abducted position, which makes finger flexion difficult and therefore forces the subject to use mostly wrist flexors/extensors muscles.

The Hi5 is designed such that EMG recordings can be performed easily on Flexor/Extensor Carpi Radialis and Ulnaris. The muscle activity of the subjects is monitored using a medically certified non-invasive 16-channel sEMG (g.GAMMAclip+g.BSamp +g.GAMMABox, g.Tec).

### **4.1.4 Redundant safety**

The interface has adjustable mechanical constraints to prevent hyper flexion/extension of the wrist. Electro-mechanical switches attached to these constraints halt the current flow to the DC motor. Emergency switches are at reach to both the experimenter and the participants.

Electronic circuits limit the maximum current supplied to the motor. Redundant sensors and a software program monitor system failures or faults. A watchdog circuit is implemented to immediately halt the system ("OFF state") when any safety issue is detected. This prevents high torques to be applied to the human wrist. To return the system to an "ON state", a reset button must be pressed. This button is accessible only to the experimenter.

The system has been approved for its use in motor learning/control experiments by the Ethics Committee at Imperial College of Science Technology and Medicine and has been assessed successfully by the Health and Safety Committee at the Department of Bioengineering of the same institution.

### **4.1.5 Real-time performance**

The robustness of the real-time configuration was tested and its results were reported in (Melendez-Calderon et al., 2011). A ten-minute test, on which the real-time system had to execute high-demanding tasks for both CPU processor and RAM memory, was performed. The execution time within the control loop was monitored at every iteration. In 93% of the cases it was comprised between 0.99ms and 1.01ms (i.e. it had 1% error or less), and it was always between 0.95ms and 1.05ms (i.e. the maximal error was less than 5%).

## **4.2 Experimental protocol**

### **4.2.1 Participants**

Nine subjects, aged between 24 and 34 ( $27.7 \pm 4.0$ ), 5 males and 4 females, participated in the experiment.

All subjects were naïve to the experiment conditions and had no known disorders or recent injury on the right wrist. The experiments were performed at the Department of Bioengineering of Imperial College, London. The study was approved by the ethical committee of Imperial College London and all subjects gave their informed consent prior to participation.

### **4.2.2 Setup**

Experiments were conducted on the aptic interface Hi5 (Fig 4.3A).

Two steel bars can be adjusted to correspond to each subject's wrist range of motion (Figure 4.3B-C). The monitor, placed in front of the subject, gave a feedback of subject's wrist angle or of the torque that the subject exerted to the wrist (Figure 4.3D). Wrist extensions, and the corresponding torques exerted during a wrist extension, were considered positive, while wrist flexions, and the corresponding torques exerted during a wrist flexion, were considered negative. Wrist angular position and torque were recorded at 100 Hz (Figure 4.3E). Surface electromyographic signals (sEMG) of the Flexor Carpi Radialis (FCR) and the

Extensor Carpi Radialis longus (ECR) muscles were collected at 1000 Hz and resampled at 100 Hz (see Surface Electromyography, Paragraph 4.2.3).

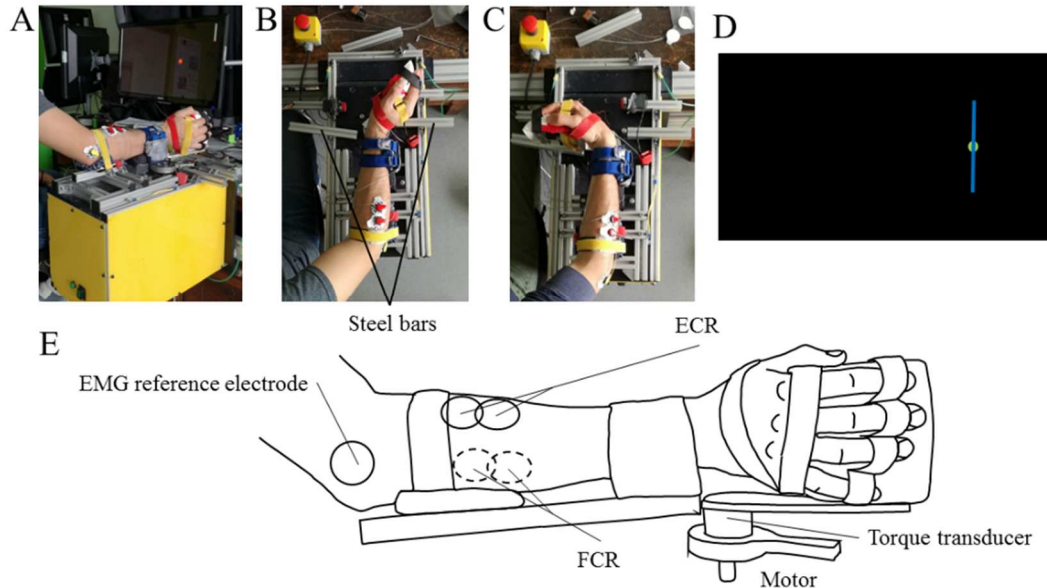


Figure 4.3: Setup. A. The Hi5 interface. B. Wrist completely extended, the steel bars against which the subject exerted the isometric force are indicated. C. Wrist completely flexed. D. An example of the scene shown by the display. E. Scheme of the setup in which the torque sensor, the motor, and the EMG positioning are indicated.

### 4.2.3 Surface electromyography

sEMG was measured from FCR and ECR (Figure 4.4), which are prime movers of the wrist flexion and extension in a midway position (Melendez-Calderon et al., 2015).

The electrode position was determined for each muscle using functional maneuvers, and the area was cleansed with alcohol. Disposable pre-gelled adhesive electrodes (Kendall/Tyco H135SG) were fixed to the subject's skin (inter-electrode distance:  $\sim 1$  cm) and a ground electrode was fixed on the subject's lateral epicondyle. The EMG signals were pre-amplified using active clip connectors (g.GAMMAclip + g.GAMMABox, g.Tec, Austria) and amplified using a medically-certified amplifier (g.BSamp, g.Tec, Austria). Signals were recorded at 1000 Hz using a National Instrument data acquisition card (NI 6221, National Instruments, USA). EMG data were processed offline for subsequent analysis. A zero-lag fourth-order 20–500 Hz band-pass Butterworth filter was first used to filter out cable movements' artifacts and high frequency noise components. The

signal was then rectified and low-pass filtered using a zero-lag fourth order Butterworth filter with 5 Hz cut-off frequency.

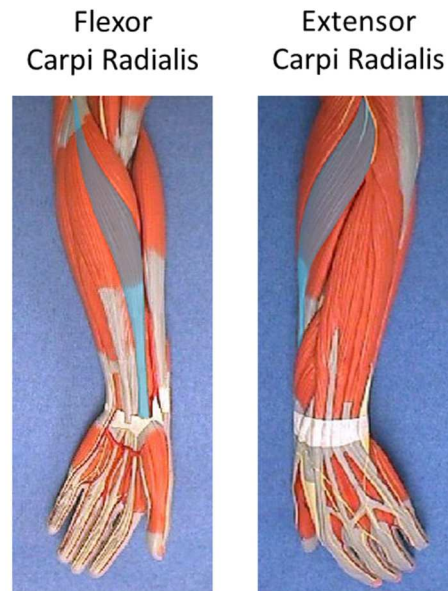


Figure 4.4: Muscles recorded. FCR on the left, ECR on the right.

#### 4.2.4 Protocol

The experiment was composed of five sessions for each subject, performed in different days. Figure 4.5 visually describe the protocol. After the identification of the zero and the wrist range of motion, the maximum co-contraction was measured and used to normalize the EMG signals. Then the maximum voluntary torques of flexion and extension were calculated to normalize the force. Seven isometric tasks, in which the subject was asked to reach a torque target, alternated with six tracking tasks, in which the subject was asked to move his wrist tracking a virtual cursor while an external perturbation was applied. The perturbation level depends on the session. Finally, the subject was asked to exert the maximum voluntary torques of flexion and extension again.

The number of tracking tasks, and consequently the number of isometric tasks, was defined based on the results of four pilot experiments. During the pilot experiments, isometric tasks were alternated with tracking tasks with Baseline session characteristics in terms of trial duration and perturbation. After any isometric task, the Borg RPE CR10 scale was administered to the subject. The number of

repetitions was selected as that repetition in which the subject experimented a feeling of fatigue that he identifies between 13 ('Somewhat hard') and 15 ('Hard') (see Paragraph 4.2.4.3). Based on these four subjects the number of tracking task repetitions was selected to be equal to 6.

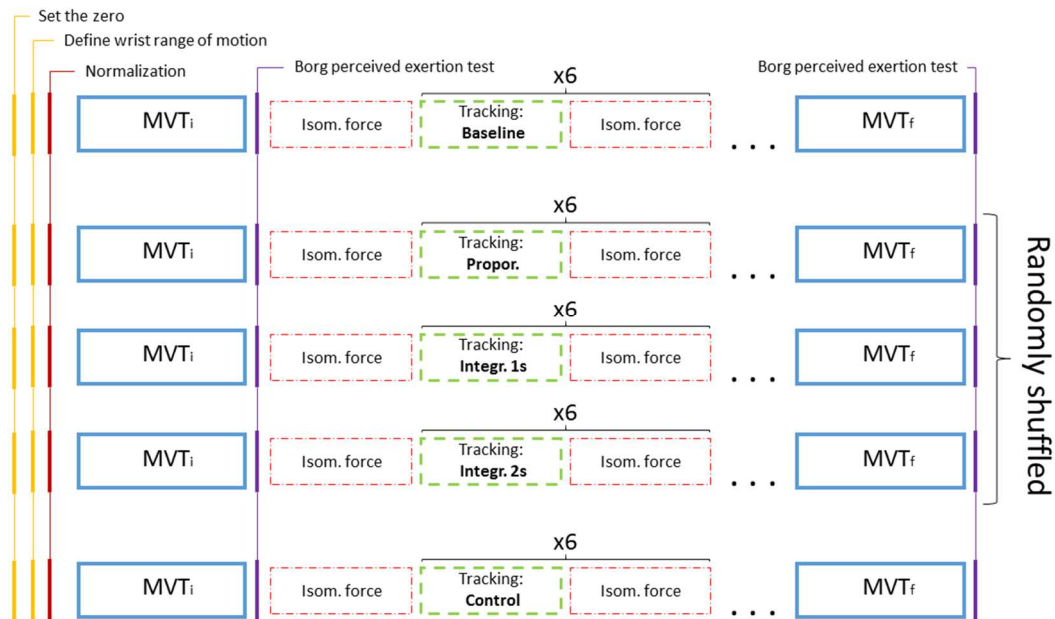


Figure 4.5: Experimental protocol.

#### 4.2.4.1 Zero setting, wrist range of motion definition, and normalization

Subjects hold the Hi5 handle and their forearm and hand were fixed to the device.

At the beginning of each session, subjects were asked to relax their muscles and leave the wrist to assume the most comfortable position. This position was set to be the zero.

Then, subjects were asked to maximally flex and extend their wrist to reach the maximum angle they felt comfortable. Two steel bars were fixed correspondingly to the maximum comfortable flexion (angleF, positive) and extension (angleE, negative) angles, identifying the wrist range of motion (Figure 4.3B-C).

Each subject started the experiment with a four-part EMG calibration procedure, defined in a predefined function, consisting of (Melendez-Calderon et al., 2015): i) relaxation, ii) flexion, iii) extension and iv) co-contraction sessions.

Each part of the calibration lasted for 4 s; the last 2 s of each recording was used to calculate the parameters for the normalization of FCR and ECR. A rest time of 20 s was given between parts. The whole calibration procedure was conducted four times (four calibration sessions), with 60 s of rest given between consecutive sessions to avoid fatigue. In particular, the four parts consisted of:

i) Relaxation: the subject was asked to relax his forearm as much as possible and not to move. The device was blocked at  $0^\circ$  and the subject had visual feedback of the torque he applied to the wrist to motivate them to be relaxed.

ii-iii) Flexion–extension: the subject was instructed to either flex or extend his wrist and keep a constant level of torque. The torque level required from the subject varied from 1 to 4 Nm with 1 Nm step between sessions. A cursor was programmed to respond to individual torque measurements amplified fourfold (i.e. 1 Nm of applied torque moved the cursor by  $4^\circ$ ), which provided the subject with visual feedback of the applied torque level. The subject was asked to apply the force necessary to keep the cursor inside a target.

iv) Co-contraction: the subject was asked to co-activate maximally and to try to keep the cursor within the target positioned at  $0^\circ$  for 4 s. The device perturbed the wrist to help the subject to achieve his maximum voluntary co-contraction (MVCC) level. The perturbation consisted of a  $0^\circ$ -centered, 3 Hz sinusoidal trajectory of  $10^\circ$  amplitude using a PD controller ( $K_p = 28.6 \text{ N}\cdot\text{m}/\text{rad}$  and  $K_d = 0.01 \text{ N}\cdot\text{m}\cdot\text{s}/\text{rad}$ ).

The sEmg data of both FCR and ECR were normalized with respect to the mean maximum co-activation, recorded in iv), while the mean rest value, recorded in i), was subtracted.

#### **4.2.4.2 Initial maximum voluntary torque ( $MVT_i$ )**

After the normalization, the subject was asked to flex his wrist, to exert the maximum torque against the steel bar that was previously set to correspond to the maximum comfortable flexion angle (angleF) and were required to maintain it until

the monitor scene changed. The subject had 10 seconds to reach the steel bar and exert the maximum voluntary torque of flexion (MVTFi). After the exertion of the maximum torque the subject was asked to relax and make his wrist to reach the comfortable position set to zero. After 5 s of rest the subject was asked to extend his wrist, to exert the maximum force against the steel bar which indicates the maximum comfortable extension (angleE) and to maintain it until the scene changed. The subject had 10 seconds to reach the steel bar and exert the maximum voluntary torque of extension (MVTEi). After the exertion of the maximum torque the subject was asked to relax and allow his wrist to reach the comfortable position set to zero, resting for 5 s. The same procedure of exerting the maximum flexion torque and extension torque was repeated a second time.

During the exertion of all the repetitions of maximum torque the subject was encouraged to exert his maximum torque with verbal advises like 'go', or 'more'.

The peak of the torque was calculated for both the two repetitions of the maximum voluntary torque of flexion and the maximum between the two repetitions was defined as the initial maximum voluntary torque of flexion (MVTFi). The peak of the absolute value of the torque was calculated during both the two repetitions of the maximum voluntary torque of extension and the maximum between the two repetitions was defined as the initial maximum voluntary torque of extension (MVTEi).

#### **4.2.4.3 The Borg rating of perceived exertion scale**

In order to identify the subject perceived exertion, the Borg RPE CR10 (Category Ratio) scale was administrated before the beginning of the experiment core.

The Borg rating of perceived exertion (RPE) scale, or Borg perceived exertion test (Borg, 1998), is a subjective qualitative measure of perceived exertion during physical activity. The Borg RPE scale rated the exertion of a patient or an athlete on a scale of 6-20 (see Table 4.1), and it was set based on the general heart rate of a healthy young adult by multiplying by 10. The test administrated to subjects was reported in the Appendix A.

Table 4.1: The Borg RPE CR10 scale

#	Level of exertion
6	No exertion at all
7	
7.5	Extremely light
8	
9	Very light
10	
11	Light
12	
13	Somewhat hard
14	
15	Hard (heavy)
16	
17	Very hard
18	
19	Extremely hard
20	Maximal exertion

#### 4.2.4.4 Visual feedback

Two different visual feedbacks were defined depending on the task: angle for the tracking task or torque for the isometric task.

Tracking: An angle scale factor converted the wrist angle into the cursor position on the monitor. It was defined as the ratio between half of the monitor horizontal size and the highest between angleF and angleE (i.e. the wrist angle boundaries), multiplied by 1.05. The zero wrist angle was visually set at the center of the monitor. Therefore, any wrist angle could be displaced by the monitor.

Isometric: The zero torque was visually set at the center of the monitor. The isometric torque flexion (extension) target, that was 0.2 MVTFi (MVTEi), was displayed in correspondence of the maximum flexion (extension) angle. Therefore, the torque scale factor was set to assure that if the subject was exerting the required 0.2 MVTFi (MVTEi) isometric force, the cursor was in correspondence with angleF (angleE).

#### 4.2.4.5 Isometric force task

A visual feedback of the exerted isometric torque was given to the subject using a blue cursor bar.

A circular target was displayed to the subject in a position corresponding to 20% the MVTFi, with a radius of 2% the MVTFi (red/green circle in Figure 4.6). Therefore, the subject was asked to flex his wrist and to exert a force against the steel bar, to make the linear cursor to reach the spherical target. The target color was red when the cursor was outside the target (i.e. the subject did not match the isometric torque request) and green when the cursor was inside the target (i.e. the subject exerts the requested torque, within the boundaries).

The subject was then asked to maintain the cursor within the target for 2 s continuously and, if subject failed, the countdown was reset.

After succeeding on the isometric flexion exertion, the same procedure was repeated for the exertion of isometric extension torque. A circular target was displayed to the subject in a position corresponding to the 20% the MVTEi, with a radius of 2% the MVTEi.

The subject was then asked to relax making his wrist to assume the zero position for 2 s so as to concentrate before the start of the next session.

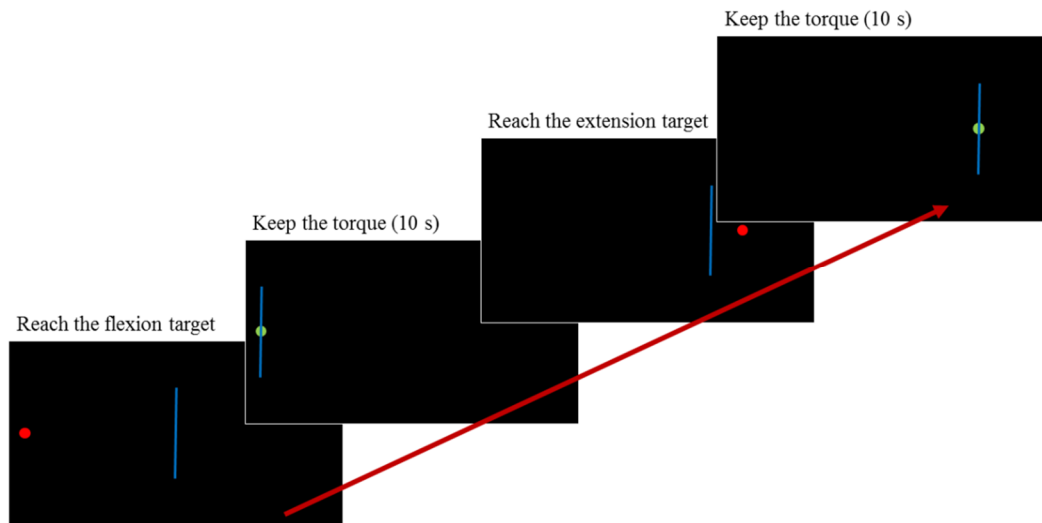


Figure 4.6: Isometric task.

#### 4.2.4.6 Tracking task

After the 2 s rest, subjects were asked to flex/extend their wrist so as to track a spherical target for 30 s. Subjects had a feedback of the wrist angle as the displacement of a blue cursor bar.

The spherical target had a radius corresponding to 2% the minimum between  $angleF$  and  $angleE$ , which were the maximum comfortable angles of flexion and extension identified in Paragraph 4.2.4.1, and moved with a sinusoidal law whose amplitude was 80% the minimum between  $angleF$  and  $angleE$  (see Figure 4.7). The amplitude of the first half of the sinusoid grows with time to permit subjects to better adapt with the task. The target frequency was set such that in 30 s the target made 7 complete sinusoids (frequency 0.23 Hz, Figure 4.7). This frequency allowed subjects to easily track the target. The target assumed the red color if the subject was not correctly tracking the target (i.e. the cursor was outside the target) and the green color if the subject was correctly tracking the cursor (i.e. the cursor was inside the target, within the boundaries).

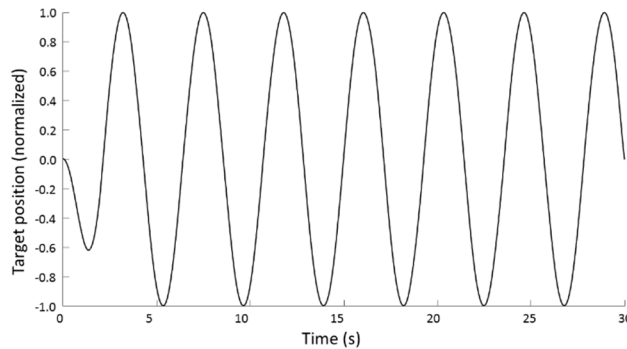


Figure 4.7: Target Position during one tracking trial.

At the same time, the test bench motors applied a perturbative torque at the wrist. The frequency of the perturbation was 3 Hz and its amplitude depended on the implemented command logic (see Paragraph 4.2.4.5). The frequency was selected to oblige the subjects to stiffen their wrist, by co-activating FCR and ECR and to prevent the subjects from voluntarily compensating the perturbation with an opposed moment.

During the tracking task, when the experimenter noticed a reduction of the performance, vocal encouragement and gratifications were given to the subject to better track the cursor, so as to reduce the performance decay due to distractions.

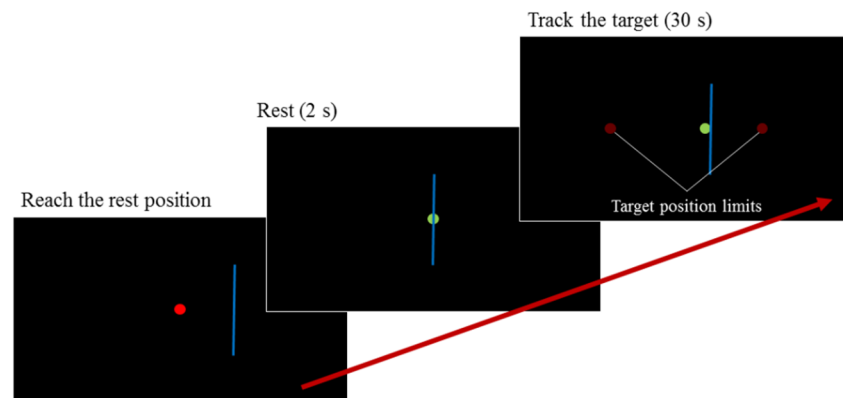


Figure 4.8: Tracking task.

#### 4.2.4.7 Command logics

The amplitude of the disturbance could be reduced in different ways, corresponding to different logics. The five sessions were:

- Baseline session: the perturbative torque amplitude was set equal to 10% the mean value between  $MVTF_i$  and  $MVTE_i$ . During this session,

the subject could only compensate the disturbance by stiffening his/her wrist.

- Proportional session: the perturbative torque amplitude was set equal to 10% the mean value between  $MVTF_i$  and  $MVTE_i$ . However, the amplitude of the perturbation was linearly reduced, via software, proportionally to the sample-by-sample co-contraction the subject was exerting (see Figure 4.8). The co-contraction was defined as the minimum between the FCR and ECR sEMG signal, rectified, Butterworth 2nd order filtered, and normalized to the maximum voluntary co-contraction (defined in Paragraph 4.2.4.1). The perturbation amplitude assumed its maximum value if no co-contraction was detected and it was equal to zero if the co-contraction was equal, or higher, than 0.25. The activation of 0.25 times the maximum voluntary contraction of a muscle could be considered a non-fatiguing contraction, because the complete pool of motor unit of a muscle was commonly recruited for muscle activations higher than 0.5 the maximum voluntary contraction (Merletti & Parker, 2004). The co-contraction threshold of 0.25, above which no perturbation was applied, was set such that the subject could voluntarily reach it without feeling too much fatigue. It was identified based on the results of four pilot experiments in which four levels of co-contraction were tested (0.15, 0.25, 0.35, 0.55). The same value allows the approximation of the endpoint stiffness major axis with the null space component of the muscle activation, as demonstrated in Chapter 3. The proportional command logic, tested in this session was inspired by the command logics implemented in those exoskeletons which enhance the operator's force based the EMG signal (Lee & Sankai, 2002; Rosen et al., 2001).
- Integral 1 s session: the perturbative torque amplitude was set equal to 10% the mean value between  $MVTF_i$  and  $MVTE_i$ . However, the amplitude of the perturbation was linearly reduced, via software, proportional to the mean co-contraction the subject was exerting 1 s before the current time. The perturbation amplitude assumed its maximum value if no co-contraction was detected in the previous 1 s and it assumed the zero value if the mean co-contraction was equal, or higher, than 0.25.
- Integral 2 s session: the perturbative torque amplitude was set equal to 10% the mean value between  $MVTF_i$  and  $MVTE_i$ . However, the

amplitude of the perturbation was linearly reduced, via software, proportional to the mean co-contraction the subject was exerting 2 s before the current time. The perturbation amplitude assumed its maximum value if no co-contraction was detected in the previous 2 s and it assumed the zero value if the mean co-contraction was equal, or higher, than 0.25.

- Control session: no perturbation is applied to the subject and the subject was only asked to track the target.

The Baseline session was performed the first day, the aided sessions (Proportional, Integral 1 s and Integral 2 s) were randomly shuffled for each subject and were performed during the second, third and fourth day, and the Control session was performed the last day.

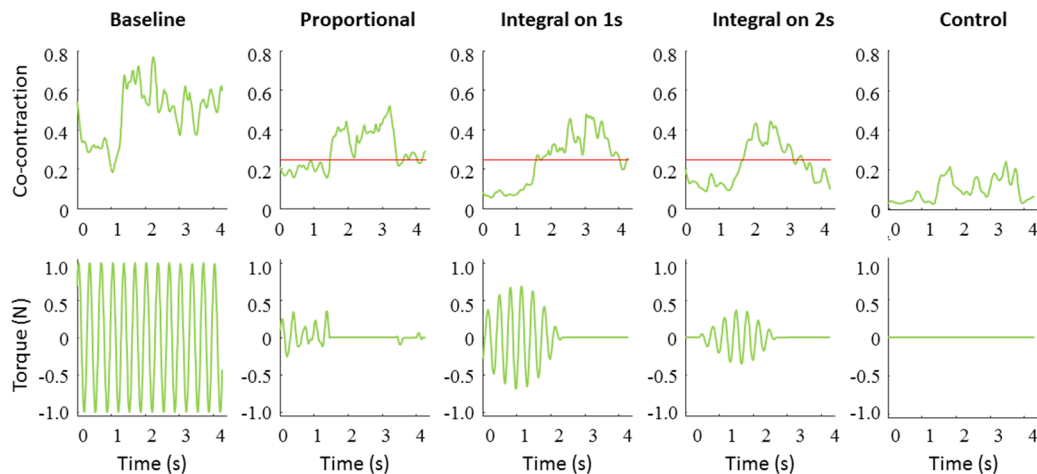


Figure 4.9: Co-contraction (upper figures) and torques (lower figures) exerted during a time interval in which the target move along a complete sinusoid. The red lines in the Co-contraction panels of the aided sessions indicates the 0.25 threshold above which no torque exertion occurs.

#### 4.2.4.8 Repetitions

The number of repetitions of the tracking task was set to 6 based on the results obtained from four pilot subjects.

Since isometric task repetitions were performed before the first tracking task repetition and after the last tracking task repetition, the number of isometric task repetitions was set to 7 for each session.

#### **4.2.4.9 Final maximum voluntary torque (MVT<sub>f</sub>) and last Borg perceived exertion**

After the last isometric task, repetition the subject was asked to exert the maximum voluntary torque of flexion (MVTF<sub>f</sub>), and extension (MVTE<sub>f</sub>). The same procedure performed at the beginning for the calculation of MVTF<sub>i</sub> and MVTE<sub>i</sub> (see Paragraph 4.2.4.2) was performed

At the very end of the experiment, the rating of perceived exertion was told to the subject, based on the Borg RPE CR10 scale (see Paragraph 4.2.4.3).

#### **4.2.4.10 Statistics**

One-way ANOVA, with a Bonferroni correction, was performed to identify significant differences between the MVTF<sub>i</sub> and the MVTE<sub>i</sub>, the perceived fatigue, and the slopes, along different repetitions of the frequency median. One-way ANOVA with repeated measurements, with Bonferroni correction, was performed to identify significant differences between the task error and the energy consumption calculated during different conditions. The GraphPad Prism 5 software was used to perform statistical analysis.

### **4.3 Analysis**

The different sessions were compared in terms of fatiguing, performance and energy consumption. The fatiguing was calculated in terms of perceived fatigue, as reported by the Borg scale RPE CR10 test, and increasing the median frequency of the EMG signals during the isometric tasks. The performance and the energy consumption was calculated during the tracking task.

#### **4.3.1 Initial Maximum voluntary torques**

The statistical difference between the initial maximum voluntary torques of flexion and extension of each subject, recorded during the different sessions, were

compared to an ANOVA test with Bonferroni correction. No statistical difference ( $p$ -value  $> 0.05$ ) was identified.

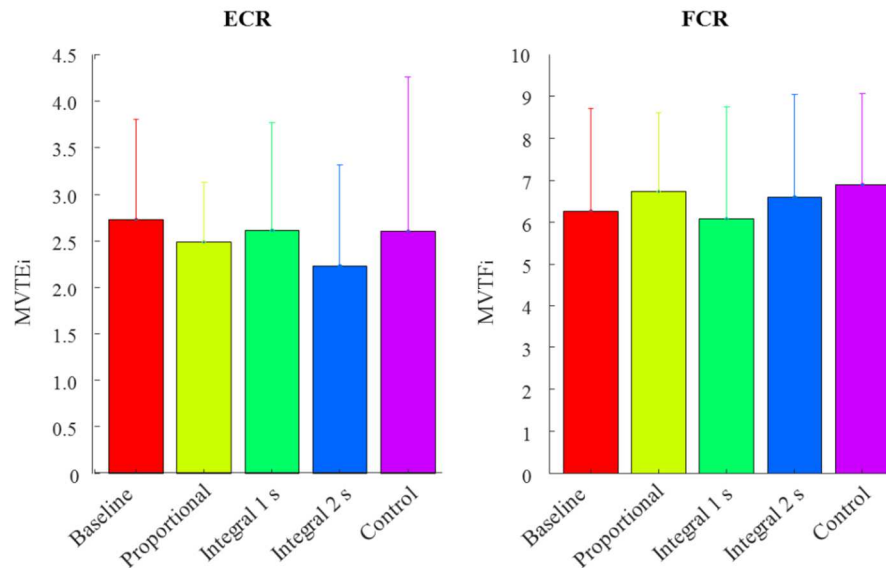


Figure 4.10: Initial maximum voluntary torque of extension (left), and flexion (right), averaged on subjects (mean  $\pm$  std).

### 4.3.2 Perceived fatigue

The perceived fatigue, estimated during all sessions with the Borg RPE CR10 scale (see Paragraph 4.2.4.3) both before the first isometric task (PF<sub>i</sub>) and after the final maximum voluntary force (PF<sub>f</sub>), were compared to a one-way ANOVA test with Bonferroni correction.

No statistical difference was identified in the perceived fatigue at the beginning of the experiment but statistical difference was identified in the fatigues perceived at the end of the different sessions (see Figure 4.11). In particular, statistical difference was identified in the fatigue perceived at the end of the Baseline session with respect to all the other sessions, among the Integral 1 s, the Proportional and Integral 2 s sessions and among the Control session, the Proportional and the Integral 2 s sessions. No statistical difference was identified between the fatigues perceived at the end of the Proportional with respect to the Integral 2 s session and between Integral 1 s with respect to the Control session.

The fatigue perceived at the end of the Baseline session, averaged along subjects, (see Figure 4.11), was higher than the fatigue perceived at the end of all

the other sessions, which suggested that subjects perceived the Baseline as the most fatiguing session. The fatigue perceived at the end of the Integral 1 s session and at the end of the Control sessions, averaged along subjects, which was lower with respect to the fatigue perceived at the end of all the other sessions, suggested that subjects perceived the Integral 1 s and the Control as less fatiguing sessions. Since, no statistical differences were identified among the fatigue perceived at the beginning of all the sessions, we can conclude that the statistical differences perceived at the end are not due to initial bias.

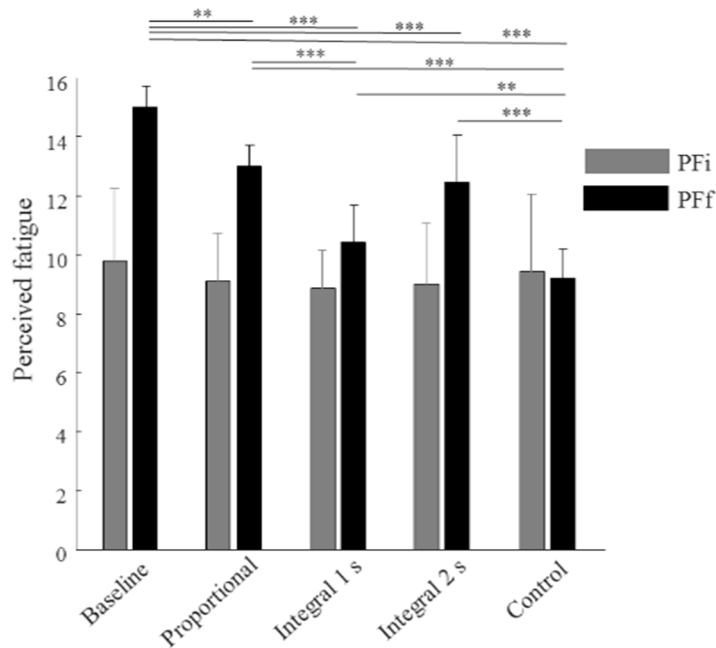


Figure 4.11: Initial (grey) and final (black) perceived fatigue of each session based on the RPE CR10 Borg scale.

### 4.3.3 The frequency median

The median frequency  $F_{median}$  was defined as the frequency value that separates the EMG power spectrum  $PS(f)$ , which is a function of the frequency  $f$ , into two parts of equal energy (González-Izal et al., 2012):

$$\int_{f_1}^{F_{median}} PS(f) \cdot df = \int_{F_{median}}^{f_2} PS(f) \cdot df$$

Where  $f_1$  and  $f_2$  are bandwidth of the sEMG signal ( $f_1$  is the lower value, i.e. 20 Hz, and  $f_2$  the upper value, i.e. 500 Hz). The ECR and FCR median frequencies were calculated during each repetition of each session of both flexion and extension isometric tasks (an example was reported in Figure 4.12).

The increase of the median frequency, which is a consequence of the higher number of motor units recruited, indicated the occurrence of fatiguing (Merletti & Parker, 2004). The median frequency of the FCR and ECR EMG signal was calculated during repetition of each session isometric tasks.

The raw EMGs, recorded at 1000 Hz during all the repetitions of the isometric flexion and extension tasks, were Butterworth 2<sup>nd</sup> order filtered between 20 and 500 Hz. The Welch's power spectral density (Mañanas et al., 2002) was calculated for each repetition of both the flexion and extension tasks (see an example in Figure 4.12), with a number of overlap points equal to 500 (0.5 s). The Matlab® function 'pwelch' was used to calculate the Welch's power spectral density.

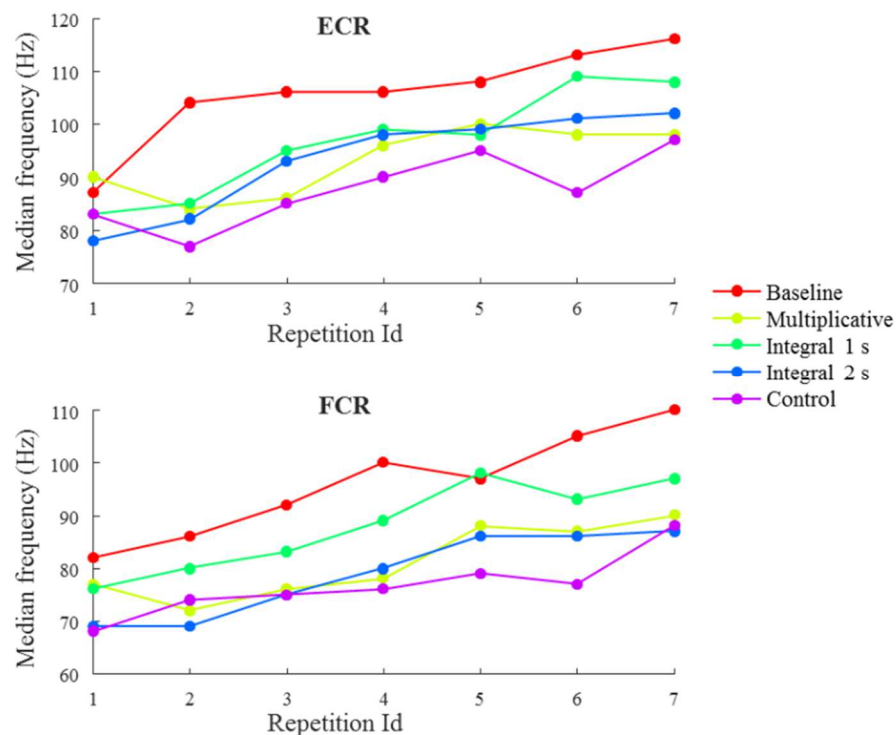


Figure 4.12: Example of the median frequency of the ECR (up), calculated during all the repetitions of the extension isometric task, and FCR (down), calculated during all the repetitions of the flexion isometric task, of subject 1.

The regression of the median frequency on the repetition was calculated from the FCR, during the isometric flexion task, and from the ECR, during the extension task, for each subject and session. The statistical difference among the slopes of the regression lines, calculated during each couple of sessions, was tested with a one-way ANOVA test with Bonferroni correction. The test did not show any statistical difference among the sessions (Figure 4.13).

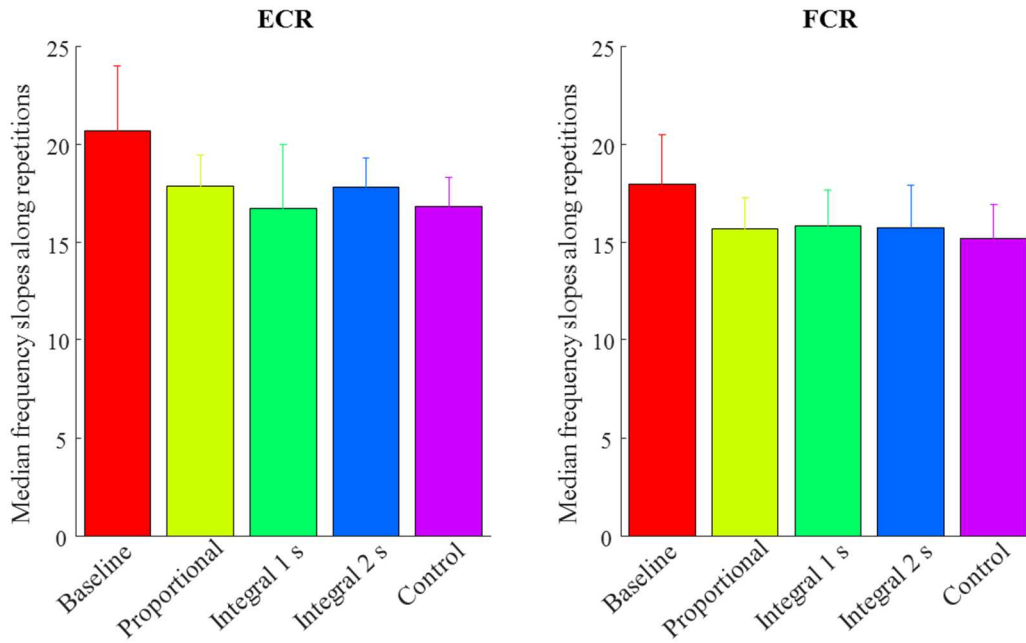


Figure 4.13: Slope of the regression of the median frequency along the repetitions of the ECR (left) and FCR (right) for each session. Mean  $\pm$  std along subjects.

#### 4.3.4 Task error during tracking task

The error the subjects committed during the tracking task was calculated for each session.

The task error  $e$  was defined as the squared root of the mean squared difference between the wrist angle  $w_a$  and the target angle  $t_a$ :

$$e = \sqrt{\frac{\sum_{i=1}^{n_{samples}} (w_{a_i} - t_{a_i})^2}{n_{samples}}}$$

Where  $n_{samples}$  is the number of samples, acquired during each repetition. The error was evaluated for each subject, session, and repetition (see Figure 4.14).

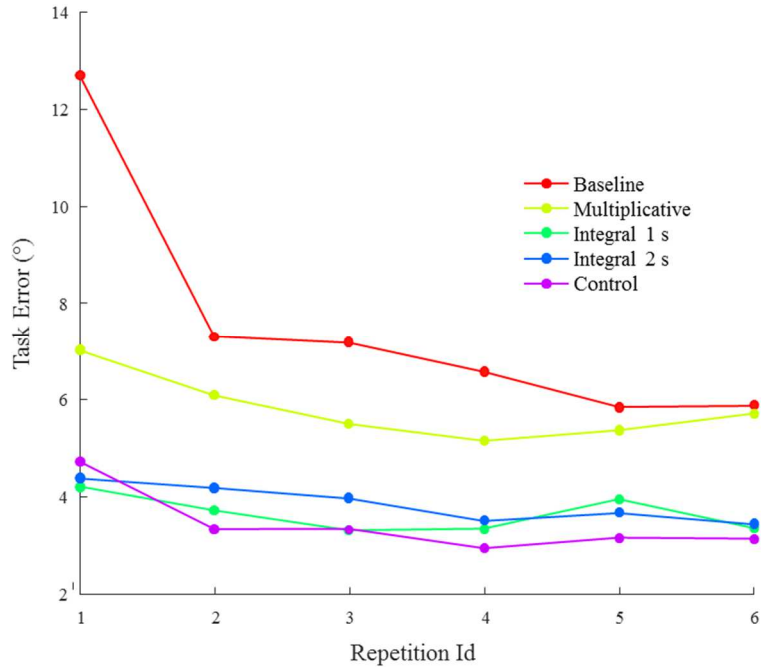


Figure 4.14: Examples of the task error committed by subject 8 during each repetition and session.

A decrease in the task error was observed between the first and the other repetitions of the Baseline session (see Figure 4.15). Since this behavior is a consequence of the learning process, the first repetition of each session was excluded from the statistical analysis to minimize this effect.

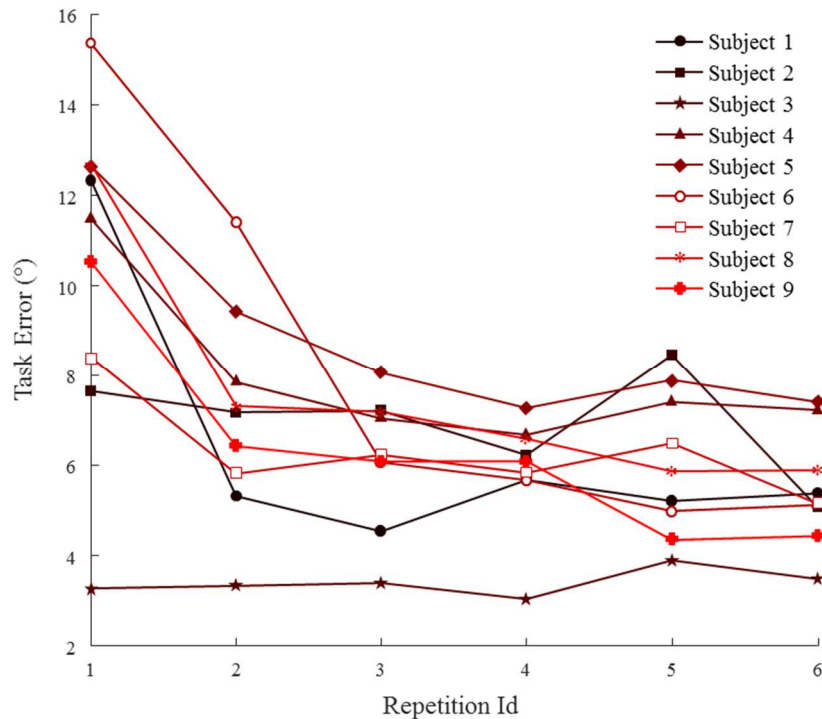


Figure 4.15: Task error committed by each subject during all the repetition of the Baseline session. A consistent decrease between the first and the second repetition was visible.

A repeated measures using one-way ANOVA, with a Bonferroni correction was conducted to test the statistical differences among the sessions.

Statistical differences were identified only between the task errors calculated during the Baseline and all the other sessions.

The higher value of the task error, averaged among subjects and repetitions, calculated during the Baseline session (mean  $\pm$  std among subjects and repetitions  $6.86^\circ \pm 2.61^\circ$ ) show a poorer performance with respect to the other sessions ( $3.60^\circ \pm 1.11^\circ$ ,  $3.57^\circ \pm 0.81^\circ$ ,  $3.69 \pm 1.27^\circ$ ,  $3.21^\circ \pm 0.94^\circ$ , respectively for the Proportional, Integral at 1 s, Integral at 2 s, and Control sessions) (see Figure 4.16).

Therefore, we can conclude that if the torque perturbation is reduced by an external aid, whose action is correlated to the level of co-contraction, beneficial effects in terms of task error could be identified. However, there is no statistical difference if the aid was given with a Proportional, Integral 1 s or Integral 2 s logic.

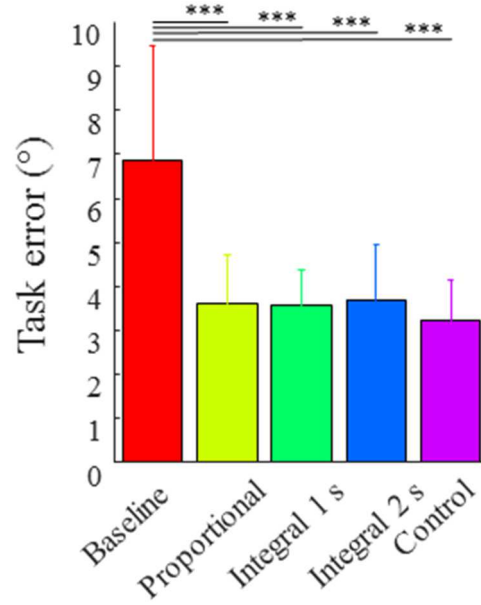


Figure 4.16: Mean  $\pm$  std among all subjects and repetitions of the task error for the different sessions.

### 4.3.5 Energy consumption during the tracking task

The energy consumption during the tracking task was calculated during all the sessions.

The energy consumption  $\varepsilon$  was defined as the sum of the squared muscle activations (Inouye & Valero-Cuevas, 2016):

$$\varepsilon = \sum_{i=1}^{n_{samples}} (m_{ECR}^2 + m_{FCR}^2)$$

where  $m_{ECR}$  and  $m_{FCR}$  are the recorded activations of the ECR and the FCR respectively. Raw EMG data, 2nd order Butterworth filtered between 20 and 500 Hz were used. The energy consumption was evaluated for each subject, session, and repetition (Figure 4.17).

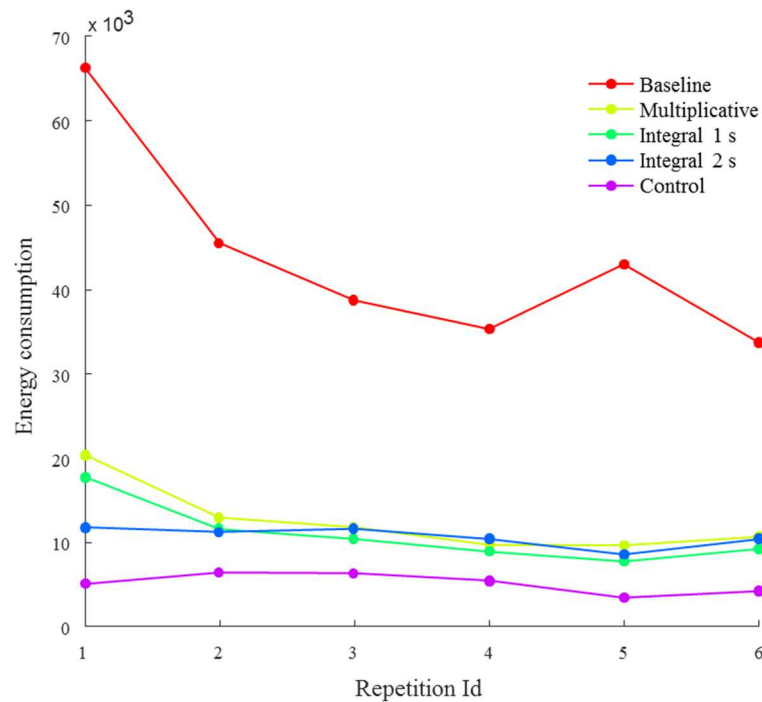


Figure 4.17: Examples of the energy consumption of subject 8 during each repetition and session.

The first repetition of all the sessions was excluded from the statistical analysis of the task error, and for the energy consumption analysis.

Repeated analysis using one-way ANOVA with Bonferroni correction was conducted to test if the energy consumption calculated during two different sessions, were statistically different.

A statistical difference was identified between the energy consumptions calculated during the Baseline session with respect to all the other sessions and during the Control session with respect to all the other sessions. A statistical difference was also identified between the energy consumption calculated during the Proportional and the integral sessions but no statistical difference was identified between the energy consumption calculated during the Integral 1 s and 2 s sessions.

The highest energy consumption, averaged between subjects and repetitions, (mean  $\pm$  std among subjects and repetitions  $68.30 \cdot 10^3 \pm 38.21 \cdot 10^3$ ) identified the Baseline session as the less efficient. Since the highest tracking error was also identified during the Baseline session, we can identify, as expected, the baseline as

the worst condition. On the other hand, the lack of external perturbation, led the Control session to require the lowest energy consumption ( $7.34 \cdot 10^3 \pm 8.17 \cdot 10^3$ ) and lowest tracking error. Subjects were able to modulate the co-contraction to exploit the external aid and reduce the tracking error together with the energy consumption ( $19.78 \cdot 10^3 \pm 1.20 \cdot 10^3$ ,  $14.93 \cdot 10^3 \pm 0.83 \cdot 10^3$  and  $16.72 \cdot 10^3 \pm 1.29 \cdot 10^3$  for the Proportional, Integral at 1 s session and Integral 2 s session respectively). Lower energy consumption mean values were calculated during the integral sessions with respect to the Proportional session (see Figure 4.18).

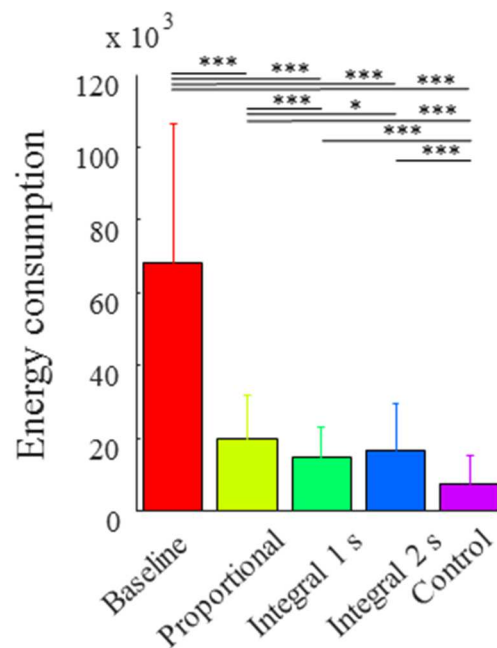


Figure 4.18: Mean  $\pm$  std among all subjects and repetitions of the energy consumption for the different sessions.

### 4.3.6 Conclusions

Subjects were able to modulate the co-contraction of two antagonist muscles of their wrist when performing a wrist flexion/extension tracking task. The statistical analysis performed on experimental data, demonstrated the beneficial effects, in terms of reducing the perceived fatigue, the task error and the energy consumption, whether an external aid, correlated to the muscle co-activation, reduces the amplitude of a perturbation. Since lower energy consumption were calculated during the integral with respect to the Proportional sessions, in light of no statistical differences in terms of task error among the different aided sessions, we may affirm that subjects were able to take advantage of the Integral control more efficiently

than the Proportional logic. In other words, the Central Nervous System was able to more efficiently coordinate the muscles if the aid follows an integral control logic. However, the Integral 1 s logic was preferred with respect to the Integral 2 s because of the lower fatigue perceived by subjects.

#### 4.4 The command parameters

The magnitude of the aid the exoskeleton should exert to help the operator may vary between 0 (i.e. the operator does not need any aid, then the exoskeleton must not exert any stiffening) to a maximum value of stiffening, which depends on the technical characteristics of the actuators that enhance the exoskeleton stiffness. Incorrect stiffening of the exoskeleton may lead to unnecessary or even dangerous situations (e.g. high stiffening exerted by the exoskeleton opposes a rapid movement the operator may need to perform in case of danger). Therefore, a relation between the muscle co-activation and the stiffness exerted by the exoskeleton was needed.

The relation between the muscle co-activation and the stiffness exerted by the exoskeleton should smoothly change from zero to the maximum stiffening, therefore a command law represented with a logistic function was proposed.

The equation of a logistic function that relates the muscle co-activation  $m$ , intended as the minimum of the normalized antagonist muscles activations, with the stiffness exerted by the exoskeleton  $K$  is:

$$K = a \frac{b \cdot e^{-m/\tau} + 1}{c \cdot e^{-m/\tau} + 1} \quad (4.1)$$

Where  $a$ ,  $b$ ,  $c$ , and  $\tau$  are four parameters that define the shape of the curve. Four muscle activations values and the corresponding four stiffness exerted by the exoskeleton determine the four logistic curve parameters. The four stiffness values selected to identify the curve parameters are:

- the minimum stiffness the exoskeleton should exert (i.e. zero),
- the maximum stiffness the exoskeleton should exert (i.e. the maximum feasible stiffness value or the maximum stiffness required by the task),

- the two stiffness values between the stiffness exerted by the exoskeleton linearly scale with the co-contraction (i.e. 0.4 and 0.6 times the maximum stiffness the exoskeleton could exert).

The corresponding four co-activations are:

- the minimum co-activation, below which the exoskeleton does not exert any stiffening,
- the maximum co-activations, above which the exoskeleton exerts the maximum stiffening,
- a range of comfortable co-activation, in which the exoskeleton linearly scales with the co-activation.

Since these co-activations are subject-specific, data from subject 8 are used as an example. Based on the experimental data, the co-activations used in the identification of the logistic function were determined as follows.

#### **4.4.1 Co-activation below which no stiffening is exerted**

The minimum value of co-contraction represents the threshold below which the exoskeleton is not required to exert any stiffening, because the operator does not need any aid.

Even if the operator is not voluntarily stiffening his limb, a co-activation might still be recorded, due to the non-negativity of the muscle activation or to unknown control law implemented in the central nervous system. The theoretical minimum physiological co-activation, recorded during an isometric task, which is needed to cope with the non-negativity of the muscle activations, could be univocally determined. However, it was demonstrated that the central nervous system does not exploit this non-negative minimization of muscle activations logic (Daniele Borzelli et al., 2013). Therefore, the minimum physiological co-activations is subject-specific and it needs to be experimentally identified during a task in which no co-activation is required. This task corresponds to the paradigm implemented in the Control session. Therefore, data collected during the Control session are processed to identify the minimum co-activation, below which the exoskeleton is not required to exert any stiffening.

The co-activation, defined as the sample-by-sample minimum between the activations of the FCR and ECR, was averaged along all the periods of all

repetitions recorded during the Control session tracking task and again time-averaged to identify the physiological co-activation required to perform the task. This value was set as the minimum co-activation, below which no contribution was required by the exoskeleton). In the example reported in Figure 4.19 and based on subject 8, the minimum co-activation was set to 0.107.

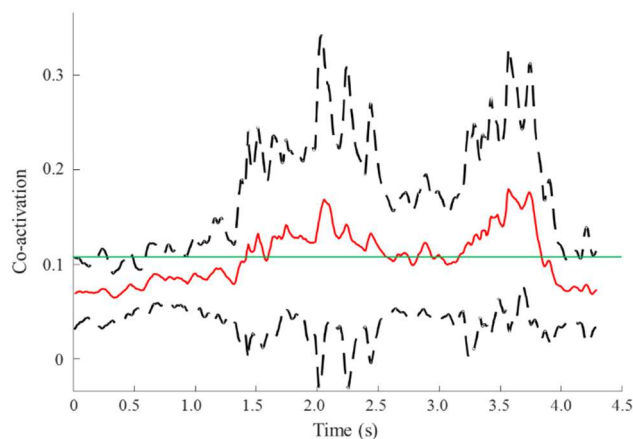


Figure 4.19: Example of the co-activations calculated from the data recorded during the Control session from subject 8. The red continuous line is the mean among all the repetitions of the co-contraction while the black dashed lines are the mean  $\pm$  the standard deviations of the co-activations. In green the mean co-contraction value.

#### 4.4.2 Co-activation above which the maximum stiffening is exerted

The maximum stiffening the exoskeleton exerts should occur when the operator exerts his maximum stiffening (i.e. co-activation equal to 1). However, high submaximal co-activations may be fatiguing too, and then the exoskeleton should be able to exert the maximum stiffness even during submaximal fatiguing co-activations.

Therefore, the exoskeleton should identify the muscle co-activations in which the operator requires ‘high’ stiffening, and consequently exert the maximum feasible stiffening. Then, the co-activation recorded during a task in which higher stiffening led to higher benefits, e.g. better performances, would allow the identification of compromise between the performance and fatigue the subject accepted, as in the paradigm implemented during the Baseline session. Then, co-activation data collected during Baseline session are processed to identify the

threshold above which the subject was assumed to try to stiffen at his maximum, and consequently above which the exoskeleton was required to exert its maximum stiffening. In the example reported in Figure 4.20 and based on subject 8, the maximum co-activation was set to 0.520.

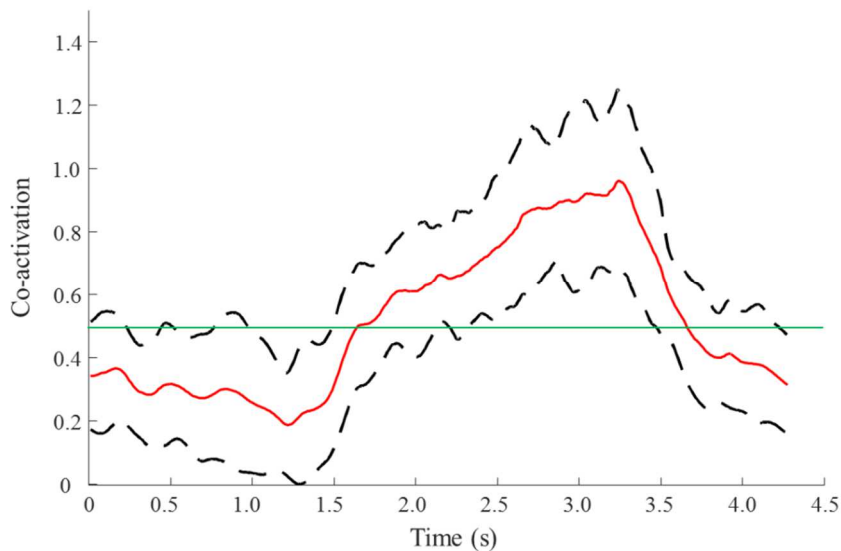


Figure 4.20: Example of the co-activations calculated from the data recorded during the Baseline session from subject 8. The red continuous line is the mean among all the repetitions of the co-contraction while the black dashed lines are the mean  $\pm$  the standard deviations of the co-activations.

#### 4.4.3 Co-activations which linearly scale with the exerted stiffening

The last two points identified the threshold in which the stiffness exerted by the exoskeleton approximately scale with the operator co-activation. This value could be proposed as the stiffness range that is more likely the operator would operate.

A comfortable exerted force is defined as the force the subject exerts if no force amplitude targets are required (Burnett et al., 2007), similarly the comfortable stiffening could be identified as the stiffening the subject exerts if no stiffening amplitude targets was required. Since in the Proportional and Integral session paradigms, a co-contraction threshold above which no perturbation occurred was set, co-contractions higher than this threshold were not required to augment the performance. Therefore, increase in the co-activations with respect to the defined threshold, could be felt by the subjects to be more comfortable. Therefore, the range

in which the exoskeleton stiffening linear scale with the co-activation is defined based on the paradigm implemented in the Proportional and the Integral sessions.

The co-activation was averaged along all the repetitions of the Proportional and integral sessions and again time averaged. The mean co-activation recorded during the Proportional session was set as the upper boundary while the mean co-activation recorded during the Integral 1 s and the Integral 2 s sessions was set as the lower boundary.

In the example reported in Figure 4.21 and based on subject 8, ranged between 0.215 and 0.266, the exoskeleton stiffness linearly scaled with the co-activation. However, this value may not only be subject dependent, but different range of co-activations may be required by the task. For example, some tasks may require high stiffening levels, therefore lower ranges of co-activations could be a better solution, on the other hand, some manipulations may require precise modulation of low stiffness levels, and therefore higher ranges of co-activations may be selected. Then, the most probable range of exoskeleton stiffness variation, that the task may require, should be earlier identified to optimize the exoskeleton action.

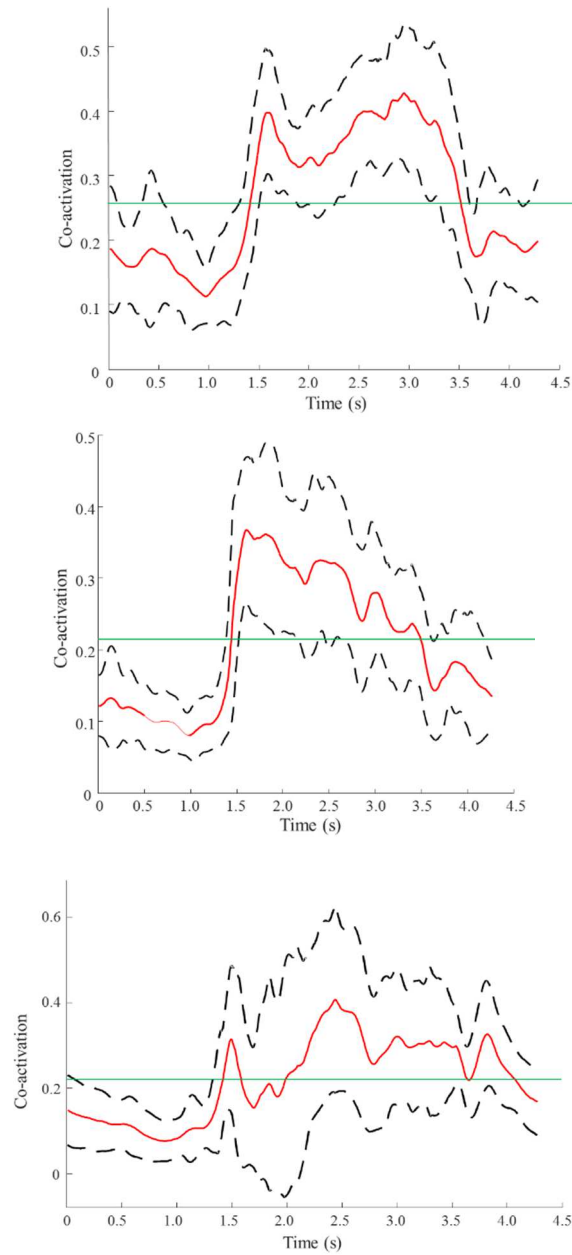


Figure 4.21: Example of the co-activations calculated from the data recorded during the Proportional (upper), Integral 1 s (middle), and Integral 2 s (lower) sessions from subject 8. The red continuous line is the mean among all the repetitions of the co-contraction while the black dashed lines are the mean  $\pm$  the standard deviations of the co-activations.

#### 4.4.4 Example of the relation between co-activation and exoskeleton stiffness

An example of the command logic based on subject 8 data, was reported in Figure 4.4. The lower asymptote of the logic function was related to those cases in which no exoskeleton effort is required, while the upper asymptote was related to those cases in which maximum feasible stiffening is required.

The equation of the logic function was described in Equation (4.1). The four couple co-activations ( $m_1, m_2, m_3, m_4$ ) and stiffness ( $K_1, K_2, K_3, K_4$ ) that univocally define the logistic curve, are  $K_1 = 0, K_2 = 0.4, K_3 = 0.6, K_4 = 1$ , and  $m_1 = 0.107, m_2 = 0.215, m_3 = 0.266, m_4 = 0.520$ . The stiffness values are normalized to the maximum stiffness the exoskeleton was required to exert, that could be equal to the maximum feasible exoskeleton stiffness or specific of the task. The co-activations were normalized to the maximum voluntary co-activation, as described in paragraph 4.2.4.1.

Since the function may identify a curve whose asymptotes are higher than 1 and lower than 0, two boundaries were fixed such that the stiffness exerted by the exoskeleton cannot be lower than zero or higher than the maximum required stiffening (see Figure 4.22).

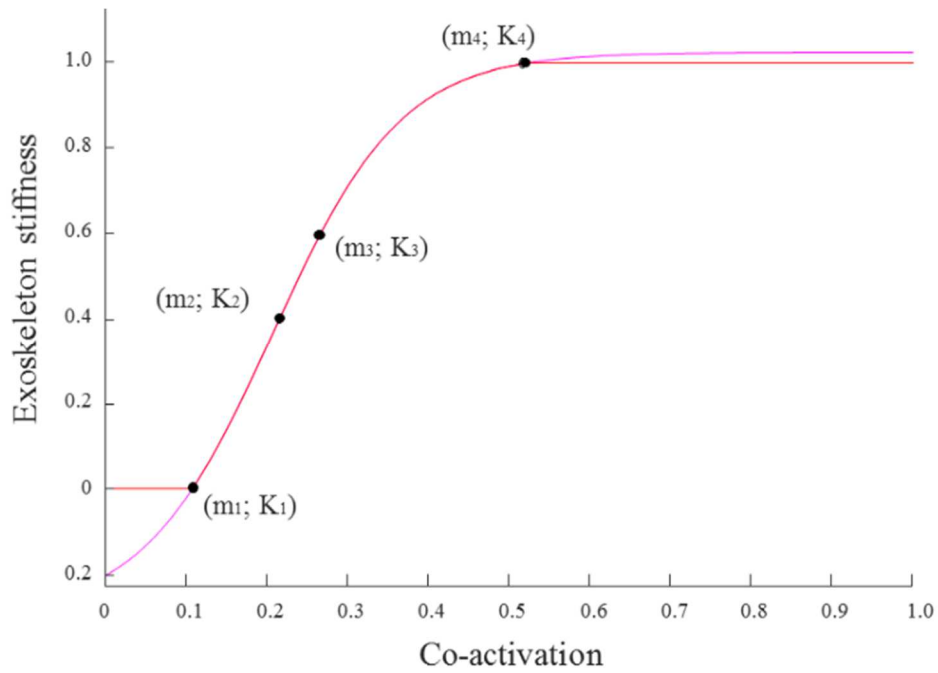


Figure 4.22: Logistic curve based on the experimental parameters. The red curve represents the curve that should be used for the control of the exoskeleton while the magenta curve represents the original logistic curve. The co-activation is normalized to the maximum voluntary co-contraction. The exoskeleton stiffness is normalized to the maximum stiffness the exoskeleton could exert.

## Chapter 5

# Selection of the variable stiffness actuators

In Chapter 3 the stiffness the operator intends to exert was estimated ('Data process' block of Figure 2.3). In Chapter 4 the command logic that determines the stiffness the device needs to exert to aid the operator was proposed ('Command logic' block of Figure 2.3). In this Chapter the device (i.e. the actuator) which exert the stiffness is proposed ('Exoskeleton' block of Figure 2.3). Therefore, in this Chapter the stiffness the exoskeleton is required to exert is defined; the question is how can the required stiffness be generated?

In this thesis, the command logic of an exoskeleton, whose only action is the enhancing of the operator end-point stiffness, was proposed. This kind of exoskeletons will help workers during different operations with respect to exoskeletons that augment operator's power. However, the implementation of both augmenting power and stiffness actions in the same device would be preferable, because of reduced costs with respect to buying two different devices, reduced time for learning how to use the device, and reduced time for wearing it if more operations are required. Therefore, the proposed logic is intended to be implemented on an already existing exoskeleton for augmenting force, on which new actuators with variable stiffness should be added to the exoskeleton design.

The new actuators with variable stiffness, which would be added to the exoskeleton design, are required to exert the required stiffness, estimated as described in Chapter 4, which depend on the stiffness exerted by the operator, estimated in Chapter 3.

The new variable stiffness actuators are required to be small and compact, so as to be easily added to the already existing exoskeleton design, and with an easy control so as to minimize delay, which would be dangerous for real-time

applications. The variable stiffness actuators are required to stiffen all the DOF of the already existing exoskeleton. Therefore, one variable stiffness actuator was expected to be added in series to the already existing stiffness actuators.

## **5.1 Actuators for the exoskeleton stiffness modulation**

All the actuators could be categorized in three different groups, based on the parameter they are controlling: position/angle, force/torque, and impedance. While the actuators that controls the position/angle and the force/torque were developed for long time, the first study that suggested the importance of the impedance control was established by Hogan (Hogan, 1985). The idea of modulating the joint impedance, through agonist-antagonist actuators, was defined in the 90s (Laurin-Kovitz et al., 1991), and other few years later a device composed of a series of elastic actuators was developed (Pratt & Williamson, 1995). However the first Variable Stiffness Actuators (VSA) prototypes could be attributed to the authors of (Bicchi et al., 2005; Hurst et al., 2004).

The publications about prototypes of Variable Impedance Actuators (VIA), and its subclass, the VSA, are rapidly increasing (Grioli et al., 2015) proposing a wide range of actuators based on different principles. Even if no “winning” design was identified, an optimal solution, which depends on the application, could be determined.

The most authoritative source for what concerns the VIA, is the VIATORS consortium (Albu-Schaeffer et al., 2009), a group of researchers of European universities, whose interests are in the development of VIA. The VIATORS consortium published a set of papers that organize the VIA state of art, and establish a common language for designers and potential users of VIA technology.

### **5.1.1 Variable impedance actuators definition**

The purposes of the traditional non-VIA (stiff actuators) are the moving of a device to a specific position, tracking a predefined trajectory, and holding the required position (ideally) whatever the external forces is (within the force limits of the device). Therefore, the mechanical impedance of stiff actuators was high and ideally infinite. A VIA in contrast deviates from its set equilibrium position, defined as the position where the VIA generates zero force or torque, depends on the external forces and the mechanical properties of the actuator (mostly inertia, stiffness and damping factors) (Vanderborght et al., 2013).

The VIA are conceived to be integrated in robotic devices which must physically interact with those unknown and dynamic environment for which the control body-actuator system must have abilities like (Vanderborgh et al., 2012):

- Efficiency e.g. natural gait generation, adaptation in legged locomotion and prosthetics for lower limbs, explosive motions such as throwing or kicking;
- Robustness to external perturbations and unpredictable model errors (changes) of the environment, of the robot kinematics and dynamics, or of the dynamics of a human interacting with it;
- Adaptability and force accuracy in the interaction with the operator, in applications in which continuous contact and accurate force exchange is necessary, such as in “hands-on” assistive devices, rehabilitation, exoskeletons and haptics;
- Safety to humans (and resilience to self-damage) in operations where the robot has fast, accurate motions, while cooperating, physically interacting or even possibly colliding with the humans and their environment, including other robots.

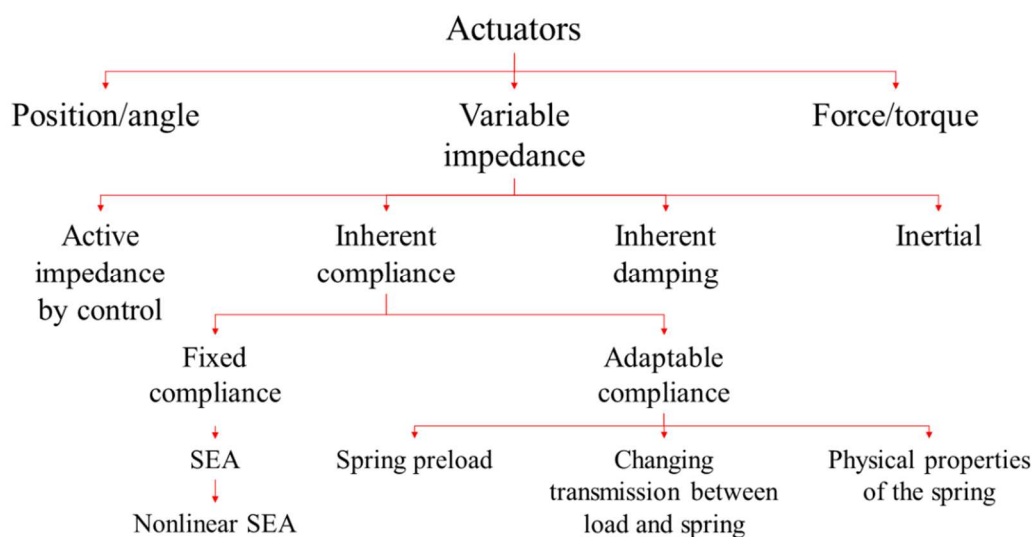


Figure 5.1: Main categorization of actuators and, in particular, of Variable impedance actuators.

Variable Impedance Actuators will be categorized depending on how their impedance can be achieved (see Figure 5.1). The first categorization can be made

between active impedance by control actuators, inherent compliance and damping actuators, and inertial actuators. A combination of them may also occur.

Since the only stiffness property is intended to be modulated, the VIA that modulated the damping (Inherent damping) and the inertia (Inertial) will not be described.

### **5.1.2 Active impedance by control**

An actuator with an Active impedance by control logic mimics the impedance behavior using software control (Albu-Schäffer et al., 2007). A correction to the measured output state is calculated and set by the (stiff) actuator. This type of VIA has an actuator, sensor and controller and can adapt both the damping and stiffness online, but no energy can be stored and no shock can be absorbed, due to the limited bandwidth of the controller. In addition, the impedance controller is quite complex and requires accurate system dynamics models. This technique, pioneered by DLR, was implemented for different applications (Boaventura et al., 2012; Fasse et al., 1994; Hyon et al., 2007), it was commercialized by Kuka, and now it is considered mature (Bischoff et al., 2010).

### **5.1.3 Inherent compliance**

In contrast to active impedance by control, passive compliance contains a passive or intrinsic compliant element. The mechanisms that own to this category can be sub-divided based on their compliant element, which may not change its stiffness (fixed compliance) with the variable impedance created by software control, or may adapt its stiffness controlling the mechanical reconfiguration.

The virtually infinite bandwidth for the passive compliance can absorb impact shocks and store energy, even if the design is usually more complex with more components than for the controlled impedance.

### **5.1.3 Fixed compliance**

The most famous inherently compliant actuator is the original Series Elastic Actuator (SEA) (Pratt & Williamson, 1995), which is a spring in series with a stiff actuator. The actuator stiffness is fixed and determined by the spring selection, thus the physical stiffness cannot be changed during operation. However, the authors of (Sugar, 2002) developed a spring-based actuator which overcome this issue. A linear spring is in series with a stiff actuator and the spring equilibrium position is

controlled to exert a desired force or stiffness, the stiffness is actively changed using a control law rather than by passively adding springs.

#### **5.1.4 Adaptable compliance properties**

Several groups have designed adaptable compliance mechanisms, with elastic elements storing energy, in addition to altering the stiffness. This concept gives intrinsic capabilities (bandwidth, impacts, energy storage) over the joint stiffness range. However, two motors are required: one to control the equilibrium position and the second to control stiffness. In this section, a classification is presented, based on the main principle on which the adaptive stiffness is obtained. The different actuators identified in literature can be classified into three major groups:

- Spring Preload: The stiffness is altered by changing the spring preload.
- Changing transmission between load and spring: The stiffness is altered by changing the transmission ratio between the output link and the elastic elements.
- Physical properties of the spring: The physical structure of the spring itself is altered.

Some devices use combinations of these three main mechanical properties.

### 5.1.4.1 Spring preload

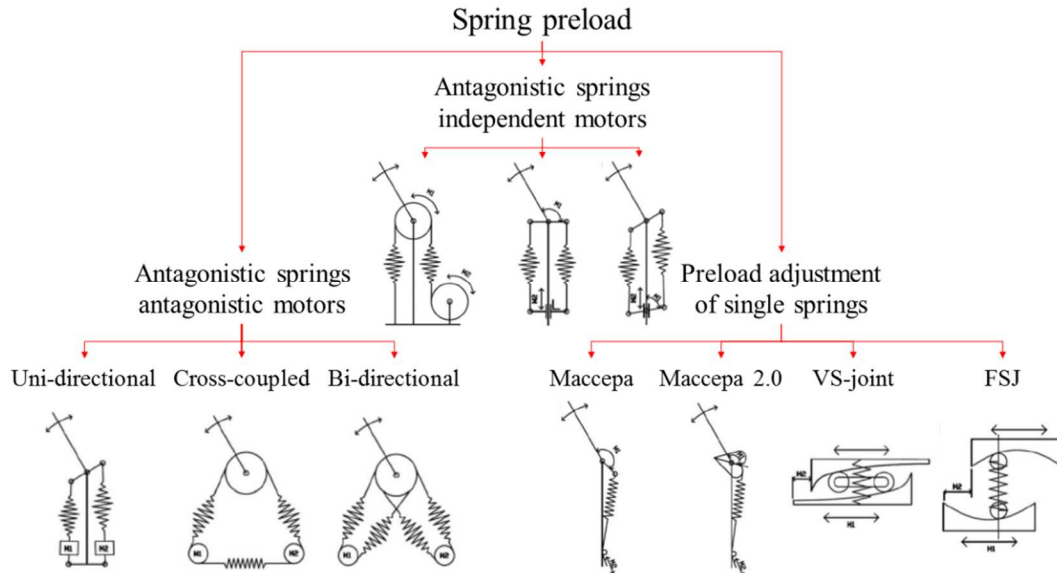


Figure 5.2: The sub-categorization of the 'spring preload' category.

In the Spring Preload category the stiffness is adjusted by changing the pretension or preload on the spring. The spring force is parallel to the spring displacement, hence energy has to be stored in the springs to change the stiffness and may not be retrievable.

This class can be further divided in the following subclasses (see Figure 5.2):

- (a) Antagonistic Springs with Antagonistic Motors: both the springs and the motors are placed in an antagonistic setup where at least two nonlinear springs are required. Both motors have to move in opposite direction to preload the springs and modulate the stiffness, while both motors have to work in the same direction to change the equilibrium position.
- (b) Antagonistic Springs with Independent Motors: similar to the previous class, except that the motors (partly) decouple the equilibrium position and stiffness control.
- (c) Preload Adjustment of Single Spring: this class is not antagonistic, 1 linear spring is enough and the preload is changed by a motor to control the stiffness. A second motor controls the equilibrium position.

### a) Antagonistic springs with antagonistic motors

As in nature, the joint stiffening modulation is commonly achieved co-activating opposite muscles (Hogan, 1984a), this actuator modulates the stiffness counter-rotating the actuators, while their rotation in the same sense generates a net joint torque. Three different possible embodiments are possible for this kind of actuators: uni-directional, cross-coupled, and bi-directional antagonistic arrangements (see Figure 5.2).

- When tension-only tendons are considered for the uni-directional case (Verrelst et al., 2006), the maximum joint torque can not be more than that of each single motor, and no net torque is available when stiffness is at maximum.
- A third compliant element (possibly different from the two antagonists) may be introduced to cross-couple the two prime movers and overcome the limitations of the uni-directional case. Cross-coupling allows setting of preload forces to tune it to nominal working conditions, using (a fraction of) each motor's torque in both directions (Tonietti et al., 2005).
- One further step introduces a fourth spring to connect each actuator to the link via two compliant elements (not necessarily symmetric) in push-pull configuration (Catalano et al., 2011; Schiavi et al., 2008; Wolf & Hirzinger, 2008). The big advantage here is that the sum of the two motor torques are available at the joint side if you drop the requirement to track a desired stiffness. The passive joint range of a setup of antagonistic springs is that both the angular and passive joint ranges are limited to the maximum extension of the springs.

### b) Antagonistic springs with independent motors

The main disadvantage of using antagonistic motors is that both motors need to work synchronously to change either the equilibrium position or the stiffness with the consequent impossible dimensioning for a specific task. The VSA with an Antagonistic Springs with Independent Motors logic, have the motors arranged to (partially) decouple the control of equilibrium position and stiffness.

- For the Quasi-Antagonistic Joint (QA-Joint) (Eiberger et al., 2010) one motor (the link drive) adjusts the link side position, while the second motor (the stiffness drive) operates the stiffness adjustment. This is a

partially decoupled system since when the stiffness is changed, the equilibrium position must be adjusted by the link side motor.

- Complete decoupling of the equilibrium position setting and the stiffness occurs when the endpoints of the two springs are mechanically coupled either by a lever arm or by a pulley (Hurst & Rizzi, 2008). Here the motor that sets the equilibrium position is not on the joint but on the other side of the nonlinear springs.
- The motor that sets the equilibrium position could be moved to the joint, with a consequent reduced complexity in the design. In this case the equilibrium position of both lever arms is horizontal, and the motor for the equilibrium position of the actual joint sets the relative position of the arm of the joint with respect to the lever arms (English & Russell, 1999). Then the angular joint range is not limited to the maximum extension of the springs, so it could be extended.

### c) Preload adjustment of single spring

The main feature of this subclass is the use of a non-linear connector between the output link and the spring element hence only one linear spring is required. The changing of the preload of the single spring modulates the stiffness.

In the Macepa device (Van Ham et al., 2007), the position of a lever arm is controlled to set the equilibrium position. The lever arm is connected to a spring loaded pivot point on the output link via a wire. When the link is moved out of the equilibrium position, the spring extends, forcing the joint back to the equilibrium position. The spring different stiffness setting can be achieved with different pre-tensioning. Similar logic was implemented in the MARIONET (Moment arm Adjustment for Remote induction Of Net Effective Torque) (Sulzer et al., 2005) in which the pre-tensioned spring was replaced with a tensioning motor.

In the Macepa 2.0 (Vanderborght et al., 2009) a cam replaced the lever arm such to allow the selection of the torque angle and stiffness-angle depending on the application.

In the VS-joint (Wolf & Hirzinger, 2008) a preload is responsible for the change of stiffness rather than a pretension. A roller is pushed by a spring to the lowest position in the cam disk that is the equilibrium position. The application of a torque led to a joint deflection of the roller and a consequent deflection of the springs. Therefore, the spring pushes back the roller and generates a force in the direction

of the lowest point of the cam disk. This design can easily be integrated into a robotic arm and the shape of the cam disk can be adjusted to obtain a progressive, regressive, or linear system behavior. Although one spring is enough, the VS joint uses three springs for symmetry. Both designs allow that two motors of different sizes can be used: a small one for the stiffness preset and a more powerful motor for the link position.

In contrast to the mechanics of the VS-joint, the new mechanics of the Floating Spring Joint (FSJ) (Wolf et al., 2011) is not equipped with a single cam system but with two opposing cam profiles. The two cam disks are coupled with each other by a single floating spring, which means that the spring has no connection to the joint base or output shaft. It is designed to use the spring energy of a single mechanical spring as good as possible to generate the desired torque and reduce losses due to pretension in order to alter the joint stiffness. One cam disk is fixed to the link side and the second to the stiffness actuator. An axial rotation led to a stiffness increasing.

### 5.1.4.2 Changing transmission between load and spring

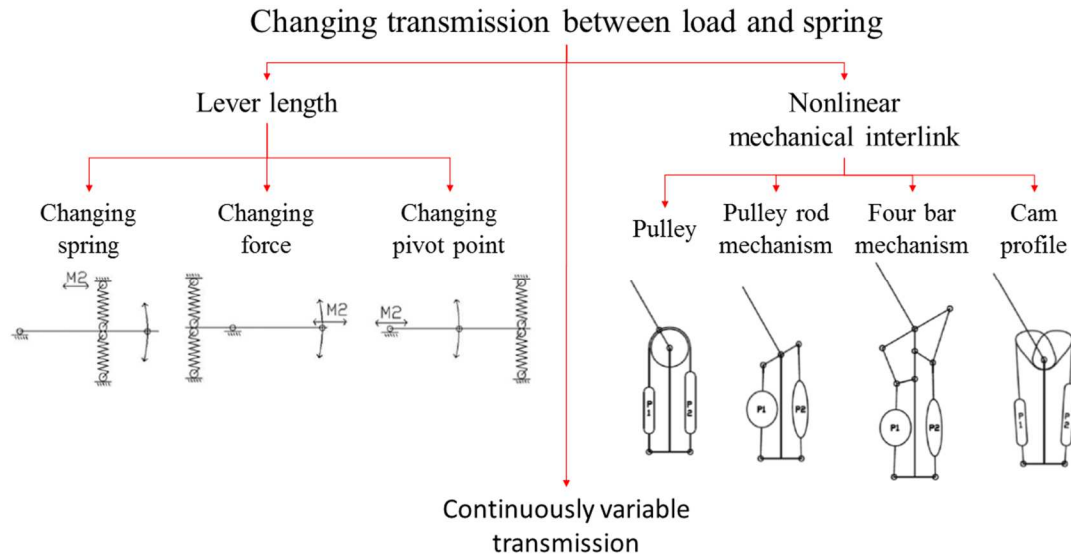


Figure 5.3: The sub-categorization of the ‘changing transmission between load and spring’ category.

The stiffness is adapted by changing the transmission ratio between the output link and the spring element. As this design does not preload the spring, theoretically at equilibrium, no energy is required to change the stiffness since the force on the spring is orthogonal to the spring displacement. However, friction has to be overcome and when the joint is not at the equilibrium position energy is still needed to adjust the stiffness. This class can be further divided into the following subclasses (Figure 5.3):

- a) **Lever length:** The stiffness is adapted by controlling the configuration of a lever mechanism.
- b) **Continuously variable transmission:** The stiffness is adapted by controlling the transmission ratio of a continuously variable transmission.
- c) **Nonlinear mechanical link:** The stiffness is adapted by controlling the properties of a nonlinear mechanical link.

#### a) Lever length

The main feature of this subclass is the use of a nonlinear connector between the output link and the spring element hence only one linear spring is required.

However, the stiffness adjustment is still performed by changing the preload on this single spring.

In the Macepa (Van Ham et al., 2007), the position of a lever arm is controlled to set the equilibrium position. The lever arm is connected to a spring loaded pivot point on the output link via a wire. When the link is moved out of the equilibrium position, the spring extends forcing the joint back to the equilibrium position. Different stiffness setting can be achieved by pre-tensioning the spring.

#### b) Nonlinear mechanical interlink

Different transmission ratios can be achieved changing the properties of the mechanical interlink. Even if no devices, that use this as the primary principle to adapt the stiffness, have been reported in literature, different connections principles exist to yield torque-deflection characteristics depending on the application.

Mostly the compliant elements are connected to the joint using a pulley. In the biped Lucy (Vanderborght et al., 2008) and in the manipulator arm developed by the authors of (Van Damme et al., 2009) a pull rod and a leverage mechanism are implemented.

#### c) Continuous variable transmission

A final approach in this class is the continuously variable transmissions incorporating designs such as Variable-diameter pulleys (VDP) or Reeves drives, Toroidal or roller-based continuously variable transmission (CVT) and Magnetic CVTs (Hollander & Sugar, 2004).

### 5.1.4.3 Physical properties of spring

Unlike the previous concepts, structure control modulates the effective physical structure of a spring to achieve variations in stiffness. The force exerted by a spring could be changed manipulating the material modulus, the cross-sectional area, or the active spring length.

The material property, which cannot be controlled by a structural change, can be changed in some materials, e.g. by changing the temperature. Unfortunately, these changes are not sufficiently rapid and there are no known VIA actuator examples.

### a) Changing of the cross-section area

One technique to alter the cross section is to use a beam with non-unity aspect ratio where stiffness can be changed by rotating the beam through  $90^\circ$  since the moment of inertia in the Bernoulli-Bar equation is the analogy to the cross section area. A prototype of a spring with variable stiffness is used in wearable robotic orthoses (Hollander & Sugar, 2004). The authors of (Kawamura et al., 2002) changed the moment of inertia by controlling the force to press together an element consisting of many layered sheets. However, if the sheets are firmly pressed together, they will not slip due to friction. As a result, the element stiffens and larger forces are needed to bend the element. This system does benefit from simple construction and a wide stiffness range, although friction makes precise control of the stiffness difficult and the shear forces are very high.

### b) Active spring length

Stiffness may also be adjusted by varying the effective length of a compliant element. An active knee brace varies the beam length to adjust the stiffness (Hollander & Sugar, 2004). The Mechanical Impedance Adjuster (Morita & Sugano, 1995) contains a leaf spring, connected to the joint by a wire and a pulley. The effective length of the spring can be changed by a slider, with a roller on the slider holding the leaf spring close to the structure. The motor rotates the feed screw, which moves the slider, and thus changes the stiffness. An advantage of this mechanisms is that it is easy to construct and easy to control since the stiffness setting and equilibrium position are completely independent. This mechanism allows all possible states between compliant and very stiff. Different variations of this method were presented by the authors of (Choi et al., 2011; Schuy et al., 2012) and applications were presented by (De & Tasch, 1996; Sugano et al., 1992).

## 5.2 Identification of the actuator

Since the best principle among the VSA cannot be determined, application-dependent optimal solutions need to be identified (Vanderborgh et al., 2013). The following Paragraphs describe a logical strategy to approach the topic of the selection of the best principle for the VSA that would modulate the stiffness of an exoskeleton (Wolf et al., 2016) .

### 5.2.1 Use-cases

In (Wolf et al., 2016), the authors identified the different requirements the actuator was required to have.

The first parameter is the use-case. The authors identified 5 main use-cases: shock absorbing, stiffness variation with constant load, stiffness variation at constant position, cyclic movements, and explosive movements.

The use shock absorbing was needed in case of fast collisions between robots with a stiff structure and rigid object with high inertia, that resulted in extremely short and high force peaks and large accelerations (Haddadin et al., 2007).

The stiffness variation at constant load allows the decoupling of two basic interactions with the environment: the exertion of the force and the modulation of the stiffness at a constant position. This task was already described in this thesis as ‘isometric task’ (See Paragraph 2.2).

When the stiffness is changing at a constant position the robot is at a certain position, or on a given track, and the modulation of the stiffness should not affect the output position. This task was already identified in this thesis as ‘dynamic task’ (See Chapter 2.2).

Cyclic movements consist of repetitive accelerations and decelerations of the robot. Here, a robot with flexible joints can take advantage of the possibility to store potential energy in the VSA springs.

Explosive movements are usually characterized by a high output velocity gained in a short period.

The task of the exoskeleton described in this thesis is required to perform, was not intended to provide high shocks, otherwise its usage would not be safe for the operator and a robotic device remotely controlled by the operator would be preferred. The operator expects no explosive movements in this phase of development, and then the exoskeleton is required to store less energy.

Therefore, the tasks the exoskeleton is required to perform are: stiffness variation with constant load, stiffness variation at constant position, and cyclic movements.

### 5.2.2 Design concepts

The main factors influencing the most common design approaches, affect the system performance and behavior. These factors are (Wolf et al., 2016) (a) the motor setup and (b) the stiffness variation.

(a) The motor setup could use an antagonistic system with two opposing motors ('antagonistic motor setup'), or a system with independent motors for joint positioning and stiffness variation ('independent motor setup').

In the 'antagonistic motor setup', movement of both motors in the same direction results in an output movement, while a co-contraction of the springs, obtained by moving both motors in the opposite direction results in a change of output stiffness. The positive effects of this setup are that the power of both motors contribute to stiffen the actuator. One drawback is the maximum power and torque, unless the antagonistic VSA is bidirectional, having only one motor and the energy storage of one spring can be used. Also, the power losses are quite high because both motors and potentially the gearboxes have to move.

An 'independent motor setup' only moves one motor to vary the output position and as a result has only the losses of one motor and if applicable one gear. Since the stiffness was changed by a dedicated motor, the size of the stiffness adjusting motor can be chosen so as to match exactly the power needed for that purpose. This results in a much smaller stiffness adjuster than the main positioning motor, so this design promises to gain smaller and lighter actuators. On the drawback, only the power of the positioning motor can be used to move the joint so that the power of the stiffness adjuster can be used to modulate the stiffness.

Since the exoskeleton concept developed in this thesis was expected to be implemented in an already existing force-augmenting exoskeleton, the independent motor setup that decouple the exertion of force and stiffness, better fits this purpose. In fact, in this case, the motor assigned to move the device was already implemented in the existing exoskeleton and the motor that modulate the stiffness needs to be added.

(b) Three methods to change the stiffness of a VSA were identified by the authors of (Wolf et al., 2016): the variation of a spring preload, the variation of the transmission ratio between output and spring, and the influence of the physical

properties of the spring. These methods could be combined with the different motor setup previously described.

Changing the stiffness preload is the simplest way to change the stiffness preset and it was realized by utilizing a few simple mechanical components. On the drawback, the potential energy stored in the spring by compression/extension cannot be used to store energy from the VSA output anymore until the pre-tension is released again.

Changing the transmission ratio between the actuator output and the spring element directly affects the displacement of the spring caused by a passive movement of the output. Therefore, this method directly affects the spring rate of the actuator output and the potential energy storage is not reduced by changing the stiffness setup, so the passive deflection range is low with respect to the preload-type actuators. Another drawback is that they are more complex than spring preload types, which results in more moving parts hence, potentially less efficient.

The adjustable physical spring properties as a way to change stiffness is still under study. However, at present the mechanism using preload or a variation of transmission ratio have higher energy capacity than the techniques related to size and weight.

The real-time continuous application needs a quick response from the VSA. A simple design is preferred compared to a complex one because to control it would be easier and the design more compact. Therefore, the preferred method to vary the stiffness is the spring preload.

### **5.2.3 Selection of the VSA**

An 'Active impedance by control' logic was discarded because the stiffening was implemented in the software control, even though this method could be useful for a continuous perturbation, it could not achieve a pre-load that was needed to compensate the spiky perturbations. Therefore, the VSA was selected from the 'Inherent compliance' VIA, and an actuator with adaptable compliance was selected because the actuators with fixed compliance does not allow an on-line stiffness modulation.

The simplest logic and structure was preferred to reduce the calculation time and the system complexity that need to be implemented on an already existing exoskeleton, and then the spring preload logic, that assures the device was compact and the control logic is simple, was selected.

The implementation on an existing exoskeleton could be performed by easily decoupling the motor that exerts the force and the motor that modulates the stiffness.

The VSA that fits the desired requirements are the ones that belong to the groups called ‘antagonist independent motors’ and ‘preload adjustment of single spring’ (see Figure 5.5). The devices, described in (Vanderborght et al., 2013), that belong to this groups, and fit the purpose this thesis are:

- The AMASC (J. Hurst & Rizzi, 2008)
- The device described by (English & Russell, 1999)
- The Macepa (Van Ham et al., 2007)
- The MARIONET (Sulzer et al., 2005)
- The Macepa 2.0 (Bram Vanderborght et al., 2009)
- The VS-joint (Wolf & Hirzinger, 2008)
- The DLR FSJ (Wolf et al., 2011)

Among these devices, some are still research concepts, the most compact are the VS-joint and its evolution, the DLR FSJ. Therefore, the proposed actuator for the required purpose is the DLR FSJ (see Figure 5.4).

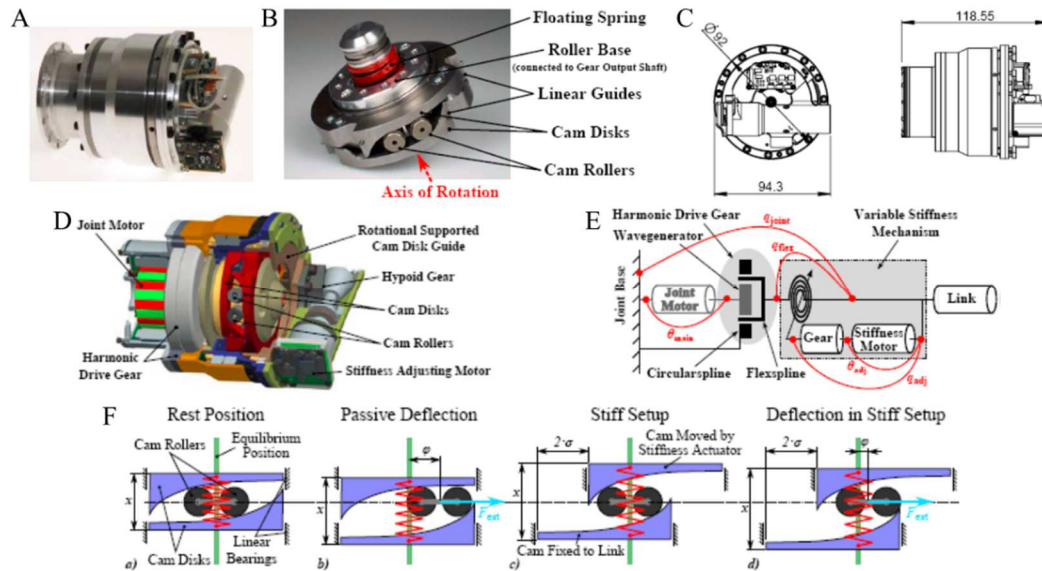


Figure 5.4: The DLR FSJ actuator. A. The DLR Floating Spring Joint. B. The FSJ mechanism. C. The DLR FSJ technical design. D. Cross section of the FSJ. E. The spring mechanism of the FSJ is located in series between the harmonic drive gear box of the main actuator and the link. F. The FSJ mechanism principle in a flattened view.

The technical sheet, that could be downloaded from the VIATORS consortium website ([www.viactors.org](http://www.viactors.org)), was reported in Appendix A, while its main functioning principles are described by the authors of (Wolf et al., 2011).

The DLR FSJ, which was already integrated in a joint prototype that was designed to serve as a modular basis for the arm and aimed to be similar to the dexterity and the capabilities of the average human arm (Wolf et al., 2011). The integration of this joint in a robotic arm yields a number of requirements for the FSJ:

- To be extremely compact to fit into the arm.
- To be highly integrated to form a joint module including the joint motors, sensors, mechanics, and the joint bearing itself.
- To be as light as possible.
- To compete with the performance of an human arm in terms of velocity.
- To have a low friction.

Otherwise, only the DLR FSJ actuator could be implemented in the joints of an already existing exoskeleton.

### **5.3 Safety systems**

Even if the described exoskeleton is not expected to operate in particularly dangerous environments, unpredicted events, which require the operator to quickly move, or retract, the limb, needs to be considered. In fact, the exoskeleton may oppose to a quick movement because of delays or unexpected malfunctioning, with possible dangerous consequences both to the device and for the operator. Therefore, a quick shut down of the exoskeleton stiffness control should be necessary to let the operator free to move his limb as soon as possible.

Consequently, a safety button, which immediately shut down the exoskeleton components that enhance the stiffness, needs to be added. This button should be easily accessible by the operator, so it should be on the frontal side of the exoskeleton. It could be added to correspond to operator shoulder, so as to be easily reachable by the other arm that does not wear the exoskeleton. A second safety button should be easily reached by other workers in case the operator cannot press the first one. This second button could be placed in the back. Finally, a third shut down button could be accessible remotely by other workers.

## Chapter 6

### Conclusions

In the last decades, a huge number of upper-limb exoskeletons were developed to help human operators in performing a large variation of tasks in clinical and rehabilitation fields, military field and, recently, in the industrial field. The introduction of exoskeletons in the industrial field was supposed to reduce the fatigue, the occurrence of musculo-skeletal diseases, and relieve operators from loads and pain during uncomfortable positions.

Despite the increased automation of the industry and the theorization of a fourth industrial revolution (Industry 4.0), one of whose characteristics is the close collaboration between the human operator and the robot, the actual standards that monitors this interaction still limits the direct contact between operator and robotic active devices. Therefore, mostly passive exoskeletons are currently engaged in the industrial field. However, the benefits of these kind of devices developed for the upper limb or trunk, is still questioned in literature. Contrarily, active upper limb exoskeletons, unloaded through the ground, could be a more valuable aid in enhancing the power exerted by the human operator. However, despite the current standards, the growing interest of the industrial field in introducing exoskeletons into the line, induced some groups to model exoskeletons specifically developed for the industrial applications and other groups to study the effect of exoskeletons on healthy subjects during manipulative works.

To the best of our knowledge, the attention of the scientific community is turned to exoskeletons that increase power, in terms of enhancing the end-point force, or aid the operator during a movement. However, a huge number of operations do not require power increase but it rather requires an increase of the stiffness exerted by the operator. Therefore, in this thesis, a command logic of an exoskeleton whose stiffness is modulated based on the operator stiffness, was proposed.

A diagram that identifies different elements of human-exoskeleton interaction was reported in Figure 2.3. The same diagram, with the contributions described in this thesis was reported in Figure 6.1.

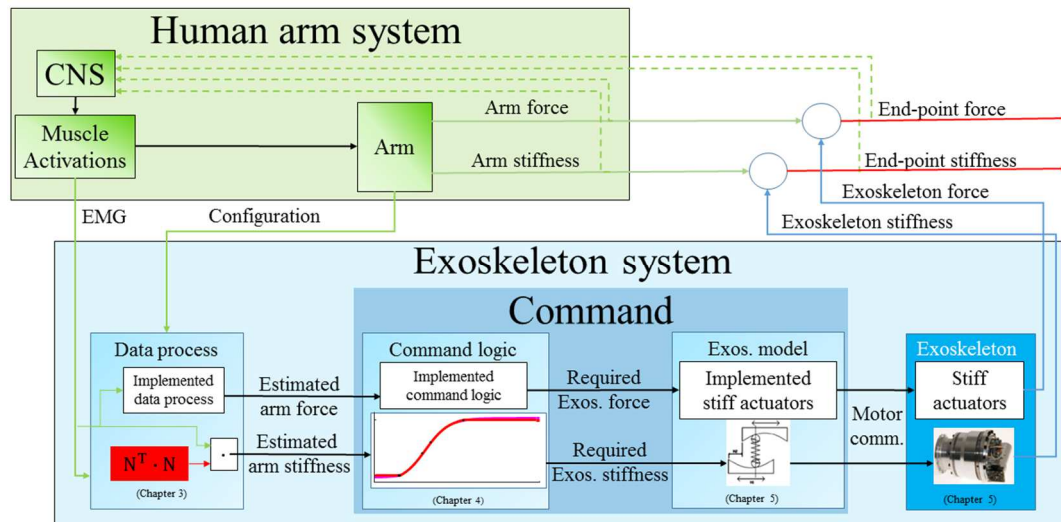


Figure 6.1: Concept of human-exoskeleton interaction with the implementations developed in this thesis. The arm stiffness was estimated as the null space projection of the recorded muscle activation, as described in Chapter 3. The stiffness required by the exoskeleton was related to the estimated arm stiffness with a logistic law, and it was exerted following an Integral 1 s command logic, as described in Chapter 5. The motor commands, that generate the required exoskeleton stiffness, are calculated based on the actuators type ('preload adjustment of single spring' actuator) and the exoskeleton design to activate the real actuators (DLR FSJ), as described in Chapter 5. The actions exerted by the exoskeleton and the operator combine to generate the end-point force and stiffness.

First, an estimation of the stiffness the operator is exerting was proposed ('Data process' block, see Chapter 3). The stiffness the operator is exerting with a limb is commonly mechanically recorded by applying an external deflection to the limb. However, this method cannot be used for limb stiffness estimation on the line because it will compromise the workers operations. Therefore, it is required to be estimated from the surface electromyographic signal recorded from muscles.

A model made of 1 joint and 2 muscles (1J2M) was developed to approximate the stiffening action exerted by two antagonist muscles acting on the elbow or the wrist joints. Then a more complex model made of 2 joints and 6 muscles (2J6M) was developed to approximate the action exerted by six muscles on the shoulder-elbow system. The 2J6M model permitted to test whether the end-point stiffness

exerted by a model of a limb could be approximated with the component of the muscle activation that does not exert any end-point force (i.e. the null space component). It was demonstrated that the null space component of the muscle activations could acceptably reconstruct the major axis of the end-point stiffness ellipse.

The presented approximation, which consists of a simple algorithm, is not computationally onerous and can be easily implemented in a device for real-time application. The ability of subjects to modulate the null space component of their muscle activations was experimentally tested in a submitted, but not yet published, paper (Borzelli et al., submitted). In this study, subjects were asked to reduce the displacement of a virtual cursor, during an isometric tri-dimensional force task, enhancing the null space component of their muscle activations (the activation of 17 arm and forearm muscles were collected). However, the model considers only six muscles, while more muscles contribute to the exertion of the end-point stiffness with a real operator joint, some of which are deep muscles whose action cannot be recorded with superficial Electromyography. The increase of the number of muscles, with the consequent increase of the number of degree of freedom of the muscle activation component that does not generate any end-point force nor end-point stiffness, may lead to a worst end-point stiffness estimation. Therefore, further experimental validation was required to test whether the same algorithm represents a valid approximation of the end-point stiffness exerted by a real human operator joint.

One of the principal elements needed for the identification of the null space component of muscle activation, is the matrix that maps the muscle activation onto the end-point force (EMG-to-force matrix). The correct identification of the selected muscles and the precise placing of the electrodes on the operator skin, together with the minimization of the components related to muscle and environment noise, are crucial to guarantee the reproducibility of the EMG-to-force matrix. Therefore, a further study whose purpose is the optimization of the design of the electrodes and their positioning on different operators, is required.

Since the EMG-to-force matrix is subject-specific, a calibration, which optimizes its duration, needs to be designed. A better end-point stiffness estimation could be achieved with the calculation of different EMG-to-force matrices for different limb postures, instead of identifying a unique matrix for all postures.

However, this calibration would take more time and the increased precision may not worth it if the operator is expected to use the exoskeleton for short period.

When the stiffness exerted by the operator was estimated, the stiffness the exoskeleton was required to exert based on this estimation, and the way it was exerted, need to be identified ('Command logic' block of Figure 6.1, see Chapter 4). The device was proposed to exert a stiffness proportional to the mean approximated stiffness the operator exerted in the previous 1 s (Integral 1 s), following a logistic law, whose parameters are subject-specific. The identification of the Integral 1 s as the best command logic for the modulation of the external device stiffness was experimentally tested, while the logistic law was only proposed and not tested on human subjects. Therefore, future experiments to test the effective control of the stiffness on external devices are required. However, the logistic law parameters are subject-specific and task-specific, consequently the optimization of the calibration for their identification are required.

The identification of the Integral 1 s as the best command logic was defined based on consistent information acquired from subjective parameter, i.e. the perceived fatigue, and objective parameters collected during isometric, i.e. the median frequency of the EMG activity, and dynamic tasks, i.e. the energy consumption and the task error. Therefore, even if the best command logic was tested on a single joint, i.e. the wrist, and only two antagonist muscles were recorded, this consistency among different parameters, may allow the assumption that results could be extended to more complex systems with more muscles acting on more joints, e.g. the whole arm. However, these extension needs to be experimentally tested.

The command logic, which defines the stiffness the exoskeleton was required to exert based on the electromyographic signal collected from the operator, was proposed to be implemented on an existing exoskeleton that already enhances the operator power, with the simple addition of variable stiffness actuators, in series with the already existing stiffness actuators. For this reason, an actuator with a 'preload adjustment of single spring' logic was proposed because of its simplicity in control and the few elements it comprises ('Exoskeleton model' block in Figure 6.1, see Chapter 5). Among the existing feasible actuators, the FSJ DLR was proposed. However, if the command logic is not expected to be implemented in an already existing exoskeleton and a new device is preferred to be developed, other solutions that does not separate the exertion of torque and stiffness could be preferred, like the 'antagonistic springs, antagonistic motors' type. On the other

hand, if the device is not intended as an exoskeleton for industrial applications, but some other applications, e.g. neuro-rehabilitation, maybe other specifications may occur, like the preponderance of cyclic movements or the necessity of energy storing, with the consequent identification of a better actuator for specific tasks.

If the proposed logic is implemented, together with the required additional actuators, to a device that already enhances the operator's power, a further investigation that compares the positive and the negative effects this exoskeleton usage would lead to, is required. In fact, the efficient control of an exoskeleton for end-point stiffness modulation may require an initial training and a practicing time. During this period, the operator would reduce his productivity on the line. Therefore, the costs related to the exoskeleton introduction, in terms of reduced productivity during practicing, cost of the exoskeleton and cost of the training, needs to be compared with the benefits related to the increase of the productivity after the operator learns how to control the exoskeleton and the reduced fatigue, diseases occurrence and discomfort during uncomfortable poses.

The worker acceptance may represent a major limitation of the usage of exoskeletons in the industrial practice. In fact, wearing an exoskeleton may led to unnatural postures that, even if not harmful, may led the operators not to agree with its usage. Therefore, investigations on how to present the device to the new operators, and then on how to design it such to simplify its acceptance, is mandatory.

Then, the further steps would require more experimental tests, which will verify whether the proposed exoskeleton command logic, estimates the stiffening exerted by the exoskeleton based on the operator electromyographic signal collected from more muscles, are feasible. Then, an efficient calibration needs to be designed to identify the EMG-to-force matrix and the parameters of the logistic law. Hence, the effects the exoskeleton would have on the operator and his productivity would be investigated. Finally, the identification of an attracting design and an efficient way to present the exoskeleton to the future operators needs to be defined.

## References

- Abdoli-Eramaki, M., Agnew, M. J., & Stevenson, J. M. (2006). An on-body personal lift augmentation device (PLAD) reduces EMG amplitude of erector spinae during lifting tasks. *Clinical Biomechanics*, *21*(5), 456–465.
- Abdoli-Eramaki, M., & Stevenson, J. M. (2008). The effect of on-body lift assistive device on the lumbar 3D dynamic moments and EMG during asymmetric freestyle lifting. *Clinical Biomechanics*, *23*(3), 372–380.
- Abdoli-Eramaki, M., Stevenson, J. M., Reid, S. A., & Bryant, T. J. (2007). Mathematical and empirical proof of principle for an on-body personal lift augmentation device (PLAD). *Journal of Biomechanics*, *40*(8), 1694–1700.
- Ajoudani, A., Tsagarakis, N., & Bicchi, A. (2012). Tele-impedance: Teleoperation with impedance regulation using a body-machine interface. *The International Journal of Robotics Research*, *0*(0), 1–14.
- Albu-Schaeffer, A., Bicchi, A., Stramigioli, S., Burdet, E., Smagt, P., Parravicini, A., ... Tsagarakis, N. (2009). VIATORS-Variable Impedance ACTuation systems embodying advanced interaction behaviors. *European Future Technologies Conference and Exhibition*, 4–5.
- Albu-Schaeffer, A., Haddadin, S., Ott, C., Stemmer, A., Wimböck, T., & Hirzinger, G. (2007). The DLR lightweight robot: design and control concepts for robots in human environments. *Industrial Robot: An International Journal*, *34*(5), 376–385.
- Anderson, R. J., & Spong, M. W. (1988). Hybrid impedance control of robotic manipulators. *IEEE Journal of Robotics and Automation*, *4*(5), 549–556.
- Anton, H. (2010). *Elementary linear algebra* (10th ed.). New York: John Wiley.
- Artemiadis, P. K., Katsiaris, P. T., Liarokapis, M. V., & Kostas, J. K. (2010). Human arm impedance: Characterization and modeling in 3D space. *2010 IEEE/RSJ International Conference on Intelligent Robots and Systems*.
- Banala, S. K., Kim, S. H., Agrawal, S. K., & Scholz, J. P. (2009). Robot assisted gait training with active leg exoskeleton (ALEX). *IEEE Transactions on Neural Systems and Rehabilitation Engineering: A Publication of the IEEE Engineering in Medicine and Biology Society*, *17*(1), 2–8.

- Belforte, G., Sorli, M., & Gastaldi, L. (1997). Active Orthosis For Rehabilitation And Passive Exercise. *WIT Transactions on Biomedicine and Health*, 4, 10.
- Bhagat, N. A., Venkatakrishnan, A., Abibullaev, B., Artz, E. J., Yozbatiran, N., Blank, A. A., ... Contreras-Vidal, J. L. (2016). Design and optimization of an EEG-based brain machine interface (BMI) to an upper-limb exoskeleton for stroke survivors. *Frontiers in Neuroscience*, 10(122).
- Bicchi, A., Tonietti, G., Bavaro, M., & Piccigallo, M. (2005). Variable Stiffness Actuators for Fast and Safe Motion Control. *Robotics Research*, 15, 527–536.
- Bischoff, R., Kurth, J., Schreiber, G., Koeppel, R., Albu-Schäffer, A., Beyer, D., ... Grunwald, G. (2010). The KUKA-DLR Lightweight Robot arm – a new reference platform for robotics research and manufacturing. *Joint 41th International Symposium on Robotics and 6th German Conference on Robotics*, 741–748.
- Bizzi, E., & Cheung, V. C. K. (2013). The neural origin of muscle synergies. *Frontiers in Computational Neuroscience*, 7(51).
- Blank, A. A., Okamura, A. M., & Whitcomb, L. L. (2014). Task-dependent impedance and implications for upper-limb prosthesis control. *The International Journal of Robotics Research*, 33(6), 827–846.
- Boaventura, T., Semini, C., Buchli, J., Frigerio, M., Focchi, M., & Caldwell, D. G. (2012). Dynamic torque control of a hydraulic quadruped robot. *2012 IEEE International Conference on Robotics and Automation*, 1889–1894.
- Bogue, R. (2009). Exoskeletons and robotic prosthetics: a review of recent developments. *Industrial Robot: An International Journal*, 36(5), 421–427.
- Borg, G. (1998). Borg's perceived exertion and pain scales. *Human Kinetics*.
- Borzelli, D., Berger, D. J., Pai, D. K., & D'Avella, A. (2013). Effort minimization and synergistic muscle recruitment for three-dimensional force generation. *Frontiers in Computational Neuroscience*, 7, 186.
- Borzelli, D., Cesqui, B., Berger, D. J., Burdet, E., & D'Avella, A. (n.d.). Muscle patterns underlying voluntary modulation of co-contraction. *Submitted*.
- Borzelli, D., Pastorelli, S., & Gastaldi, L. (2016). Model of the human arm stiffness exerted by two antagonist muscles. In *Iftomm/IEEE/euRobotics 25th International Conference on Robotics in Alpe-Adria-Danube Region– RAAD 2016*. Belgrade.

- Borzelli, D., Pastorelli, S., & Gastaldi, L. (2017a). Determination of the Human Arm Stiffness Efficiency with a Two Antagonist Muscles Model (pp. 71–78). Springer International Publishing.
- Borzelli, D., Pastorelli, S., & Gastaldi, L. (2017b). Elbow musculoskeletal model for industrial exoskeleton with modulated impedance based on operator's arm stiffness. *International Journal of Automation Technology*, *11*(3), 442–449.
- Burdet, E., Franklin, D. W., & Milner, T. E. (2013). *Human robotics*. MIT Press.
- Burdet, E., Osu, R., Franklin, D., Milner, T., & Kawato, M. (2001). The central nervous system stabilizes unstable dynamics by learning optimal impedance. *Nature*, *414*, 446–449.
- Burnett, A., Green, J., Netto, K., & Rodrigues, J. (2007). Examination of EMG normalisation methods for the study of the posterior and posterolateral neck muscles in healthy controls. *Journal of Electromyography and Kinesiology*, *17*(5), 635–641.
- Catalano, M. G., Grioli, G., Garabini, M., Bonomo, F., Mancini, M., Tsagarakis, N., & Bicchi, A. (2011). VSA-CubeBot: A modular variable stiffness platform for multiple degrees of freedom robots. In *Proceedings - IEEE International Conference on Robotics and Automation* (pp. 5090–5095).
- Cavallaro, E. E., Rosen, J., Perry, J. C., & Burns, S. (2006). Real-time myoprocessors for a neural controlled powered exoskeleton arm. *IEEE Transactions on Bio-Medical Engineering*, *53*(11), 2387–2396.
- Choi, J., Hong, S., Lee, W., Kang, S., & Kim, M. (2011). A robot joint with variable stiffness using leaf springs. *IEEE Transactions on Robotics*, *27*(2), 229–238.
- Contreras-Vidal, J. L., & Grossman, R. G. (2013). NeuroRex: a clinical neural interface roadmap for EEG-based brain machine interfaces to a lower body robotic exoskeleton. *Engineering in Medicine and Biology Society (EMBC), 2013 35th Annual International Conference of the IEEE, 2013*, 1579–1582.
- Crago, P., Houk, J., & Hasan, Z. (1976). Regulatory actions of human stretch reflex. *Journal of Neurophysiology*.
- Darainy, M., Malfait, N., Gribble, P. L., Towhidkhah, F., & Ostry, D. J. (2004). Learning to control arm stiffness under static conditions. *Journal of Neurophysiology*, *96*(6), 3344–3350.
- De, A., & Tasch, U. (1996). A two-DOF manipulator with adjustable compliance capabilities and comparison with the human finger. *Journal of Robotic*

*Systems*, 13(1), 25–34.

- de Looze, M. P., Bosch, T., Krause, F., Stadler, K. S., & O’Sullivan, L. W. (2016). Exoskeletons for industrial application and their potential effects on physical work load. *Ergonomics*.
- Delp, S. L., Anderson, F. C., Arnold, A. S., Loan, P., Habib, A., John, C. T., ... Thelen, D. G. (2007). OpenSim: Open-source software to create and analyze dynamic simulations of movement. *IEEE Transactions on Biomedical Engineering*, 54(11), 1940–1950.
- Delp, S. L., Grierson, A. E., & Buchanan, T. S. (1996). Maximum isometric moments generated by the wrist muscles in flexion-extension and radial-ulnar deviation. *Journal of Biomechanics*, 29(10), 1371–1375.
- Delp, S. L., & Loan, J. P. (1995). A graphics-based software system to develop and analyze models of musculoskeletal structures. *Computers in Biology and Medicine*, 25(1), 21–34.
- Eiberger, O., Haddadin, S., Weis, M., Albu-Schäffer, A., & Hirzinger, G. (2010). On joint design with intrinsic variable compliance: Derivation of the DLR QA-joint. In *IEEE International Conference on Robotics and Automation* (pp. 1687–1694).
- English, C., & Russell, D. (1999). Mechanics and stiffness limitations of a variable stiffness actuator for use in prosthetic limbs. *Mechanism and Machine Theory*, 34(1), 7–25.
- EWCS. (2015). Sixth European Working Conditions Survey: 2015 Data visualisation. *European Survey on Working Conditions (ESWC) 2005*.
- Fagg, A. H., Shah, A., & Barto, A. G. (2002). A computational model of muscle recruitment for wrist movements. *Journal of Neurophysiology*, 88(6), 3348–3358.
- Fasse, E. D., Hogan, N., Gomez, S. R., & Mehta, N. R. (1994). A novel variable mechanical impedance electromechanical actuator. *Dynamic Systems and Control*, 55(1), 311–318.
- Flash, T. (1987). The control of hand equilibrium trajectories in multi-joint arm movements. *Biological Cybernetics*, 57(4–5), 257–274.
- Fleischer, C., & Hommel, Gü. (2008). A Human-Exoskeleton Interface Utilizing Electromyography. *IEEE Transactions on Robotics*, 24(4), 872–882.

- Franklin, D., Burdet, E., & Osu, R. (2003). Functional significance of stiffness in adaptation of multijoint arm movements to stable and unstable dynamics. *Experimental Brain Research*.
- Franklin, D. W., Burdet, E., Osu, R., Kawato, M., & Milner, T. E. (2003). Functional significance of stiffness in adaptation of multijoint arm movements to stable and unstable dynamics. *Experimental Brain Research Brain Res.*, *151*(2), 145–157.
- Frost, D. M., Abdoli-Eramaki, M., & Stevenson, J. M. (2009). PLAD (personal lift assistive device) stiffness affects the lumbar flexion/extension moment and the posterior chain EMG during symmetrical lifting tasks. *Journal of Electromyography and Kinesiology*, *19*(6).
- Gandevia, S. C. (2001). Spinal and supraspinal factors in human muscle fatigue. *Physiological Reviews*, *81*(4), 1725–1789.
- Garrec, P., Friconneau, J. P., Méasson, Y., & Perrot, Y. (2008). ABLE, an innovative transparent exoskeleton for the upper-limb. In *2008 IEEE/RSJ International Conference on Intelligent Robots and Systems, IROS* (pp. 1483–1488).
- Godwin, A. A., Stevenson, J. M., Agnew, M. J., Twiddy, A. L., Abdoli-Eramaki, M., & Lotz, C. A. (2009). Testing the efficacy of an ergonomic lifting aid at diminishing muscular fatigue in women over a prolonged period of lifting. *International Journal of Industrial Ergonomics*, *39*(1), 121–126.
- Gollapudi, S. K., & Lin, D. C. (2009). Experimental determination of sarcomere force-length relationship in type-I human skeletal muscle fibers. *Journal of Biomechanics*, *42*(13), 2011–2016.
- Gomi, H., & Kawato, M. (1996). Equilibrium-point control hypothesis examined by measured arm stiffness during multijoint movement, *272*(5258), 117–120.
- Gomi, H., & Osu, R. (1998). Task-dependent viscoelasticity of human multijoint arm and its spatial characteristics for interaction with environments. *The Journal of Neuroscience*, *18*(21), 8965–8978.
- González-Izal, M., Malanda, A., Gorostiaga, E., & Izquierdo, M. (2012). Electromyographic models to assess muscle fatigue. *Journal of Electromyography and Kinesiology*.
- Gopura, R. A. R. C., Kiguchi, K., & Bandara, D. S. V. (2011). A brief review on upper extremity robotic exoskeleton systems. In *2011 6th International Conference on Industrial and Information Systems, ICIIS 2011 - Conference*

*Proceedings* (pp. 346–351).

- Gribble, P. L., Mullin, L. I., Cothros, N., & Mattar, A. (2003). Role of cocontraction in arm movement accuracy. *Journal of Neurophysiology*, 89(5), 2396–2405.
- Grioli, G., Wolf, S., Garabini, M., Catalano, M., Burdet, E., Caldwell, D., ... Bicchi, A. (2015). Variable stiffness actuators: The user's point of view. *International Journal of Robotic Research*, 1–17.
- Haddadin, S., Albu-schäffer, A., & Hirzinger, G. (2007). Safety evaluation of physical human-robot interaction via crash-testing. In *Robotics: Science and Systems* (pp. 217–224).
- He, W., Dong, Y., & Sun, C. (2016). Adaptive Neural Impedance Control of a Robotic Manipulator with Input Saturation. *IEEE Transactions on Systems, Man, and Cybernetics: Systems*, 46(3), 334–344.
- Hill, A. V. (1953). The Mechanics of Active Muscle. *Proceedings of the Royal Society B: Biological Sciences*, 141(902), 104–117.
- Hocaoglu, E., & Patoglu, V. (2012). Tele-impedance control of a variable stiffness prosthetic hand. *2012 IEEE International Conference on Robotics and Biomimetics (ROBIO)*.
- Hodges, P. W., & Richardson, C. A. (1999). Altered trunk muscle recruitment in people with low back pain with upper limb movement at different speeds. *Archives of Physical Medicine and Rehabilitation*, 80(9), 1005–1012.
- Hogan, N. (1984a). Adaptive control of mechanical impedance by coactivation of antagonist muscles. *IEEE Transactions on Automatic Control*.
- Hogan, N. (1984b). Impedance control: An approach to manipulation. *American Control Conference, 1984*.
- Hogan, N. (1985). Impedance Control: An Approach to Manipulation: Part III—Applications. *Journal of Dynamic Systems, Measurement, and Control*.
- Hollander, K., & Sugar, T. (2004). Concepts for compliant actuation in wearable robotic systems. *US-Korea Conference (UKC) CDROM*.
- Holmqvist, L. W., von Koch, L., & de Pedro-Cuesta, J. (2000). Use of healthcare, impact on family caregivers and patient satisfaction of rehabilitation at home after stroke in southwest Stockholm. *Scandinavian Journal of Rehabilitation Medicine*, 32(4), 173–179.

- Holzbour, K. R. S., Murray, W. M., & Delp, S. L. (2005). A Model of the Upper Extremity for Simulating Musculoskeletal Surgery and Analyzing Neuromuscular Control. *Annals of Biomedical Engineering*, 33(6), 829–840.
- Hu, X., Murray, W., & Perreault, E. (2011). Muscle short-range stiffness can be used to estimate the endpoint stiffness of the human arm. *Journal of Neurophysiology*, 105(4), 1633–1641. Retrieved from <http://jn.physiology.org/content/105/4/1633.short>
- Hurst, J., & Rizzi, A. (2008). Series compliance for robot actuation: Application on the electric cable differential leg. *IEEE Robotics & Automation Magazine*.
- Hurst, J. W., Chestnutt, J. E., & Rizzi, A. a. (2004). An actuator with physically variable stiffness for highly dynamic legged locomotion. *IEEE International Conference on Robotics and Automation, 2004. Proceedings. ICRA '04. 2004*, 5, 4662–4667.
- Hyon, S. H., Hale, J. G., & Cheng, G. (2007). Full-body compliant human-humanoid interaction: Balancing in the presence of unknown external forces. In *IEEE Transactions on Robotics* (Vol. 23, pp. 884–898).
- Iannotti, J. P., & Parker, R. D. (2013). *The Netter Collections of Medical Illustrations: Musculoskeletal System, part I - Upper Limb*. (F. H. Netter, Ed.) (2nd ed., Vol. 6). Philadelphia, PA: Saunders.
- Inouye, J. M., & Valero-Cuevas, F. J. (2016). Muscle Synergies Heavily Influence the Neural Control of Arm Endpoint Stiffness and Energy Consumption. *PLoS Computational Biology*, 12(2), e1004737.
- Ison, M., & Artemiadis, P. (2015). Multi-Directional Impedance Control with Electromyography for Compliant Human-Robot Interaction. *2015 IEEE International Conference on Rehabilitation Robotics (ICORR)*.
- Johnson, M., & Feng, X. (2007). Potential of a suite of robot/computer-assisted motivating systems for personalized, home-based, stroke rehabilitation. *Rehabilitation*.
- Karavas, N., & Ajoudani, A. (2013). Tele-impedance based stiffness and motion augmentation for a knee exoskeleton device. *2013 IEEE International Conference on Robotics and Automation (ICRA)*, 2194–2200.
- Kawamura, S., Yamamoto, T., Ishida, D., Ogata, T., Nakayama, Y., Tabata, O., & Sugiyama, S. (2002). Development of passive elements with variable mechanical impedance for wearable robots. *2002 IEEE International Conference on Robotics and Automation*, 1(May), 248–253.

- Kiguchi, K., Tanaka, T., & Fukuda, T. (2004). Neuro-Fuzzy Control of a Robotic Exoskeleton With EMG Signals. *IEEE Transactions on Fuzzy Systems*, 12(4), 481–490.
- Kilicarslan, A., Prasad, S., Grossman, R. G., & Contreras-Vidal, J. L. (2013). High accuracy decoding of user intentions using EEG to control a lower-body exoskeleton. *Conference Proceedings : ... Annual International Conference of the IEEE Engineering in Medicine and Biology Society. IEEE Engineering in Medicine and Biology Society. Annual Conference, 2013*, 5606–5609.
- Kistemaker, D. A., Wong, J. D., & Gribble, P. L. (2010). The central nervous system does not minimize energy cost in arm movements. *Journal of Neurophysiology*, 104(6), 2985–2994.
- Kutch, J. J., & Valero-Cuevas, F. J. (2012). Challenges and new approaches to proving the existence of muscle synergies of neural origin. *PLoS Computational Biology*, 8(5), e1002434.
- Lacquaniti, F., Carrozzo, M., & Borghese, N. A. (1993). Time-varying mechanical behavior of multijointed arm in man. *Journal of Neurophysiology*, 69(5), 1443–1464.
- Lasi, H., Fettke, P., Kemper, H. G., Feld, T., & Hoffmann, M. (2014). Industry 4.0. *Business and Information Systems Engineering*, 6(4), 239–242.
- Latash, M. (1992). Independent control of joint stiffness in the framework of the equilibrium-point hypothesis. *Biological Cybernetics*, 67, 377–384.
- Latash, M. L., Scholz, J. P., & Schönner, G. (2002). Motor control strategies revealed in the structure of motor variability. *Exercise and Sport Sciences Reviews*, 30(1), 26–31.
- Laurin-Kovitz, K. F., Colgate, J. E., & Carnes, S. D. R. (1991). Design of components for programmable passive impedance. *Proceedings. 1991 IEEE International Conference on Robotics and Automation*, (April), 1476–1481.
- Lee, S., & Sankai, Y. (2002). Power assist control for walking aid with HAL-3 based on EMG and impedance adjustment around knee joint. In *IEEE/RSJ International Conference on Intelligent Robots and System* (Vol. 2, pp. 1499–1504). IEEE.
- Lee, S., & Sankai, Y. (2005). Virtual impedance adjustment in unconstrained motion for an exoskeletal robot assisting the lower limb. *Advanced Robotics*, 19(7), 773–795.

- Liang, P., Yang, C., Wang, N., & Li, Z. (2014). Implementation and Test of Human-Operated and Human-Like Adaptive Impedance Controls on Baxter Robot. *Advances in Autonomous ....*
- Lotz, C. A., Agnew, M. J., Godwin, A. A., & Stevenson, J. M. (2009). The effect of an on-body personal lift assist device (PLAD) on fatigue during a repetitive lifting task. *Journal of Electromyography and Kinesiology*, 19(2), 331–340.
- Lucas, L., DiCicco, M., & Matsuoka, Y. (2004). An EMG-controlled hand exoskeleton for natural pinching. *Journal of Robotics and Mechatronics*, 16, 482–488.
- Magnusson, S. P., Aagaard, P., Rosager, S., Dyhre-Poulsen, P., & Kjaer, M. (2001). Load-displacement properties of the human triceps surae aponeurosis in vivo. *The Journal of Physiology*, 531(1), 277–288.
- Makinson, B. J. (1971). *Research and Development Prototype for Machine Augmentation of Human Strength and Endurance. Hardiman I Project*. Schenectady, NY.
- Mañanas, M. a, Jané, R., Fiz, J. a, Morera, J., & Caminal, P. (2002). Influence of estimators of spectral density on the analysis of electromyographic and vibromyographic signals. *Medical & Biological Engineering & Computing*, 40(1), 90–98.
- Marieb, E. N., & Hoehn, K. (2007). *Human Anatomy & Physiology*. Pearson Benjamin Cummings.
- McDaid, A. J., Song Xing, & Xie, S. Q. (2013). Brain controlled robotic exoskeleton for neurorehabilitation. In *2013 IEEE/ASME International Conference on Advanced Intelligent Mechatronics* (pp. 1039–1044). IEEE.
- McIntyre, J., Mussa-Ivaldi, F., & Bizzi, E. (1996). The control of stable postures in the multijoint arm. *Experimental Brain Research*.
- McMahon, T. A. (1984). Muscles, reflexes, and locomotion BT - Reflexes and Motor Control. In *Reflexes and Motor Control* (p. 331).
- Melendez-Calderon, A., Bagutti, L., Pedrono, B., & Burdet, E. (2011). Hi5: A versatile dual-wrist device to study human-human interaction and bimanual control. In *2011 IEEE/RSJ International Conference on Intelligent Robots and Systems* (pp. 2578–2583). IEEE.
- Melendez-Calderon, A., Komisar, V., & Burdet, E. (2015). Interpersonal strategies for disturbance attenuation during a rhythmic joint motor action. *Physiology*

- & *Behavior*, 147, 348–358. <https://doi.org/10.1016/j.physbeh.2015.04.046>
- Merletti, R., & Farina, D. (2016). *Surface Electromyography: Physiology, Engineering and Applications*. *Surface Electromyography: Physiology, Engineering and Applications*.
- Merletti, R., & Parker, P. (Philip A. . (2004). *Electromyography : physiology, engineering, and noninvasive applications*. IEEE Press.
- Mghames, S., Laghi, M., Della Santina, C., Garabini, M., Catalano, M., Grioli, G., & Bicchi, A. (2017). Design, control and validation of the variable stiffness exoskeleton FLExo. In *2017 International Conference on Rehabilitation Robotics (ICORR)* (pp. 539–546). IEEE.
- Milner, T. (2002). Adaptation to destabilizing dynamics by means of muscle cocontraction. *Experimental Brain Research*.
- Milner, T., & Cloutier, C. (1993). Compensation for mechanically unstable loading in voluntary wrist movement. *Experimental Brain Research*, 94, 522–532. Retrieved from <http://link.springer.com/article/10.1007/BF00230210>
- Morita, T., & Sugano, S. (1995). Design and Development of a new Robot Joint using Mechanical Impedance Adjuster. *IEEE International Conference on Robotics and Automation*, 2469–2475.
- Mulas, M., Folgheraiter, M., & Gini, G. (2005). An EMG-controlled exoskeleton for hand rehabilitation. *9th International Conference on Rehabilitation Robotics, 2005. ICORR 2005*.
- Munoz, L. M. (2017). Ergonomics in the Industry 4.0: Exoskeletons. *Journal of Ergonomics*, 08(01).
- Muramatsu, Y., Kobayashi, H., Sato, Y., Jiaou, H., Hashimoto, T., & Kobayashi, H. (2011). Quantitative performance analysis of exoskeleton augmenting devices - muscle suit - for manual worker. *Int. J. Automation Technol.*, 5(4), 559–567.
- Mussa-Ivaldi, F., Hogan, N., & Bizzi, E. (1985). Neural, mechanical, and geometric factors subserving arm posture in humans. *The Journal of Neuroscience*, 5(10), 2732–2743.
- Nazari, M. A., Perrier, P., & Payan, Y. (2013). The distributed lambda ( $\lambda$ ) model (DLM): a 3-D, finite-element muscle model based on Feldman's  $\lambda$  model; assessment of orofacial gestures. *Journal of Speech, Language, and Hearing*

*Research : JSLHR, 56(6), S1909-23.*

- Nef, T., Mihelj, M., & Riener, R. (2007). ARMin: a robot for patient-cooperative arm therapy. *Medical & Biological Engineering & Computing, 45(9)*, 887–900.
- Osu, R., Franklin, D. W., Kato, H., Gomi, H., Domen, K., Yoshioka, T., & Kawato, M. (2002). Short- and long-term changes in joint co-contraction associated with motor learning as revealed from surface EMG. *Journal of Neurophysiology, 88(2)*, 991–1004.
- Osu, R., & Gomi, H. (1999). Multijoint muscle regulation mechanisms examined by measured human arm stiffness and EMG signals. *Journal of Neurophysiology, 81(4)*, 1458–1468.
- Osu, R., Kamimura, N., Iwasaki, H., Nakano, E., Harris, C. M., Wada, Y., & Kawato, M. (2004). Optimal impedance control for task achievement in the presence of signal-dependent noise. *IEEE Transactions on Systems, Man, & Cybernetics - Part B: Applications and Foundations, 34(12)*, 1199–1215.
- Overduin, S. A., D'Avella, A., Roh, J., & Bizzi, E. (2008). Modulation of muscle synergy recruitment in primate grasping. *The Journal of Neuroscience : The Official Journal of the Society for Neuroscience, 28(4)*, 880–892.
- Peattie, A., Korevaar, A., & Wilson, J. (2009). Automated variable resistance system for upper limb rehabilitation. *Australasian Conference on Robotics and Automation*.
- Perreault, E. (2002). Voluntary control of static endpoint stiffness during force regulation tasks. *Journal of Neurophysiology, 87(6)*, 2808–2816.
- Perreault, E. J., Kirsch, R. F., & Crago, P. E. (2002). Voluntary Control of Static Endpoint Stiffness During Force Regulation Tasks. *J Neurophysiol, 87(6)*, 2808–2816.
- Poulin, V., Korner-Bitensky, N., Bherer, L., Lussier, M., & Dawson, D. R. (2017). Comparison of two cognitive interventions for adults experiencing executive dysfunction post-stroke: a pilot study. *Disability and Rehabilitation, 39(1)*, 1–13.
- Pratt, G. a., & Williamson, M. M. (1995). Series elastic actuators. *IEEE/RSJ International Conference on Intelligent Robots and Systems. "Human Robot Interaction and Cooperative Robots," 1(1524)*, 399–406.
- Pratt, J., Krupp, B., Morse, C., & Collins, S. (2004). The RoboKnee: an exoskeleton for enhancing strength and endurance during walking. In *IEEE Int. Conf. on*

- Robotics and Automation, 2004. Proceedings. ICRA '04* (Vol. 3, pp. 2430–2435). IEEE.
- Reinkensmeyer, D. J., Pang, C. T., Nessler, J. A., & Painter, C. C. (2002). Web-based telerehabilitation for the upper extremity after stroke. *IEEE Transactions on Neural Systems and Rehabilitation Engineering*, 10(2), 102–108.
- Rocon, E., Belda-Lois, J. M., Ruiz, A. F., Manto, M., Moreno, J. C., & Pons, J. L. (2007). Design and validation of a rehabilitation robotic exoskeleton for tremor assessment and suppression. *IEEE Transactions on Neural Systems and Rehabilitation Engineering: A Publication of the IEEE Engineering in Medicine and Biology Society*, 15(3), 367–378.
- Romero, D., Bernus, P., Noran, O., Stahre, J., & Berglund, Å. F. (2016). The operator 4.0: Human cyber-physical systems & adaptive automation towards human-automation symbiosis work systems. In *IFIP Advances in Information and Communication Technology* (Vol. 488, pp. 677–686).
- Rosen, J., Brand, M., Fuchs, M. B., & Arcan, M. (2001). A myosignal-based powered exoskeleton system. *IEEE Transactions on Systems, Man, and Cybernetics - Part A: Systems and Humans*, 31(3), 210–222.
- Sacco, K., Cauda, F., D'Agata, F., Duca, S., Zettin, M., Virgilio, R., ... Geminiani, G. (2011). A combined robotic and cognitive training for locomotor rehabilitation: evidences of cerebral functional reorganization in two chronic traumatic brain injured patients. *Frontiers in Human Neuroscience*, 5, art.n. 146 ppl-9.
- Sanger, T. D., Krakauer, J. W., Diedrichsen, J., Schweighofer, N., Schmit, B., Rymer, W., ... Hong, Y. (1994). Optimal unsupervised motor learning for dimensionality reduction of nonlinear control systems. *IEEE Transactions on Neural Networks*, 5(6), 965–973.
- Scataglini, S., Andreoni, G., & Gallant, J. (2015). A Review of Smart Clothing in Military. In *Proceedings of the 2015 workshop on Wearable Systems and Applications - WearSys '15* (pp. 53–54). New York, New York, USA: ACM Press.
- Schiavi, R., Grioli, G., Sen, S., & Bicchi, A. (2008). VSA-II: A novel prototype of variable stiffness actuator for safe and performing robots interacting with humans. In *Proceedings - IEEE International Conference on Robotics and Automation* (pp. 2171–2176).

- Schuy, J., Beckerle, P., Wojtusich, J., Rinderknecht, S., & Von Stryk, O. (2012). Conception and evaluation of a novel variable torsion stiffness for biomechanical applications. In *Proceedings of the IEEE RAS and EMBS International Conference on Biomedical Robotics and Biomechatronics* (pp. 713–718).
- Selen, L. P. J., Franklin, D. W., & Wolpert, D. M. (2009). Impedance control reduces instability that arises from motor noise. *Journal of Neuroscience*, *29*(40), 12606–12616.
- Shadmehr, R. (1993). Postural force fields of the human arm and their role in generating multijoint movements. *The Journal of Neuroscience*. Retrieved from <http://www.jneurosci.org/content/13/1/45.short>
- Smith, A. M. C., Yang, C., Ma, H., Culverhouse, P., Cangelosi, A., & Burdet, E. (2015). Novel hybrid adaptive controller for manipulation in complex perturbation environments. *PloS One*, *10*(6), e0129281. <https://doi.org/10.1371/journal.pone.0129281>
- Soekadar, S. R., Witkowski, M., Vitiello, N., & Birbaumer, N. (2015). An EEG/EOG-based hybrid brain-neural computer interaction (BNCI) system to control an exoskeleton for the paralyzed hand. *Biomedizinische Technik*, *60*(3), 199–205.
- Spada, S., Ghibaudo, L., Gilotta, S., Gastaldi, L., & Cavatorta, M. P. (2017). Measurement procedure of parameter to assess an exoskeleton introduction in industrial reality: main issues and EAWS risk assessment. *Procedia Manufacturing*.
- Spada, S., Ghibaudo, L., Gilotta, S., Gastaldi, L., & Cavatorta, M. P. (2018). Analysis of exoskeleton introduction in industrial reality: Main issues and EAWS risk assessment. In *Advances in Intelligent Systems and Computing* (Vol. 602, pp. 236–244).
- Strang, G. (1993). The Fundamental Theorem of Linear Algebra. *The American Mathematical Monthly*, *100*(9), 848.
- Sugano, S., Tsuto, S., & Kato, I. (1992). Force control of the robot finger joint equipped with mechanical compliance adjuster. *Proceedings of the 1992 IEEE/RSJ Int. Conf. on Intelligent Robots and Systems*.
- Sugar, T. G. (2002). A novel selective compliant actuator. *Mechatronics*, *12*(9–10), 1157–1171.
- Sulzer, J. S., Peshkin, M. A., & Patton, J. L. (2005). MARIONET: An exotendon-

- driven rotary series elastic actuator for exerting joint torque. In *Proceedings of the 2005 IEEE 9th International Conference on Rehabilitation Robotics* (pp. 103–108).
- Sylla, N., Bonnet, V., Colledani, F., & Fraisse, P. (2014). Ergonomic contribution of ABLE exoskeleton in automotive industry. *International Journal of Industrial Ergonomics*, *44*(4), 475–481.
- Teasell, R. W., & Kalra, L. (2004). What's New in Stroke Rehabilitation. *Stroke*, *35*(2).
- Theurel, J., Desbrosses, K., Roux, T., & Savescu, A. (2018). Physiological consequences of using an upper limb exoskeleton during manual handling tasks. *Applied Ergonomics*, *67*, 211–217.
- Thoroughman, K. A., & Shadmehr, R. (1999). Electromyographic Correlates of Learning an Internal Model of Reaching Movements. *The Journal of Neuroscience*, *19*(19), 8573–8588.
- Todorov, E., & Jordan, M. I. (2002). Optimal feedback control as a theory of motor coordination. *Nat Neurosci*, *5*(11), 1226–35.
- Tonietti, G., Schiavi, R., & Bicchi, A. (2005). Design and control of a variable stiffness actuator for safe and fast physical human/robot interaction. In *Proceedings - IEEE International Conference on Robotics and Automation* (pp. 526–531).
- Toussaint, H. M., de Winter, A. F., de Haas, Y., de Looze, M. P., Van Dieën, J. H., & Kingma, I. (1995). Flexion relaxation during lifting: Implications for torque production by muscle activity and tissue strain at the lumbo-sacral joint. *Journal of Biomechanics*, *28*(2), 199–210.
- Tresch, M. C., & Jarc, A. (2009). The case for and against muscle synergies. *Current Opinion in Neurobiology*.
- Ulrey, B. L., & Fathallah, F. A. (2013a). Effect of a personal weight transfer device on muscle activities and joint flexions in the stooped posture. *Journal of Electromyography and Kinesiology*, *23*(1), 195–205.
- Ulrey, B. L., & Fathallah, F. A. (2013b). Subject-specific, whole-body models of the stooped posture with a personal weight transfer device. *Journal of Electromyography and Kinesiology*, *23*(1), 206–215.
- Valero-Cuevas, F. J., Venkadesan, M., & Todorov, E. (2009). Structured

- Variability of Muscle Activations Supports the Minimal Intervention Principle of Motor Control. *Journal of Neurophysiology*, 102(1), 59–68.
- Van Damme, M., Vanderborght, B., Verrelst, B., Van Ham, R., Daerden, F., & Lefeber, D. (2009). Proxy-based Sliding Mode Control of a Planar Pneumatic Manipulator. *The International Journal of Robotics Research*, 28(2), 266–284.
- Van Der Kooij, H., Veneman, J., & Ekkelenkamp, R. (2006). Design of a compliantly actuated exo-skeleton for an impedance controlled gait trainer robot (pp. 189–193).
- Van Ham, R., Vanderborght, B., Van Damme, M., Verrelst, B., & Lefeber, D. (2007). MACCEPA, the mechanically adjustable compliance and controllable equilibrium position actuator: Design and implementation in a biped robot. *Robotics and Autonomous Systems*, 55(10), 761–768.
- van Nijhuijs, B., van der Heide, L. A., Jansen, J. W., Gysen, B. L. J., van der Pijl, D. J., & Lomonova, E. A. (2013). Overview of Actuated Arm Support Systems and Their Applications. *Actuators*, 2(4), 86–110.
- Vanderborght, B., Albu-Schaeffer, A., Bicchi, A., Burdet, E., Caldwell, D., Carloni, R., ... Wolf, S. (2012). Variable impedance actuators: Moving the robots of tomorrow. In *IEEE International Conference on Intelligent Robots and Systems* (pp. 5454–5455).
- Vanderborght, B., Albu-schaeffer, A., Bicchi, A., Burdet, E., Caldwell, D. G., Carloni, R., ... Wolf, S. (2013). Variable impedance actuators: A review. *Robotics and Autonomous Systems*, 61(12), 1601–1614.
- Vanderborght, B., Tsagarakis, N. G., Semini, C., Ham, R. Van, & Caldwell, D. G. (2009). MACCEPA 2.0: Adjustable compliant actuator with stiffening characteristic for energy efficient hopping. In *Proceedings - IEEE International Conference on Robotics and Automation* (pp. 544–549).
- Vanderborght, B., Van Ham, R., Verrelst, B., Van Damme, M., & Lefeber, D. (2008). Overview of the Lucy Project: Dynamic Stabilization of a Biped Powered by Pneumatic Artificial Muscles. *Advanced Robotics*, 22(10), 1027–1051.
- Veneman, J. F., Kruidhof, R., Hekman, E. E. G., Ekkelenkamp, R., Van Asseldonk, E. H. F., & van der Kooij, H. (2007). Design and Evaluation of the LOPES Exoskeleton Robot for Interactive Gait Rehabilitation. *IEEE Transactions on Neural Systems and Rehabilitation Engineering*, 15(3), 379–386.
- Verrelst, B., Van Ham, R., Vanderborght, B., Lefeber, D., Daerden, F., & Van

- Damme, M. (2006). Second generation pleated pneumatic artificial muscle and its robotic applications. *Advanced Robotics*, 20(7), 783–805.
- Vorm, J. van der, Nugent, R., & O’Sullivan, L. (2015). Safety and Risk Management in Designing for the Lifecycle of an Exoskeleton: A Novel Process Developed in the Robo-Mate Project. *Procedia Manufacturing*, 3(6th Int.l Conf. on Appl. Human Factors and Ergonomics (AHFE 2015) and the Affiliated Conferences), 1410–1417.
- Wang, S., Wang, L., Meijneke, C., Van Asseldonk, E., Hoellinger, T., Cheron, G., ... Van Der Kooij, H. (2015). Design and Control of the MINDWALKER Exoskeleton. *IEEE Transactions on Neural Systems and Rehabilitation Engineering*, 23(2), 277–286.
- Wang, T., Dordevic, G., & Shadmehr, R. (2001). Learning the dynamics of reaching movements results in the modification of arm impedance and long-latency perturbation responses. *Biological Cybernetics*, 85(6), 437–448.
- Whitfield, B. H., Costigan, P. A., Stevenson, J. M., & Smallman, C. L. (2014). Effect of an on-body ergonomic aid on oxygen consumption during a repetitive lifting task. *International Journal of Industrial Ergonomics*, 44(1), 39–44.
- Wolf, S., Eiberger, O., & Hirzinger, G. (2011). The DLR FSJ: Energy based design of a variable stiffness joint. *2011 IEEE International Conference on Robotics and Automation*, 5082–5089.
- Wolf, S., Grioli, G., Eiberger, O., Friedl, W., Grebenstein, M., Hoppner, H., ... Albu-Schaffer, A. (2016). Variable Stiffness Actuators: Review on Design and Components. *IEEE/ASME Transactions on Mechatronics*.
- Wolf, S., & Hirzinger, G. (2008). A new variable stiffness design: Matching requirements of the next robot generation. In *Proceedings - IEEE International Conference on Robotics and Automation* (pp. 1741–1746).
- Yagi, E., Harada, D., & Kobayashi, M. (2009). Upper-Limb Power-Assist Control for Agriculture Load Lifting. *International Journal of Automation Technology*, 3(6), 716–722. <https://doi.org/10.20965/ijat.2009.p0716>
- Yoshikawa, T. (1985). Manipulability of Robotic Mechanisms. *The International Journal of Robotics Research*, 4(2), 3–9.
- Young, A., & Ferris, D. (2016). State-of-the-art and Future Directions for Robotic Lower Limb Exoskeletons. *IEEE Transactions on Neural Systems and Rehabilitation Engineering*, 25(2).

- 
- Zhou, S., Lawson, D. L., Morrison, W. E., & Fairweather, I. (1995). Electromechanical delay in isometric muscle contractions evoked by voluntary, reflex and electrical stimulation. *European Journal of Applied Physiology and Occupational Physiology*, 70(2), 138–145.
- Zoss, A. B., Kazerooni, H., & Chu, A. (2006). Biomechanical design of the Berkeley lower extremity exoskeleton (BLEEX). *IEEE/ASME Transactions on Mechatronics*, 11(2), 128–138.

## **Appendix A: The administrated Borg scale**

While doing physical activity, we want you to rate your perception of exertion. This feeling should reflect how heavy and strenuous the exercise feels to you, combining all sensations and feelings of physical stress, effort, and fatigue. Do not concern yourself with any one factor such as wrist pain or shortness of breath, but try to focus on your total feeling of exertion.

Look at the rating scale below while you are engaging in an activity; it ranges from 6 to 20, where 6 means "no exertion at all" and 20 means "maximal exertion." Choose the number from below that best describes your level of exertion. This will give you a good idea of the intensity level of your activity, and you can use this information to speed up or slow down your movements to reach your desired range.

Try to appraise your feeling of exertion as honestly as possible, without thinking about what the actual physical load is. Your own feeling of effort and exertion is important, not how it compares to other people's. Look at the scales and the expressions and then give a number.

---

#	Level of exertion
6	No exertion at all
7	
7.5	Extremely light
8	
9	Very light
10	
11	Light
12	
13	Somewhat hard
14	
15	Hard (heavy)
16	
17	Very hard
18	
19	Extremely hard
20	Maximal exertion

---

Borg RPE scale (Borg CR10 scale)

© Gunnar Borg, 1

## Appendix B: The DLR FSJ data sheet

